

Hybrid power supply for automotive powertrain

Modelling and comparison of average EV and FCV

Master's thesis in Electric Power Engineering (MPEPO)

Alfred Kulldorff

MASTER'S THESIS 2020

Comparison of PEMFC and LiB in automotive use


Modelling 3 cases of different design methods for the same drive
cycle, HWFET

Alfred Kulldorff



Department of Energy and Environment
Division of Electric Power Engineering
CHALMERS UNIVERSITY OF TECHNOLOGY
Gothenburg, Sweden 2020

Comparison of PEMFC and LiB in automotive use
Modelling 3 cases of different design methods for the same drive cycle, HWFET.
Then comparing their footprint and cost
Alfred Kulldorff

 Unless other mentioned Alfred Kulldorff, 2020.

Supervisor: Peter Boman, AFRY, Electrical & Atex Design
Examiner: Torbjörn Thiringer, Energy and Environment

Master's Thesis 2020
Department of Electrical Engineering
Division of Electric Power Engineering
Chalmers University of Technology
SE-412 96 Gothenburg
Telephone +46 31 772 1000

Cover: Visualization of model principles constructed in Matlab.

Typeset in L^AT_EX
Printed by Chalmers Reproservice
Gothenburg, Sweden 2020

Comparison of PEMFC and LiB in automotive use
Modelling 3 cases of different design methods for the same drive cycle, HWFET

Alfred Kulldorff
Department of Electric Power Engineering
Chalmers University of Technology

Abstract

The thesis investigates pros and cons of different types, combinations and dimensions of energy storage in vehicles. Such as capacity, weight, power, cost (LCA), environmental impact and safety. With other words comparing their sustainability aspects.

Three cases of different power supply design methods are modelled for the same drive train with a repeated HWFET cycle. The 3 cases are then designed to be able of driving +630km of this cycle. Case A is an EV, case B and C is FCV where case B uses a low power FC stack with a larger energy buffer compared to case C.

Then the difference of dynamic performance of the 3 cases are analysed and compared. With the lifetime and derogation of performance is investigated which enables a comparable cost analysis of each case, both environmental and economical.

The conclusion of the investigation shows cost, environmental, high power performance during shorter periods and lifetime benefits with FCV compared to EV. Crucial areas such as infrastructure needed is neglected, that includes cost of hydrogen compared to electricity from the grid.

Keywords: Vehicle, Car, fuel-cell, PEMFC, Lithium-ion, LiB, comparison, capacity, weight, performance, cost, LCA, sustainability

Acknowledgements

First I would like to thank the whole community in this area of field, wherever I have turned I have received the support they can give.

Thanks to...

Torbjörn Thringer, for his crucial feedback which simplified the work

Peter Boman, Lennart Alfredsson and the rest of the Electrical and Atex department for their support and knowledge about stationary hydrogen solutions

Jonathan Hillander, for his crucial feedback from his experience with HT-PEMFC systems

Stefan Skoog, for his eye-opening work [89] [88] [90]

Emma Arfa Grunditz work that verifies many assumption made in this thesis [28]

Evelina Wikner work that inspired the idea for control system for FCV that extends the LiB life time [103]

And last but not least my family and friends for their support.

Without your help and previous work my work would not be possible. Thank you!

Alfred Kulldorff, Gothenburg, June 2020

Contents

| | |
|--|-------------|
| List of Figures | xiii |
| List of Tables | xiii |
| List of Abbreviations | xiii |
| 1 Introduction | 1 |
| 1.1 Background | 1 |
| 1.2 Purpose of work | 1 |
| 1.3 Contributions | 1 |
| 2 Theory | 3 |
| 2.1 Lithium-ion Cells - LiB | 3 |
| 2.1.1 Efficiency | 4 |
| 2.1.2 Anode materials | 5 |
| 2.1.3 Cathode materials | 5 |
| 2.1.4 Characteristics of batteries | 5 |
| 2.1.4.1 LiB Dynamics / kinetics | 6 |
| 2.1.4.2 Impedance ladder model | 7 |
| 2.1.5 Lifetime | 8 |
| 2.2 DC-link | 9 |
| 2.3 Proton-exchange membrane fuel cell | 9 |
| 2.3.1 Principle | 9 |
| 2.3.2 Variations | 12 |
| 2.3.3 Characteristics V-I | 13 |
| 2.3.4 Control | 15 |
| 2.3.5 Temperature dependence | 16 |
| 2.3.6 Fade - life time | 16 |
| 2.3.7 Losses | 16 |
| 2.3.8 Humidifier | 17 |
| 2.4 Hydrogen | 18 |
| 2.4.1 Generation | 18 |
| 2.4.2 Storage - Fuel tank | 18 |
| 2.4.2.1 Dynamics | 19 |
| 2.4.3 Safety | 20 |
| 2.5 DC/DC - Converter | 20 |
| 2.6 DC/AC - Inverter | 20 |

| | | |
|----------|--|-----------|
| 2.6.1 | Harmonics | 20 |
| 2.7 | Permanent Magnet Synchronous Motor | 21 |
| 2.8 | Vehicle dynamics | 21 |
| 2.9 | Driving cycles | 22 |
| 2.10 | Sustainability | 22 |
| 2.10.1 | Footprint | 23 |
| 3 | Methods | 29 |
| 3.1 | Drive cycle | 29 |
| 3.1.1 | Verification | 30 |
| 3.2 | PMSM - Modeling | 32 |
| 3.2.1 | Parameters | 32 |
| 3.3 | DC/AC - Inverter | 34 |
| 3.3.1 | Harmonics | 34 |
| 3.4 | DC-link | 34 |
| 3.4.1 | Parameters | 36 |
| 3.5 | LiB - Modelling | 37 |
| 3.5.1 | Parameters | 37 |
| 3.6 | PEM - Modeling | 39 |
| 3.6.1 | DC/DC - converter | 40 |
| 3.6.2 | Controller | 41 |
| 3.6.3 | Hydrogen - Fuel tank | 41 |
| 3.6.3.1 | Design | 41 |
| 3.6.4 | Air - Compressor | 42 |
| 3.6.5 | Water | 43 |
| 3.6.6 | Verification of dynamics | 43 |
| 3.7 | Dynamics of systems | 45 |
| 3.7.1 | PEMFC and LiB | 45 |
| 3.7.2 | LiB & PEMFC potential of life | 48 |
| 3.8 | Cost | 49 |
| 3.8.1 | DC-Link | 49 |
| 3.8.2 | LiB | 49 |
| 3.8.3 | PEMFC | 52 |
| 3.8.4 | Cost - fuel | 55 |
| 3.9 | Material usage - Manufacturing footprint | 56 |
| 3.9.1 | DC-Link | 56 |
| 3.9.2 | LiB | 56 |
| 3.9.3 | Material used for PEMFC system | 60 |
| 3.9.4 | Environmental impact - Cases | 60 |
| 4 | Results | 63 |
| 4.1 | System verification | 63 |
| 4.1.1 | EV - Case A | 63 |
| 4.1.2 | FCV with DC/DC - Case B | 64 |
| 4.1.3 | FCV - Case C | 65 |
| 4.1.4 | Limitation to model | 66 |
| 4.2 | Comparison of cases | 67 |

| | | |
|----------|---|-----------|
| 4.2.1 | Cost comparison | 70 |
| 4.2.2 | Environmental impact comparison | 70 |
| 5 | Conclusion | 73 |
| 6 | Future work | 75 |

List of Abbreviations

| | |
|--------|--|
| Li | Lithium |
| LiB | Lithium ion Battery |
| BOL | Beginning of Life |
| MOL | Middle of Life |
| EOL | End of Life |
| SOC | State of Charge (0-100%) |
| OCV | Open Circuit Voltage |
| C-rate | The rate at which a battery is completely discharged or charged in 1 h. |
| FCE | Full Cycle Equivalent (Total current throughput over rated initial capacity) |
| CC | Constant Current |
| CV | Constant Voltage |
| RMS | Root Mean Square |
| EIS | Electrochemical Impedance Spectroscopy |
| OCV | Open Circuit Voltage |
| CPE | Constant Phase Element |
| FFT | Fast Fourier Transform |
| CE | Coulombic efficiency |
| PE | Positive Electrode |
| NE | Negative Electrode |
| LTO | Lithium Titanium Oxide |
| LFP | Lithium Iron Phosphate |
| NMC | Lithium Nickel Manganese Cobalt oxide |
| NCA | Lithium Nickel Cobalt Aluminium oxides |
| WLTC | The Worldwide harmonised Light vehicles Test Cycles |
| PEM | Proton-exchange membrane |
| FC | Fuel cell |
| FCV | Fuel cell vehicle |
| EV | Electric vehicle |
| HT | High temperature |
| LT | Low temperature |
| BOP | Balance of Plant |
| LCA | Life cycle analysis |
| DC | Direct current |
| AC | Alternative current |
| DC/DC | DC to DC converter |
| DC/AC | DC to AC converter |
| ASSB | All-solid-state batteries |

| | |
|---------------------------|--|
| MLCC | multi-layer ceramic capacitor |
| SSE | solid-state electrolyte |
| SSLB | Solid-state Lithium battery |
| NASCION | Sodium (Na) Super Ionic CONductor |
| CPE | Constant Phase Element |
| GSM | Global System for Mobile Communications |
| SEI | Solid solid electrolyte interface |
| TF | Transfer function |
| AECD | Apparent exchange current density |
| EPSA | Electrochemical Pt surface area (of the cathode and anode layer) |
| MLI | Multi level inverter |
| FSHE | Fundamental Selective Harmonic Elimination |
| EOL | End of lifetime |
| GHG | Greenhouse gasses |
| CAFE | Corporate Average Economy |
| GREET | Greenhouse Gases, Regulated Emissions, and Energy Use in |
| Transportation (software) | |
| BatPac | Battery Manufacturing Cost Estimation (software) |

1

Introduction

1.1 Background

The demand of electrical vehicles is increasing and companies are yet to saturate the market and fulfil its potential and compete with combustion solutions. Fuel-cells have been used more and more in high capacity solutions and have found its way into the car industry.

There are split beliefs all over the world of what is optimal solutions, not only because of different priorities.

The world's resources are limited and new solutions enables the flexibility to diversify them where it's needed the most. This is crucial for a sustainable future.

The manufacturing of lithium batteries keeps getting more sustainable, but fuel cells can be a good complement to many applications, such as FCV. As later will be discussed will depend on what climate it's used in and what infrastructure opportunities the specific country has.

1.2 Purpose of work

To investigate pros and cons of different types, combinations and dimensions of energy storage's in automotives. This includes aspects such as capacity, weight, power, cost, environmental impact and safety. With other words normalising the cases specifications to then be able to measure their individual sustainability difference.

1.3 Contributions

According to the author the following contributions have been made with this thesis.

- A Matlab model that automatically compares the cases implemented in various aspects.
- Collecting data about sustainable aspects of multiple cell types, cost, performance and environmental impact.
- Comparing the three main sustainability aspects of FCV and EV.
- Identifying potential of increase of life time of both LiB and FC when working in synergy with another. For NMC/LMO-G cell it's around 20% SOC.

2

Theory

2.1 Lithium-ion Cells - LiB

Although LiB cells have a lot research attention there is still a lot to improve. Both regarding manufacturability, cost, performance and footprint. The difference between the actual and theoretical capacity can be seen in table (2.1).

Solid state batteries are still under experimental stages but are expected to have higher lifetime and with higher current density with less hysteresis [105]. Which can improve the more environmentally friendly cells like LFP cathode see figure 3.34.

All types of cells have different cons and pros which makes them more effective in some applications then others. For example cells like LFP and LTO have a relatively constant potential in a wide range of their SOC as can be seen in [62]

For each chemistry type there are pros and cons to in several aspects to consider when applying them in the design in question. Most of them are shown and compared approximately in figure 2.1. In addition to this their individual environmental footprint are different and will be compared later in this report.

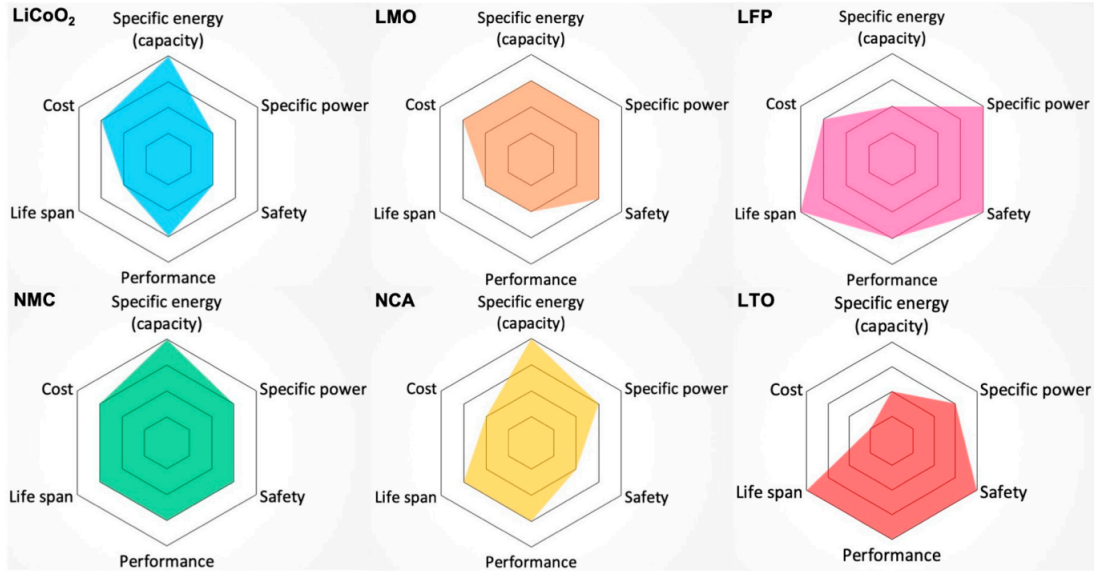


Figure 2.1: Comparison between chemistry performance in different aspects [62]

By using different material and combining different anode with cathode material you can design the cell for the specific application, that it will be used to satisfy the specifications needed with as little material as possible.

Table (2.1) shows an example on how far each chemistry reached its theoretical capacity. It can already be seen here that LTO uses both lithium and titanium which is the reason why they cost more.

Table 2.1: Comparison of actual and theoretical capacity of different types of anode and cathode materials, data from BatPac

| Material | MW g/mol | Actual Capacity Ah/kg | Theoretical Capacity Ah/kg | Full Name |
|----------|-------------|-----------------------------|----------------------------------|---------------------------------|
| NMC333 | 93,88 | 155 (52%) | 300 | Li1.05(Ni1/3Mn1/3Co1/3)0.95O2 |
| NMC622 | 94,39 | 180 (60%) | 298 | Li1.05(Ni0.6Mn0.2Co0.2)0.95O2 |
| NMC532 | 94,03 | 161 (54%) | 299 | Li1.05(Ni0.5Mn0.3Co0.2)0.95O2 |
| NMC811 | 94,72 | 212 (71%) | 297 | Li1.05(Ni0.8Mn0.1Co0.1)0.95O2 |
| NCA | 96,10 | 200 (71%) | 279 | LiNi0.80Co0.15Al0.05O2-Graphite |
| LFP | 157,76 | 150 (88%) | 170 | LiFePO4 |
| LMO | 176,02 | 108 (63%) | 167 | Manganese-Spinel |
| LTO | 459,26 | 170 (72%) | 233 | Li4Ti5O12 |
| G | 72,00 | 360 (96%) | 372 | Graphite |

2.1.1 Efficiency

Each anode or cathode chemistry's total efficiency can be divided into 3 factors and their individual efficiency and comparison of their specific energy can be seen in Richard Schmuck work [82].

Coulombic efficiency (CE), also called faradaic efficiency or current efficiency, is the charge efficiency by which electrons are transferred in batteries. With other words the ratio between the total charge and the output. Which is normally around 99% [82].

Voltaic efficiency, Since the charging voltage is higher than the rated voltage to be able to activate the chemical reaction within the battery losses occur. With other words the efficiency is the ratio of the average discharge voltage to the average charge voltage. To increase efficiency it is important to charge the battery slowly so as small voltage difference.

By increasing its efficiency its lifetime can be increased as well. Which also means it will also reduce the heat generated during use. This is described in Wikners work [103] that a lower temperature will extend the cell capacity and lifespan [62].

Energy Efficiency relates to the charge and discharge C-rate. With a charge rate of 0.05C, the energy efficiency can be as high as 99%. Normally the higher the C rate the lower the efficiency. At 0.5C the energy efficiency is around 97%. This means that it is important to have an oversized battery to be able to reach higher efficiency.

NMC cells is a good example of how doped anodes or cathodes can change its dynamics. The cobalt and aluminium gives the NCA cell better capacity retention, a smaller tendency for transition metal dissolution (no Mn) and power. There are many types with this NCM chemistry. Compared to the rest of its family the NMC-811 shows more favourable properties regarding the thermal stability.

This is one of the reasons why Lithium metals are used more and more in EV applications [82]. Li-rich and Mn-rich oxides (LMR–NMC) are cheap but the voltage & capacity tends to fade allot, lower crystallographic density results with slow kinetics and large voltage hysteresis [82].

2.1.2 Anode materials

There are mainly three types of negative electrode materials that are used Artificial-(SGs), Natural graphite's (NGs) and Amorphous (Hard and soft) carbons [82]. SGs shows outstandingly high levels of purity and less fluctuating quality compared to NGs. Commonly SG are combined with Amorphous to reach the power and energy ratio that is needed in the system [82].

As an example, small amounts of silicon (mostly as SiO_x) are added to the carbon anode to further enhance specific cell energy. The draw back with the added silicon is that the battery will expand more during load which can be dangerous.

Another example is combining titanite to the lithium which resulting in low cell voltage and high-power capability with all-solid-state batteries (ASSBs) which is used in Li-metal polymer [82]. For more information and comparison between each of the cell type and material, read Miaos article [62].

2.1.3 Cathode materials

The mainly used materials in the cathode in EV applications is NCA and NMC due to their high specific energy capability [82]. But also combinations with LMO and LFP are used. LFP cells needs to be operating in higher temperature to reach a lower internal resistance that is comparable with other alternatives [90]. As discussed earlier LFP cells has a low energy capability compared to other NCA and NMC.

With the new solid state (NASICON-based) technology the lifespan, thermal runaway up to 300°C of LFP cells will be improved. SSLBs will have longer lifetime because of the suppressed chemical “cross talk” between electrodes [105]. Normal thermal runaway conditions can be around 100°C [8]. Even the cells operating range is normally up to 60°C [62].

2.1.4 Characteristics of batteries

Impedance spectroscopy (EIS) can be used for analysing the dynamic behavior of batteries [80], within several frequency areas different specific parameters can be derived to be able to model the internal impedance. Figure 2.2 describes the impedance from the EIS sweep. The locations of the characteristic parameters of the cell as different operation areas and specifications that are used for the model.

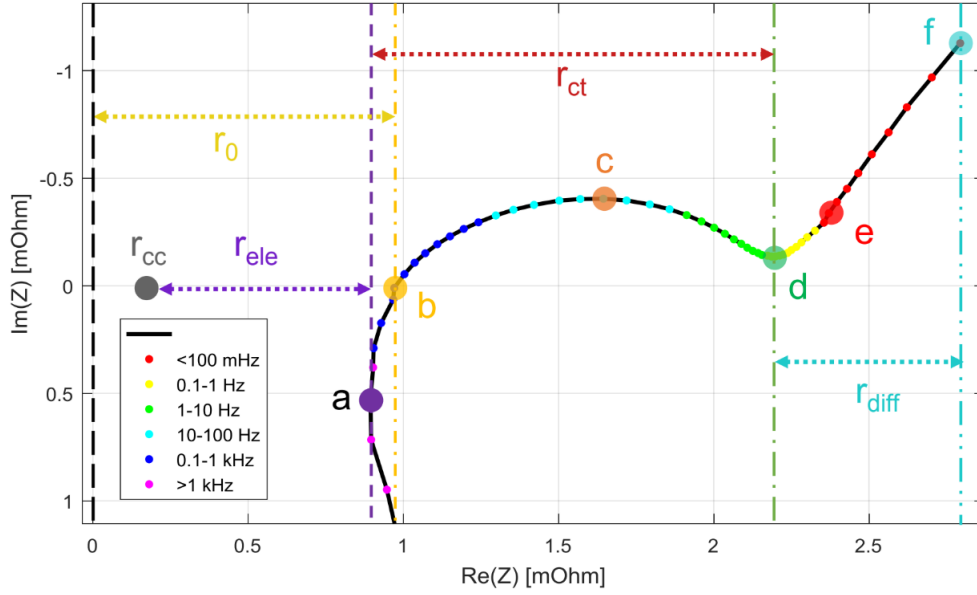


Figure 2.2: Point of interests on a typical EIS sweep. Measurement are for the cell NMC+LMO/G at 41% SOC and 6° C with linear interpolation between sample points.[90] ©

Each dot in figure 2.2 are noted with their respective representation which can be described as

- Z_a is the contact resistance (current collectors, r_{cc}), the electrode active material, separator and the electrolyte.
- Z_b is when the complex part is equal to 0 which, in the model this is called R_0 .
- Z_c , this maximum is not visible in all cell types and temperatures. But it is used for the time constant of the first RC part τ_1 . It is located in the middle of the passing through area denoted r_{ct} .
- Z_d represent the transition between double layer effects and mass transport effects. This can vary a lot depending on lifetime, SOC and temperature conditions.
- Z_e is a fixed frequency point at 100mHz which is where the battery typically is operating during acceleration deceleration.
- Z_f is the slow-diffusion impedance which can change a lot also depending on SOC, temperature and age, also typically called Warburg impedance. The diffusion area is denoted r_{diff} and is between point Z_f and Z_d .

2.1.4.1 LiB Dynamics / kinetics

There are many effects change the cells performance. Ageing of batteries influences its performance in several ways, such as impedance, max capacity which in its turn affect's dynamics as well.

Reversible effects for LiB is mainly the memory effect which can last up to years. It can be refreshed by applying a full cycle [45] .

SOC effects changes most characteristics of the cell such as equivalent circuit parameters which results with different impedance. With other words different time

constants, losses, voltage hysteresis during different operations [45]. Example of this change can be seen in Figure 3.10 and 3.9 or directly from Skoogs work [89].

Cycling with an GSM discharge with an effective current of 1.73 C would result with 3 times the heat generation. $P_{loss} = R * I_{eff}^2$. The heat will change for example its lifetime and internal resistance. [45]. But as seen in Skoogs work [88] a higher temperature will result lower impedance.

Mass transportation is either done with diffusion or migration. Diffusion of ions though the solid electrolyte interface (SEI) will change the electric behavior of the battery especially with aged cells where the SEI have changed [45]. Its parameter can be seen in the low frequency spectrum of the impedance spectroscopy (mHz). see r_{diff} in figure 2.2.

Another effect LiB cells have is a relaxation period after a pulse test where it's terminal voltage will increase back to its steady state after a heavy load, as can be seen in Skoogs work [89].

The heat generated by the cell is either joule heat or entropy heat. The entropy heat potential changes depending on SOC and will drop around 0-15 % SOC which means that the main contribute to heat generation is the joule heat which is mainly from the internal resistance.

Since the entropy heat is even negative at this lower SOC level the zero heat current can be very high, with other words high discharge current without generating any heat.

In addition to this there is a charge transfer impedance that affects the temperature as well. But since it's fast acting typically around 1s it is usually neglected. It can be included in R_0 to compensate for this [88].

2.1.4.2 Impedance ladder model

All cells can be modelled with a R-2RC ladder wear each stage represents a time constant. This approximation is relatively accurate in most applications as can be seen in Skoogs work [89]. The time constant of the cell is calculated for the derived parameters from the EIS as

$$\tau = RC \quad (2.1)$$

This is done for the hole R-2RC ladder which can be written as

$$G = \frac{V_{over}(s)}{I(s)} = R_0 + \frac{R_1}{\tau_1 s + 1} + \frac{R_2}{\tau_2 s + 1} + \frac{R_3}{\tau_3 s + 1} \quad (2.2)$$

When the total impedance is expressed as a TF a bode plot can easily be made to show the cells internal impedance and phase shift depending on the frequency of the applied load. As seen in bode diagram 2.3 the impedance at higher frequency is close to R_0 which was expected. For this specific case the impedance at lower frequencies is the lowest around 60% SOC while at higher frequencies 50% SOC is beneficial.

The drawback with a R-2RC model is that it does not cover the inductive properties of the battery as is seen in 2.2. But since the loads used in the model used in this thesis it can be neglected.

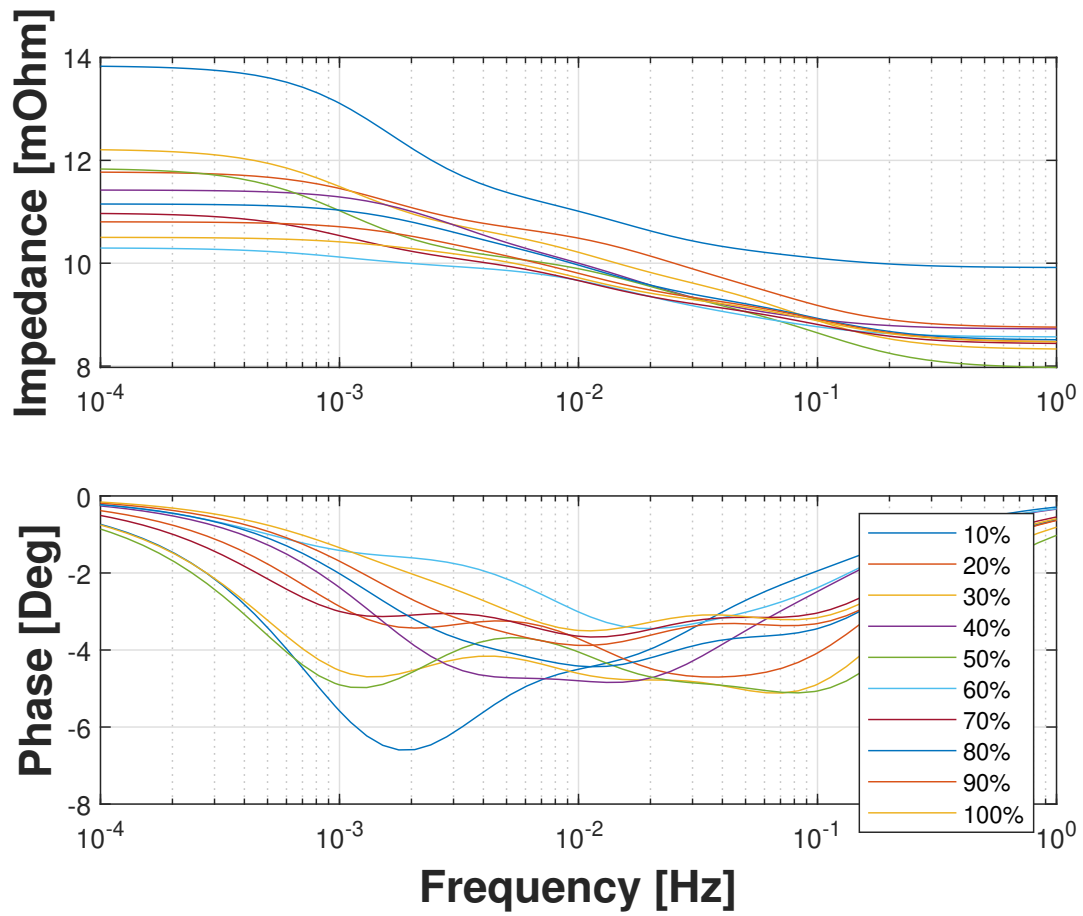


Figure 2.3: Impedance of LMO cell pack depending on SOC at $20C^\circ$, Matlab TF

When a stack of cells is formed in series or parallel its total ladder impedance changes. Each cell is never the same but for simplicity sake they are assumed to be identical. When they are stacked in series each of the same stage of R is doubled and the C is halved, in parallel it is the opposite.

This means that the time constant is always the same but the total internal resistance can be reduced by using more cell stacks in parallel.

2.1.5 Lifetime

The lifetime of LiB can change a lot but the principle on how to save their performance as long as possible are similar. In this section the lifetime NMC/LMO+G will be discussed specifically from Wikners results [103].

To retain the battery life, it is recommended that after the 4 year test to operate between 10-20% SOC around 40° with $\pm 4C$ loads. But the degradation of internal resistance and capacity is much higher than same DOD and range around $35C^\circ$, but for some reason their capacity fluctuates a lot at the end of cycle test.

The reason why the lower DOD drops from $>95\%$ to 80% is unknown from the 4 year experiment. After troubleshooting a theory is that the fluctuations are linked to processes such as temporary blocking of active material or other reversible processes[103]. This is something that would be interesting to investigate to see if a

strict mono type of cycling can affect it's performance.

To still be able to regenerate power back to the battery it common that the battery needs to be cooler than 40°C, as seen in all cell data-sheets. This is because it puts higher stress on the cell compared to discharging.

In Wikners work it is illustrated how it is preferable to control the SOC around 0-20% to both keep its capacity and internal resistance optimal. To approximate their lifetime an empirical ageing model are used which was developed after many tests. This model can be implemented with other models, which makes it very useful. Read more about this in Wikners thesis [103].

2.2 DC-link

There are multiple options on what extra energy buffer to use, this mainly depends on what application its used for. The main reason to implement one is to make sure that the voltage ripple during heavy loads are not to large which makes it hard for the DC/AC inverter to control the output power and thereby be ineffective. In large EV it is usually unnecessary because the high power battery pack can usually provide a lot more power when normally requested.

Normally there are a small DC-link on all DC/AC inverter right by its terminal so the worst ripple voltage from harmonics will be tolerable. Which is why it will not be a part of this thesis. Usually double-layer capacitors are used, also called super- or ultra capacitors. They have also become doped with lithium to be able to hold even higher energy called lithium-ion capacitors (LIC). But in FCV this is not enough if the FC degradation [20]. But this is of course depending on what loads are expected to tolerate.

Instead power batteries are used such as LTO cells. They are very energy dense compared to capacitors with similar power density compared to normal capacitors. As can be seen in table (3.1) a 100F capacitor has similar power density but a factor of almost 8 smaller specific energy capabilities then the LTO.

2.3 Proton-exchange membrane fuel cell

There are multiple types of fuel cells but in this work only Proton-exchange membrane (PEM) will be considered since others is not practical for cars because of its efficiency and its high specific power capabilities.

When solid state cells develops HT-PEMFC might be usable due to their high thermal tolerance [83]. This will result in other benefits as well which will be discussed later in this thesis.

2.3.1 Principle

The overall operating principle of a PEMFC is relatively simple. Hydrogen is fed to the cells anode and oxidized (HOR), while oxygen is reduced at the cathode (ORR). Since catalysts are used on both sides of the PEM the gasses are combined and water is produced.

The protons produced at the anode from the hydrogen are conducted through the PEM to the cathode. But since the PEM is not electronically conductive, the electrons released at the anode have to flow along an external circuit, which can be used however, eventually the electrons recombines with the protons on the cathode side. This is illustrated schematically in 2.4.

The proton-conducting membrane sandwiched between the two catalysts and electrodes are called the membrane electrode assembly (MEA). Normally a platinum-impregnated porous electrode is used. [91].

The main electrochemical reactions take place on the triple phase boundary where the electrolyte, the catalyst, and the reactant (gas) are all in contact [91]. This is illustrated in figure 2.4.

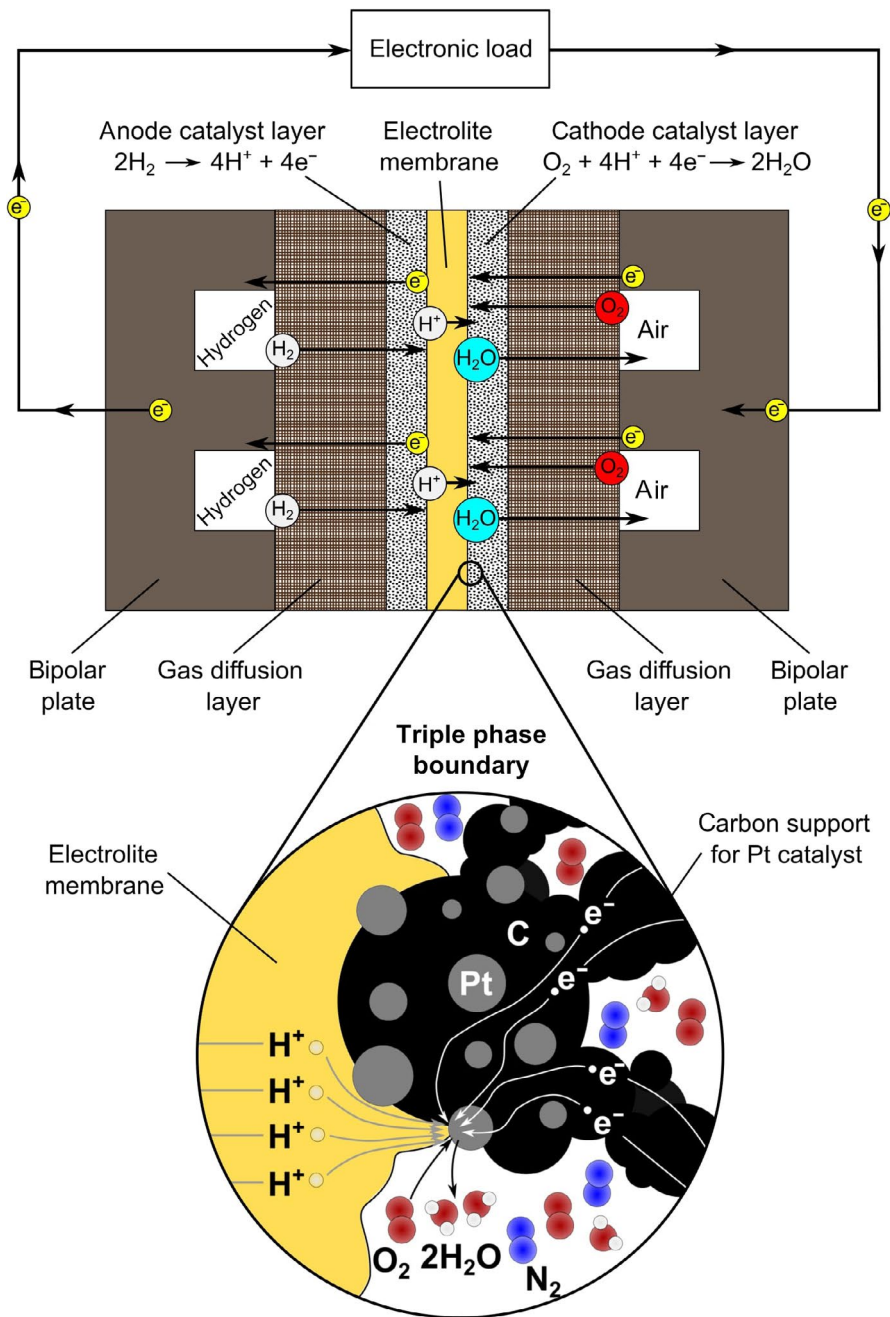
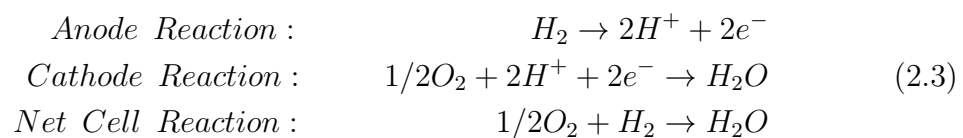


Figure 2.4: Layout and principle of FC , [91]

As described in previous section that a hydrogen gas molecule separates to hydrogen proton and two free electrons which then is conducted through the electric load. The anode, cathode, and net cell reactions of the PEMFC can be described as



The membrane within the fuel cell needs to stay in hydrated state to have high

ion conductivity and durability in LT-PEMFC, which requires proper humidification. With other words water is required as the charge carrier for the proton conductivity inside the Nafion membrane [67].

This results with higher operation range with higher power and higher efficiency. The difference of only wet and dry air used can be seen in [16]. The PEM is made from sulfonated polymers that are highly proton conductive and have hydrophobic properties (contains liquid water).

By decreasing the thickness of the PEM the water can be controlled around depending on what pressure applied on the anode or cathode, there by using an internal humidification system [32]. This system is used in the Toyota Mirai but in most LT-PEMFC system an external humidifier is used to humidify the inlet gas to the cell [76].

The catalyst membranes used the FC needs to be a specific temperature depending on choice of material to be able to full fill its function. This requires the FC to heat up before usage. LT-PEMFC can be started fastest and can be heated up around $10C^{\circ}/min$ while other stationary types can only be heated $1C^{\circ}/min$ up to even higher temperatures which means that it can take hours before they are done.

2.3.2 Variations

There are several new solutions emerging that uses less rare materials. The flexible air-breathing passive PEMFC removes the extra conductor used as electrode and connect directly to breathable conductor that is on the MEA and use light weight plastic instead of heavy metal. Which normally is cobalt steel [67]. Instead of the diffusion layer a breathable carbon nanotubes (CNT) membrane with holes are used together with carbon paper as electrodes. This layout has high gas permeability and conductivity capabilities which is essential for the cells electrical and mass transfer efficiency [67].

The electrodes are electrically insulated and separated by the PEM, which also serves as a barrier for the reactant gases, but still allows the protons to migrate across it as described previously.

The catalyst has high electrical conductivity and materials with good hydrogen storage capabilities are used. Since air naturally diffuses into the PEMFC due to the CNT with holes. There is no need for a compressor, therefor called a passive cell. The plates that are removed are responsible for around 80% of total stack weight, 90% of stack volume and about 30% of the cost [67].

Not only will this passive cell cost less it will also have a higher specific power than normal cells. It can reach $2.2kW/kg$ compared to Toyota's cell $2kW/kg$ which has the highest specific power capability used in cars. The normalised V-I characteristics of the two types of cells indicates a decrease in losses in the ohmic region, which can be seen in Nings article [67].

It is unclear if this passive cell can be used in higher power applications such as cars compared to the medical applications it is used for today [67]. There are new method using this flexible passive cell together with a bifunctional catalyst that enables an energy storage in the cell [99]. Its theoretical specific energy capability is $722Wh/kg$ and are already made with $135Wh/kg$ where NCA LiB cells are around

170Wh/kg [99], see table (3.1) for comparison.

High temperature PEMFC (HT-PEMFC) are mainly used in stationary applications because of its low specific power and operating temperature. Its electrolyte is polybenzimidazole doped with phosphoric acid to create ionic conductivity. This makes it possible to operate at above 100 °C since the membrane does not need to be humidified. Normal operation range is around 120 to 180 °C [47].

This enables a simplified water management and thermal management of the system. Another advantage is its high tolerance towards fuel impurities like carbon monoxide and hydrogen sulphate [47]. It also shows promising performance with iron carbide based catalyst, with other words without noble metals.

A 3 layer membrane type are developed where its lifetime can be increased. With three-layered PBI membranes with the middle layer acting as an acid reservoir. This improves its durability as compared to conventional cells with single layered post doped PBI membranes. Degradation are tested of only 0.00008 %/h in a 9000 h test [47].

There is no standard way to test FC yet so it is hard to compare but in GREET software LT-PEMFC life expectancy is less then 5000h for automotive use. What is the main factor of its derogation is impurities from the air or hydrogen that clog up the catalyst which reduces the effective area that can be deionize the hydrogen.

2.3.3 Characteristics V-I

The V-I characteristics of FC can be divided into three sections, the activation-, ohmic- and mass diffusion regime. which are visible in figure 2.5 3.11 in same order from low to high power. The linear V-I region is the ohmic regime. After the red dot shown in figure 2.5 which shows the maximum power of that cell comes the mass diffusion regime where the efficiency and output power drops drastically.

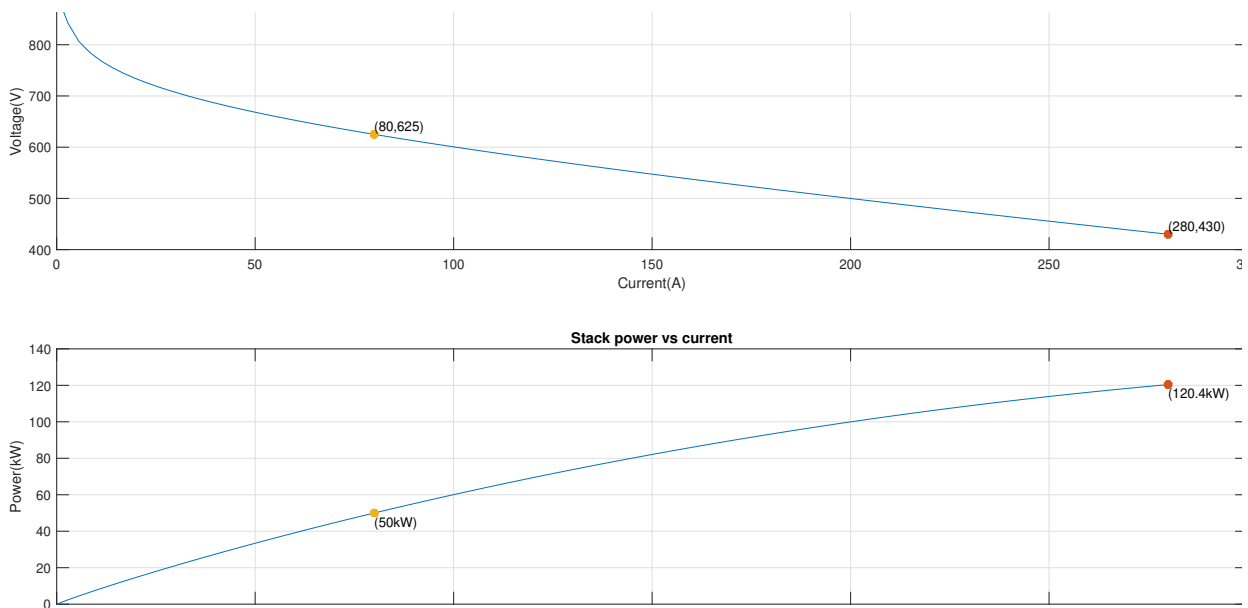


Figure 2.5: Operating range of PEMFC, V-I characteristics

The 3 different operation regimes that affects the output voltage where their equivalent resistance can be used in the model. The activation regime has high efficiency but is unstable to operate in if the cell is alone without any support such as a battery. The voltage contribution can be expressed as

$$V_{\text{act}} = \frac{RT}{\alpha z F} \ln \left(\frac{I}{I_0} \right) = T[a + b \ln(I)] \quad (2.4)$$

The Ohmic regime is the normal operation area which in normal LT-PEMFC has an efficiency around 57% at nominal power output. Its voltage contribution can be described with (2.5) and (2.6). Where R_{ohm} is also a function of current and temperature.

$$V_{\text{ohm}} = V_{\text{ohm,a}} + V_{\text{ohm,membrane}} + V_{\text{ohm,c}} = IR_{\text{ohm}} \quad (2.5)$$

$$R_{\text{ohm}} = R_{\text{ohm0}} + k_{R1}I - k_{RT}T \quad (2.6)$$

Concentration- and also called Mass diffusion regime voltage contribution can with Fick's first- and Faraday's law [65] be used to derive the relation between the surface concentration and the bulk concentration to the cells equivalent resistance. The equation is expressed as

$$R_{\text{conc}} = \frac{V_{\text{conc}}}{I} = -\frac{RT}{zFI} \ln \left(1 - \frac{I}{I_{\text{limit}}} \right) \quad (2.7)$$

where α = Electron transfer coefficient
 a, b = constant terms in Tafel equation (V/K)
 R = Gas constant, 8.3143 J/(mol*K)
 T = Temperature [K]
 z = Number of electrons participating.
 F = Faraday constant (96487 coulombs per mol)
 C = Specific heat capacity of species [J/(mol*K)]

All of them combined affects the total voltage drop as seen in the Figure 2.6 together with other dynamics of the cell that can be used in model.

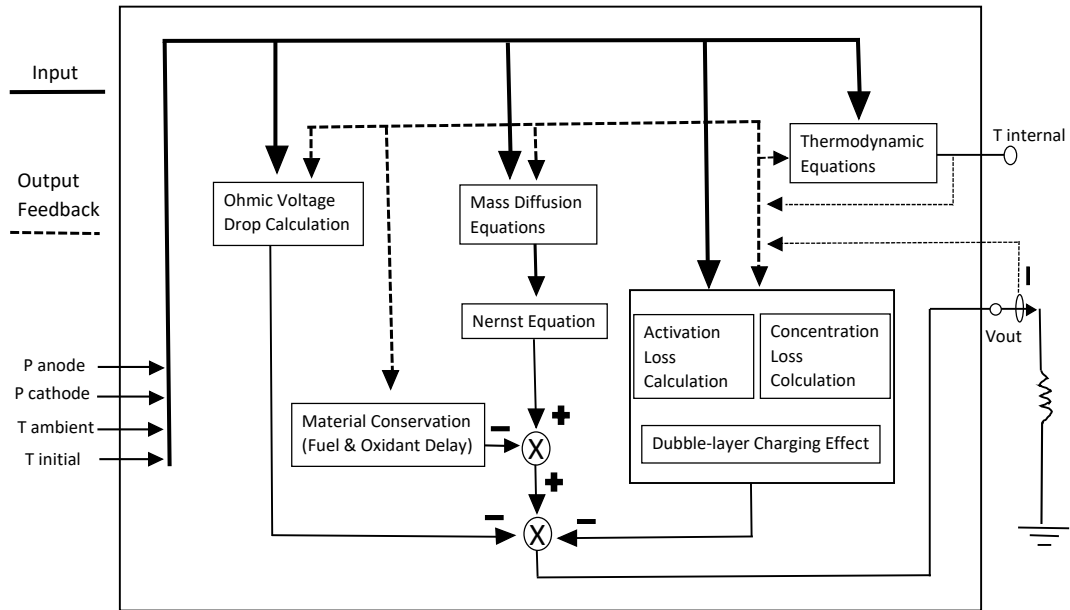


Figure 2.6: Model layout with between different [51] ©

As is shown in Pukrushpans article [76] it is preferable to operate the FC not only at lower current then rated but let it operate slowly to reduce ohmic losses to improve efficiency. More exactly lower frequency then 5.7 Hz in this specific cell. Current signals with frequencies smaller than 0.1 rad/s cause six times lower impedance than currents with frequencies larger than 10 rad/s. The phase change in this region changes almost 50 degrees.

2.3.4 Control

The hydrogen and air relation to the current wanted is linear [79]. Only a compressor for the air intake is needed due to the hydrogen tank has its high pressure where only the valve is needed to regulate the flow. The compressor is much slower to be regulated than the valve but since there are no drawbacks with saturation of air in the cathode as long as it keeps hydrated the air can be compressed more than needed to hide its dynamics. The same principle works with the reuse loop of hydrogen where a compressor is used to compress it back to its inlet.

Thereby it is assumed to be possible to neglect their dynamics in the model, with other words both catalysts is always saturated. The drawback in practice is that this will allow more contamination into the cell which as preciously described decrees its efficiency. There are investigations involving ways to flush the system to clean the catalysts to increase its lifetime.

2.3.5 Temperature dependence

As described in Esfeha article the apparent exchange current density (AECD) is related to the activation losses. The increase of temperature decreases the concentration losses but decreasing the activation over-potential up to $80C^\circ$ [21]. The AECD is dependent of the partial pressure of reactant, temperature and the electrochemical Pt surface areas of the cathode and anode layer (EPSA) as shown in equation (2.8).

It is also shown in the article how the open voltage relation to temperature is linear and changes 8% over the temperature span between 20 to $120 C^\circ$. At $90 C^\circ$ the membrane resistance is the lowest which leads to its highest efficiency. The resistance changes around 50% linearly between $20C^\circ$ and its operational point at $90C^\circ$. The following relations hold

$$\begin{aligned} i_c^0 &= (EPSA)_c I_{O_2(Pt/P_{to})}^0 \left(\frac{P_{O_2}}{P_{O_2}^0} \right)^{\alpha_c} \\ i_a^0 &= (EPSA)_a I_{H_2(Pt)}^0 \left(\frac{P_{H_2}}{P_{H_2}^0} \right)^{\alpha_a} \end{aligned} \quad (2.8)$$

2.3.6 Fade - life time

A normal internal combustion engine is usually assumed to have a lifetime of approximately 5000 hours, in comparison with a fuel cell that has a lifetime of 2000 hours. The degradation is mainly due to the high dynamic load that the cell is operating against during cycle.

If the speed were constant the lifetime could be increased with a factor of 10 to 20 [48]. According to GREET software the lifetime of the FC are assumed to be around the same lifetime expectancy as combustion cars.

2.3.7 Losses

The hydrogen utilisation factor at the anode is expressed as u_{H_2} in (2.9). This is normally very high since a re-loop is commonly used which reuses the hydrogen that was not activated, the cost is the power usage for the compressor needed. Which will be assumed to be draw a total of 1kW together with the rest of the BOP needed for the FC to operate as expected.

$$u_{H_2} = \delta = \frac{Mass_{of H_2 reacted}}{Mass_{of H_2 as input}} \quad (2.9)$$

$$P_{electrical} = (x_{H_2} + 4x_{CH_4} + x_{CO})u_{H_2}[-\Delta g(T) - n_e F(V_{act} + V_{ohm} + V_{con})] \quad (2.10)$$

$$\eta_{PEM} = \frac{P_{electrical}}{(x_{H_2} + 4x_{CH_4} + x_{CO})u_{H_2}(-\Delta g(T))} \quad (2.11)$$

where the dry gas molar compound is:

$$x_{H_2} + 4x_{CH_4} + x_{CO} \quad (2.12)$$

Hydrogen utilisation factor at the anode

u_{H_2}

Where dry gas molar ratio at anode

xa is

| | |
|--------------------------------|---------------|
| Number of electrons | n_e |
| Faraday constant | F |
| Molar ratio | x |
| Gibbs function change of gases | $\Delta g(T)$ |
| Efficiency | η |

There are mainly three ways to produce hydrogen. Steam reforming power usage according to Zhangs article [107] can be approximated with the relation as

$$P = (1 + x)(x_{H_2}q_{LHV}(H_2) + x_{CO}q_{LHV}(CO) + x_{CH_4}q_{LHV}(CH_4)) \quad (2.13)$$

This allows you to calculate the total efficiency from heat and water back to electricity. Normally electrolysis efficiency has the highest efficiency which is around 70-90% depending on how much potassium hydroxide and what input voltage used as is described in [56].

2.3.8 Humidifier

Because the air and hydrogen are usually relatively dry it is natural for the inlet to become dry, the closer to the outlet the more humidified will the membranes be due to the water creation in the cathode catalyst and all membranes has hydrophobic properties. With other words allows water to travel through the cell to the anode side. Common practice is to have the two inlets going through in opposite direction so the water re-circulates.

There are mainly two ways to make sure that the membranes in the FC are kept humidified, internal and external. By reduce the thickness of the PEM membrane to promote the diffusion of water generated downstream in the air system humidify the system using the moisture at the anode.

This measure humidifies the cathode inlet, which is susceptible to drying, Since the H₂ and air flow is counter directed [32]. This also reduce evaporation which leads to poor ion conductivity. The coolant flow at the cathode inlet was increased to restrict evaporation caused by temperature increases.

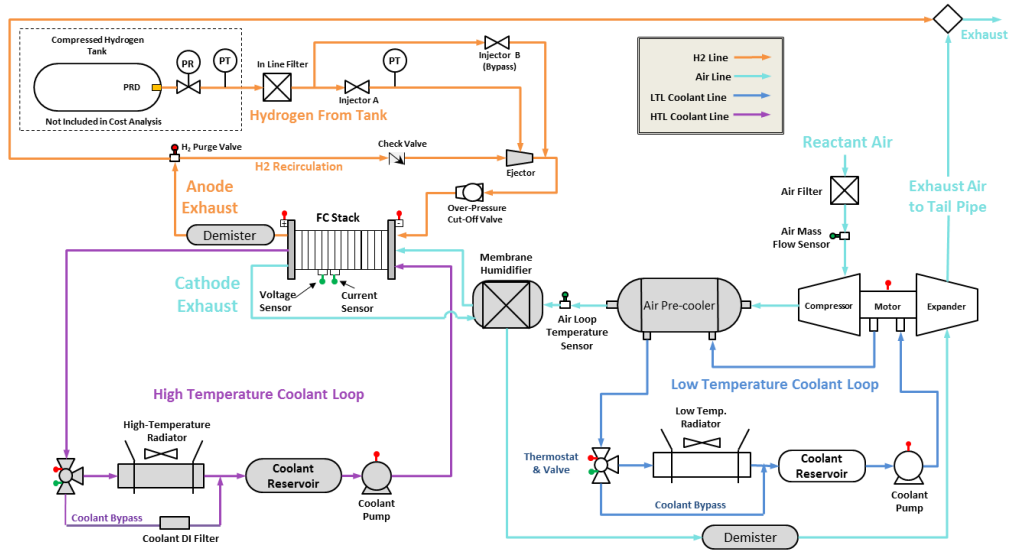


Figure 2.7: BOP hydrogen system layout and FC stack , from James work [43]

2.4 Hydrogen

2.4.1 Generation

There are mainly 3 methods of producing hydrogen:

Electrolysis separates water into its two primary elements—hydrogen (H_2) and oxygen (O_2). This is done by conducting an electrical current through the water to extract hydrogen. The benefit with this method is that it can be sourced from clean, renewable energy such as wind, solar, or hydro. Which is perfect in smaller green energy systems where there might be an over production of energy that cannot be stored or distributed. This is also the most energy efficient method [56]. Mainly because the other methods are using heating/ burning methods.

Steam reforming of methane is a common method of hydrogen production today. It starts with liquids or gases containing hydrogen like natural gas or sustainable biogas sourced from landfills. The fuel then reacts with steam at high temperatures in the reformer, where hydrogen then can be extracted.

The **Gasification** process uses organic materials like crops and livestock waste. Its converted into hydrogen by expose the organic materials for high temperatures which triggers a reaction that separates the hydrogen.

2.4.2 Storage - Fuel tank

Normal storage pressure in FCV are around 700 bar. Since FC have relatively low efficiency it's needed capacity almost needs to be doubled compared to normal a normal EV. This translates to around 120l storage which results with a total hydrogen mass of 5kg.

Hydrogen is around 14 times lighter than air which makes its escape route predictable in our atmosphere. This is fortunate because it is very combustible, dust

particles can be enough to ignite it in some cases [6]. A specific foam material that binds and limits the maximum flow so a puncture will not empty the tank all at once, if there was a leakage. To prevent an extreme explosion [6]. This foam is temperature dependent and will be not be effective over a certain temperature [6].

The total capacity of a fuel tank can be calculated as in equation (2.15), the mass of the flow of hydrogen can be calculated similarly as

$$n = \frac{p_{drop}}{RT} \int Q dt = \frac{pV}{RT} = \frac{pV}{TN_A k_b} \quad (2.14)$$

$$Energy = H_{2_{J/kg}} H_{2_{mass}} n \quad (2.15)$$

where:

p is the pressure of the gas [Pa]

V is the volume of the gas [m³]

n is the number of moles [mol]

R is the universal gas constant, 8,314 J/(molK)

k_B is the Boltzmann constant

N_A is the Avogadro constant

T is the absolute temperature of the gas [Kelvin]

Q is cubic meter per second [m³/s]

The layout of the tank can be different, Toyota's Mirai FCV tank uses 3 layers and is illustrated in it's specification description [1].

1. The inner polymer-lined layer contains the hydrogen.
2. The middle structural layer of carbon-fiber-reinforced polymer provides strength.
3. The outer fiber-glass reinforced polymer layer helps protect from surface abrasions.

2.4.2.1 Dynamics

To control the hydrogen flow a seat valve is commonly used that can handle high pressure low flow gasses accurately. Its delay can be vary a lot all depending on the actuators used. According to a Siemens support [104] it is around 0.2s. The air compressor on the other hand is slower and can be approximated to 1 second, but this also can vary allot on both control system and components used.

Since the PEMFC stack is dependable on both the input pressure and flow rate of which the valve has control over. To simplify the model none of these dynamics are used as mentioned before that both sides are presumed to be saturated. The less pressure that is left in the tank the more the valve needs to be open to be able to supply the pressure required for the PEMFC, which is around 1.5-3 bar.

In general small zone/seat valves that operate 1-3Cv and can easily be closed within 1 second according to Emerson support. Again, it all depends on the actuators used. The equation used to calculate how fast the valve can be closed depending on what application can be expressed as

$$K_v = Q \sqrt{\frac{SG}{\Delta P}} \quad (2.16)$$

K_v is the flow factor

Q is the flow rate m^3/h

SG is the specific gravity of the gas, (Air = 1)

ΔP is the differential pressure across the device [bar]

2.4.3 Safety

According to the MSB which sets the standards to legal hydrogen tanks amongst other things have decided that combustible gases outside in public may not exceed 60l [30]. With other words by decreasing the maximum container the size also decreases the potential explosion magnitude in case of an accident or failure. This means that to be able to store high enough amount of energy 2 storage units is needed. Which is often the case in most FCV.

2.5 DC/DC - Converter

Since the fuel cell will be a compliment to the LiB and they do not have the same terminal voltage, a converter is needed [37]. If the FC voltage is higher than the LiB no DC/DC is needed since the internal voltage of the cell is not stiff and can move close to the LiB voltage depending on the fuel flow rate [37].

According to Wais article, step up converters with coupled-inductor can reach an efficiency of 97.5 %, however as seen in the article the efficiency is not linear. But the lowest efficiency is 95% which makes the nominal efficiency still high [97], and this is for a conversion from 30 to 400V which is a much larger difference in voltage then what is used in Case B in this thesis.

2.6 DC/AC - Inverter

The inverter is used to transform the power potential of the battery to a 3-phase voltage that can power the PMSM. There are multiple types of DC/AC types and transistors that can be used. The most effective is currently SiC transistors which can reach a peak of efficiency of 99.5% which can be achieved during 3/4 of its operational range [108]. It is also shown how its losses are linear depending on output power, which makes the model implementation very simple. Compared to thyristors types converters they can operate in higher frequency with lower losses which results a reduced minimum DC-link

2.6.1 Harmonics

Depending on what control method used different harmonics is expected. Square wave inverters have their harmonics starting right after the fundamental frequency. PWM on the other hand has its harmonics around the switching frequency, which is a lot easier to filter away since it usually is around 1kHz [108]. Normally every odd number of harmonics makes the most noise. In a 3-phase system which usually

is used in automotive, the 3d harmonic is cancelled out in the l-l voltage since the sum of the 3 harmonics is zero.

The line to line harmonic voltage can be approximated with (2.17). The harmonics that could reach the battery is usually handled with an integrated DC-link on the inverter that takes care of the most harmonics, so this will be neglected in the model.

$$U_{l-l} = \frac{\sqrt{6}}{n\pi} u_{dc} \quad (2.17)$$

2.7 Permanent Magnet Synchronous Motor

There are many types of motors but the most effective with highest specific power usage for both breaking and propelling are Permanent Magnet Synchronous Motor (PMSM). Nominal efficiency is usually around 96% [66]. The motor used in this thesis model has a peak of 95% [3].

Advantage compared to other motor alternatives is that the permanent magnets will generate back power whenever there is a negative torque of the rotor. Depending on what speed and mass of the vehicle, the efficiency of the regenerative breaking will change a lot. An excellent illustration of this can be seen in Grunditz work [28].

A usual control strategy is the Maximum Torque Per Ampere (MTPA) method, where the angle ϕ between the d- and q-axis currents is found such that the highest torque can be produced for a certain magnitude of current. This relation can be expressed as

$$\sin(\phi) = -\frac{\Psi_m}{4(L_d - L_q)I_s} - \sqrt{\left(\frac{\Psi_m}{4(L_d - L_q)I_s}\right)^2 + \frac{1}{2}} \quad (2.18)$$

2.8 Vehicle dynamics

Grading force neglected due long distance back and forth will equal to 0.

Table 2.2: Fundamental equations for forces affecting the vehicle

| Parameter | Equation |
|---------------------|---|
| Rolling resistance | $F_{rr} = mg\mu_u \cos(\theta)$ |
| Aerodynamic drag | $F_{areo} = 0.5\rho C_w A_f V^2$ |
| Gradient resistance | $F_{hc} = mg\sin(\theta)$ |
| Propelling force | $F_{xi} = 1.05ma$ |
| Gearbox resistance | $F_{gearR} = 1.05$ [28] |
| Tractive force | $F_{tractive} = F_{gearR}(F_{xi} + F_{hc} + F_{aero} + F_{rr})$ |

Depending on how the aerodynamics and dimension of the car its modeld constants are changed. In table (2.3) the average parameters for different types of cars are shown, according to Grunditz work [28].

Table 2.3: Parameters of three types of cars [28] ©

| Parameter | City | HW | Sport | Unit |
|-------------------------------|-------|-------|-------|------------|
| Seats: | 4-5 | 5 | 2 | kg |
| Mass: | 1200 | 1700 | 1900 | kg |
| Acceleration 0-100 km/h: | 13 | 10 | 4 | s |
| Top speed: | 135 | 150 | 210 | km/h |
| WLTC EH Range: | 108 | 144 | 240 | km |
| Aerod. drag coeff. C_d : | 0.3 | 0.28 | 0.35 | - |
| Area: | 2.05 | 2.3 | 2.0 | m^2 |
| Wheel radius: | 0.31 | 0.32 | 0.34 | m |
| Rolling resist. coeff C_r : | 0.009 | 0.009 | 0.012 | - |
| Energy: | 19.3 | 29.9 | 56.6 | kWh |
| Series cells: | 98.04 | 98.04 | 98.04 | |
| Parallel cells: | 1.76 | 2.73 | 5.17 | |
| V_t , SOC 90%, $P_{EM,max}$ | 325 | 317 | 283 | V |
| R_{dis} | 160.4 | 103.4 | 54.6 | m ω |
| R_{ch} | 134 | 86.4 | 45.6 | m ω |
| Propulsion efficiency | 86 | 85 | 82 | % |
| Braking efficiency | 83 | 82 | 79 | % |
| Net efficiency | 77 | 73 | 71 | % |

2.9 Driving cycles

There are many types of drive cycles that approximate travel routine of different areas both globally and types of roads [17]. To approximate reality, often several drive cycles are combined to be able to see if the automotive can handle it.

The Highway Fuel Economy Driving Schedule (HWFET) represents highway driving conditions under 100 km/h. Which makes a HWFET cycle similar to country road driving. A middle ground between city driving and highway traffic in Sweden.

2.10 Sustainability

There are many aspects to design systems in a sustainable manner. Generally there are 3 pillars that holds it up, social, environmental and economic. The social pillar can symbolise that the car is user friendly and fulfill the drivers performance requirements and safety.

Environmental requirements can be that not only the manufacturing process is inefficient but also the rest of the life cycle of the car such as recycling, fuel, repair/serving it. The same cycle has to be thought through economically as well. The measurement of these parameters are hard to compare to another but are essential to build a sustainable system around a car for example. With other words the whole life cycle of the product and system is needed to be considered.

A good start is to summarise the 3 pillars for the different design alternatives that are available to then be able to compare them with another. Depending on how

the rest of infrastructure and other products system are designed the new design might need to compensate for it.

For example if most previous solutions have been on the heavy side of being economically beneficial it is necessary to start to compensate for that to be able to build a sustainable future. This works in all three directions.

2.10.1 Footprint

There are many kinds of footprints the material used can leave in the manufacturing process. It is usually divided into energy used, emissions released. Figure 2.8 represents the emissions that common materials used a lot for structural purposes commonly used in cars. Figure 2.10 represents the emissions that common materials used that leave a large footprint but are usually used in small amounts for a specific reason due to their appropriate specifications. These are commonly used in electric automobiles.

Rare earth is a group of metals in the periodic table which are for example commonly used in magnets or batteries.

2. Theory

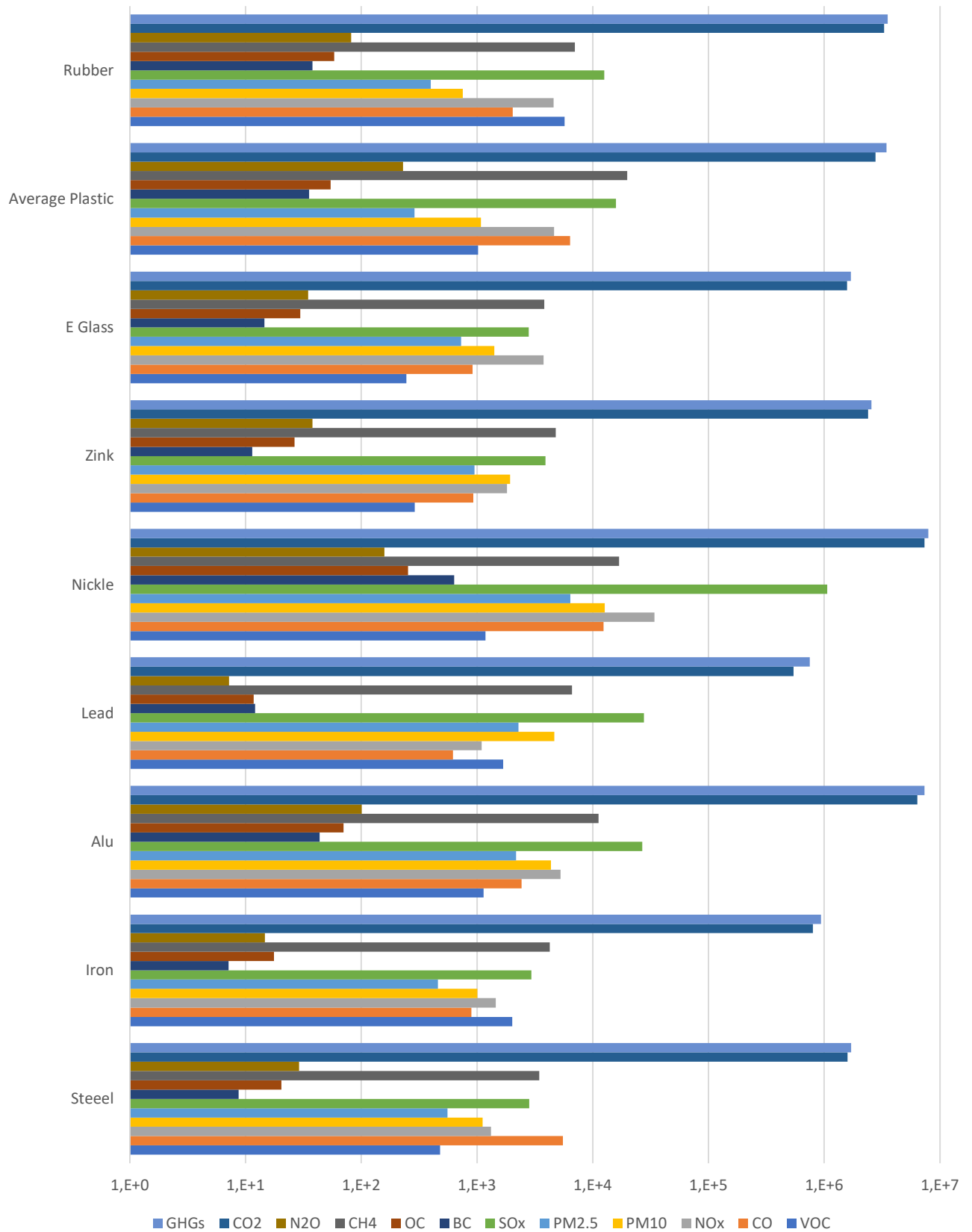


Figure 2.8: Greenhouse gas emissions [g] after manufacturing one ton of each common material used in automotives for constructive purposes.
NOTE logarithmic scale. The parameters are taken from GREET

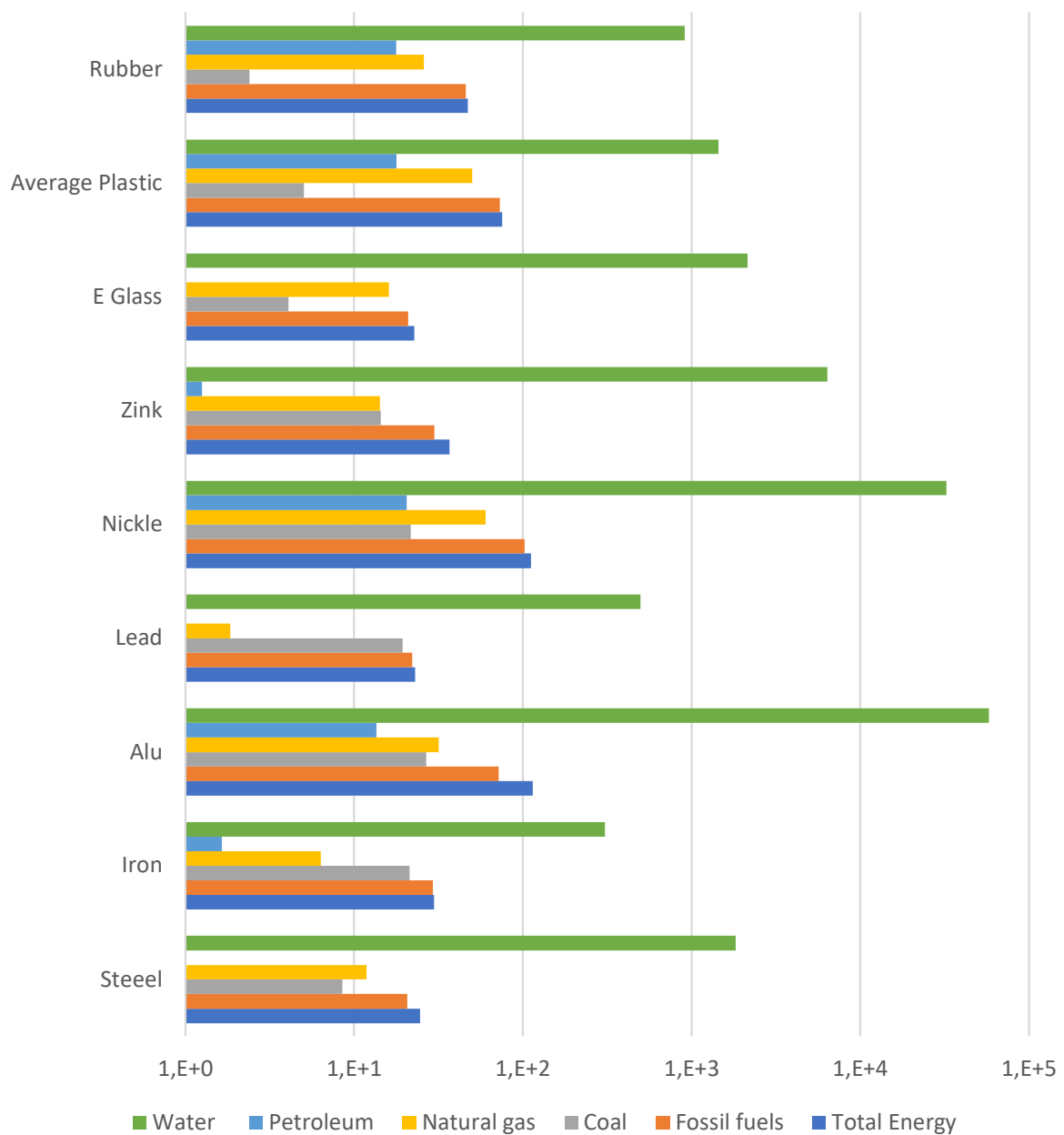


Figure 2.9: Energy used [mmBtu] during manufacturing one ton of each common material used in automotive for constructive purposes.

NOTE logarithmic scale. The parameters are taken from GREET

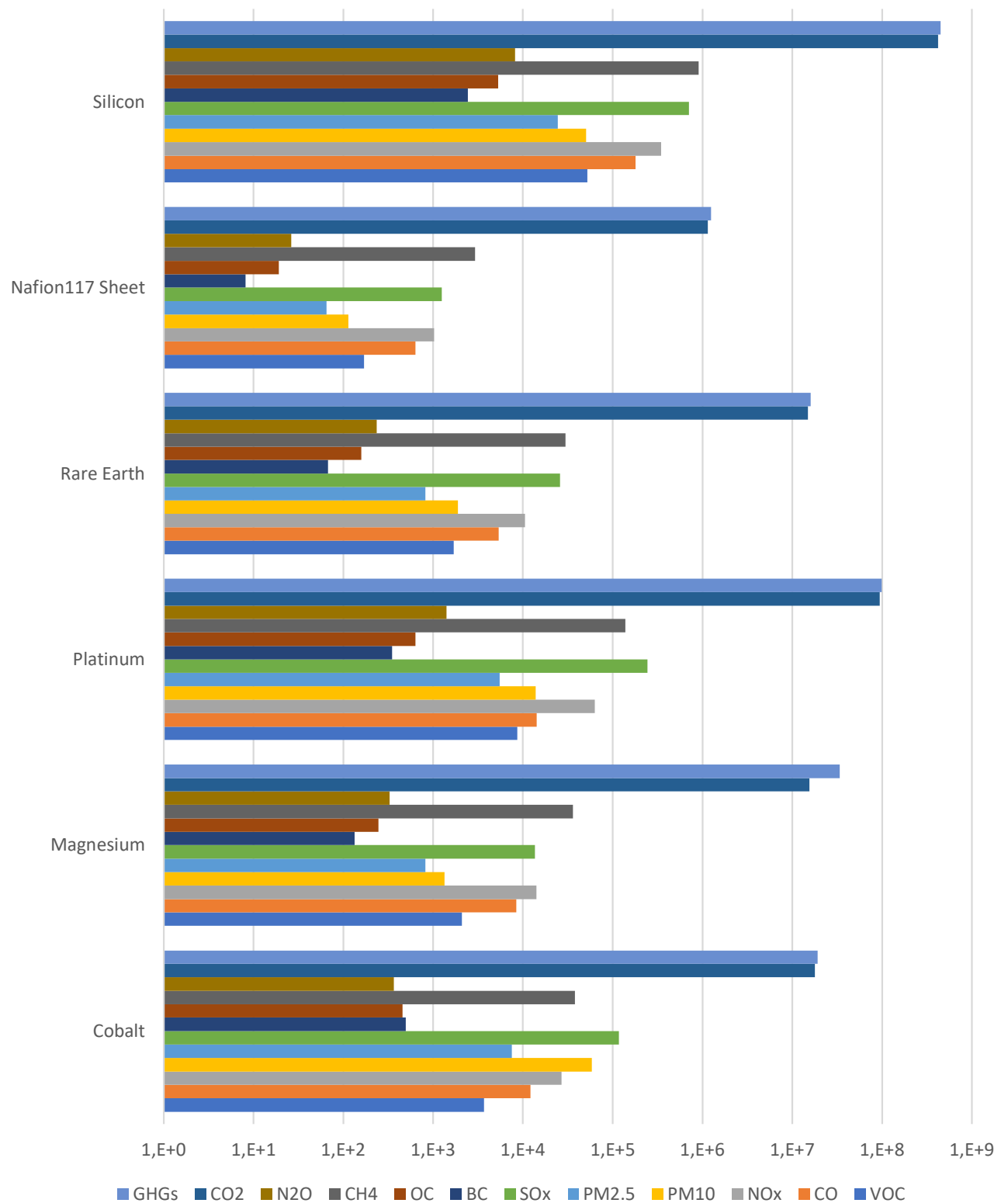


Figure 2.10: Greenhouse gas emissions [g] after manufacturing one ton of each common material used in automobiles for their unique properties. NOTE logarithmic scale. The parameters is taken from GREET

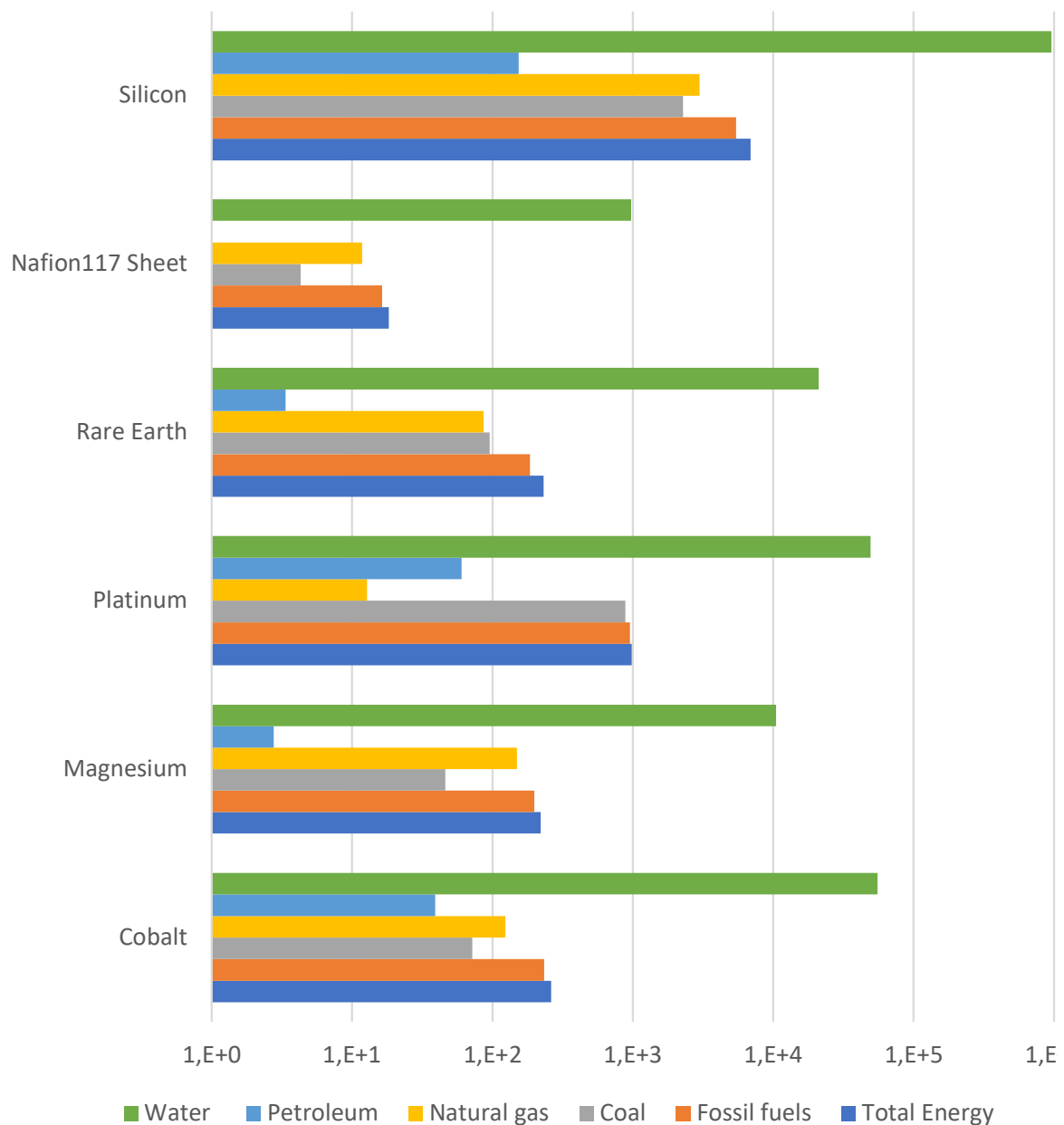


Figure 2.11: Energy used [mmBtu] during manufacturing one ton of each common material used in automotive for their unique properties.
NOTE logarithmic scale. The parameters is taken from GREET

3

Methods

This thesis will investigate and model the most critical parts in Simulink and find three different solution strategies which then can be compared in a sustainable aspects. The Social aspect will be the performance of each case. Such as weight, losses, dynamics, range and safety.

By investigating and comparing different types and dimensions of fuel cells, hydrogen tanks, lithium-cells and DC-Links an acceptable solution will be established for each case. Already established and commercialised products will be investigated and implemented. When each case solutions performance has been analysed the cost and environmental aspects will be estimated and reflected upon.

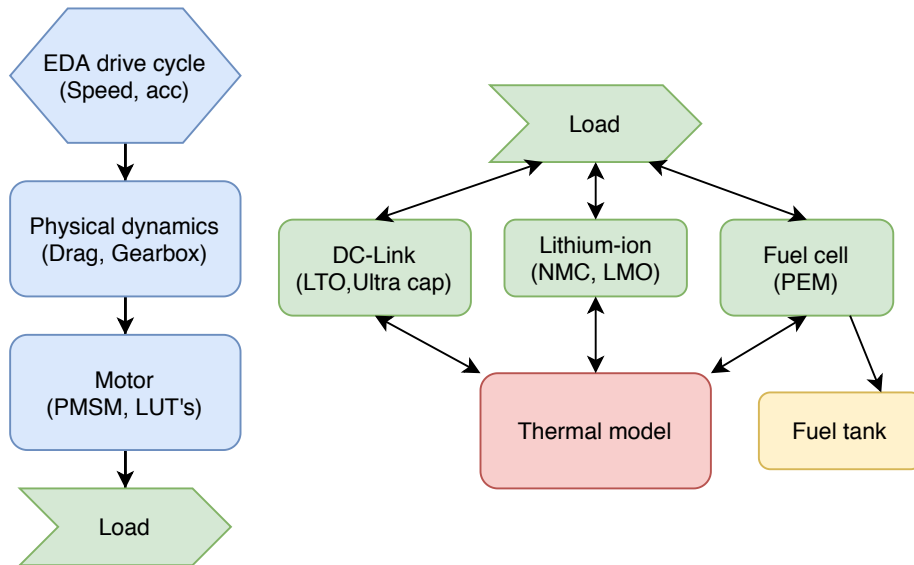


Figure 3.1: Simple overview of simulink model

3.1 Drive cycle

One of the more everyday driving cycle in the more rural areas that does not involve that many stops are similar to the HWFET cycle. Where the highest speed is below 100km/h.

The cycle used can be seen in Figure 3.2. According to Tesla's prediction of distance 2012 [63] their top range is around 40km/h. Tesla is using the WLTF cycle instead which is a more dynamic driving cycle with many more stops compared to the HWFET which only stops once every 13min.

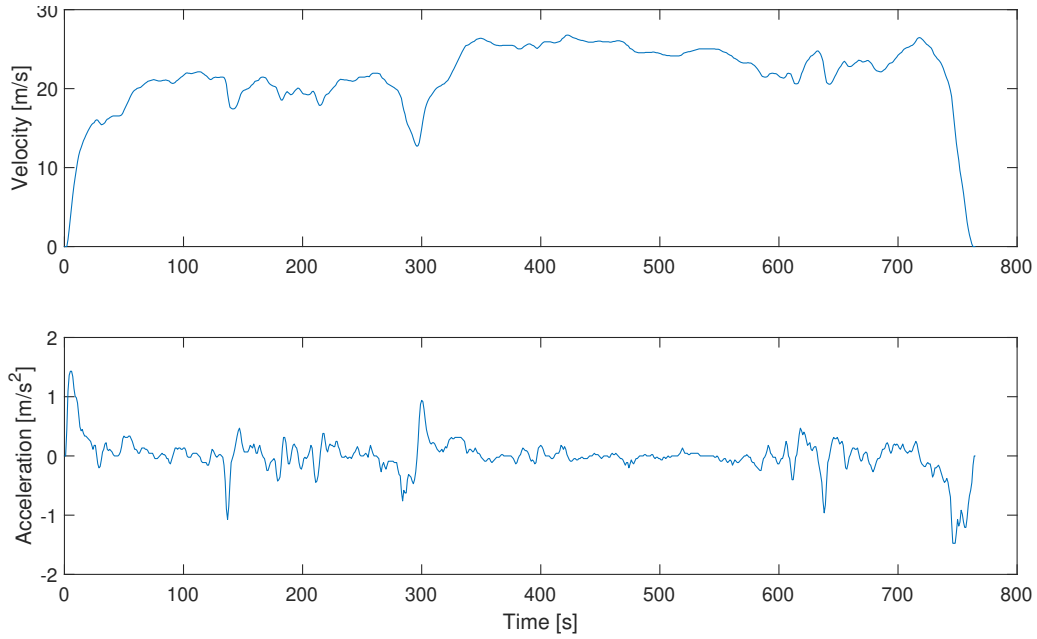


Figure 3.2: The Highway Fuel Economy Driving Schedule (HWFET)

3.1.1 Verification

For this model in this thesis the parameters in table (2.3) are used according to the HW option. The mass will vary depending on which case is used and can be seen in 4.11. Comparing the results that can be seen in Figure 3.3 are similar with Grunditz results with the same cycle and vehicle parameters [28]. Which is a max power cycle 29kW P_{wheel} .

Since the electrical regeneration when decelerating is not as efficient an average of 70% is used as discussed in previous section (2.3) and in Grunditz work [28] showing the efficiency depending on what speed and braking power used, with other words the higher braking force, the higher efficiency.

The large difference between the regenerated power and the wheel power verifies that this is implemented in the intended way. During braking the electrical power is much lower than similar power usage during propelling.

The highest point of regeneration power is 25kW at a vehicle mass of 2ton. The highest electrical power output is 38kW. But keep in mind that the maximal designed output will still be 120kW.

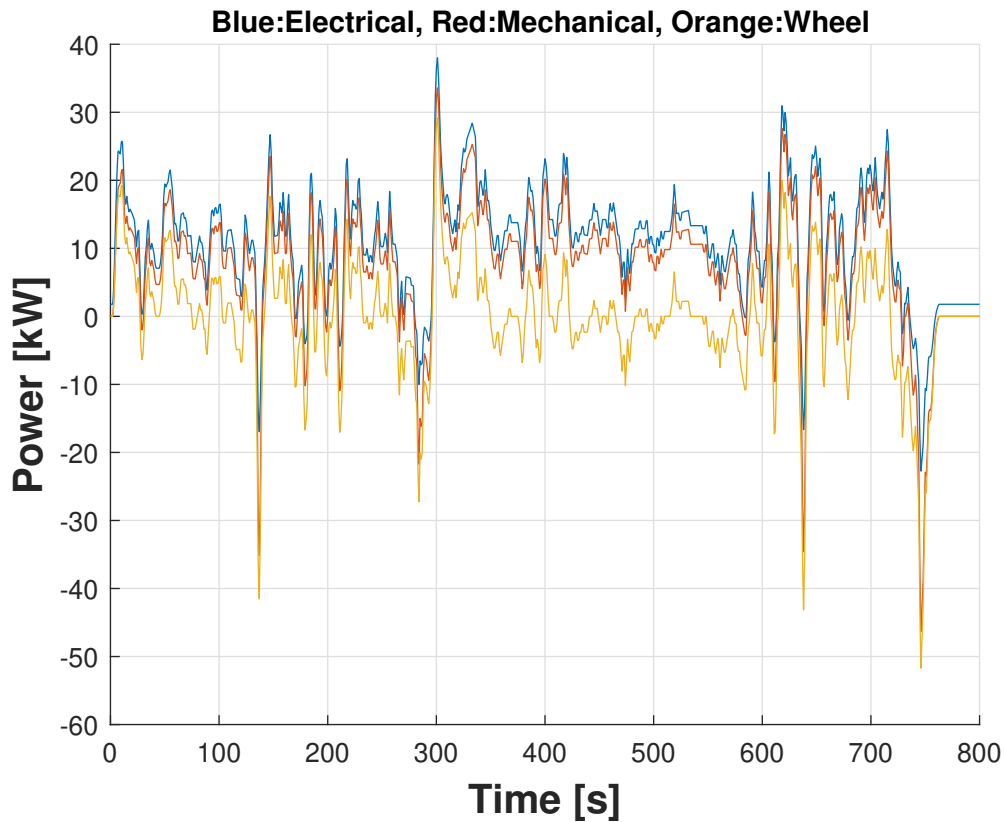


Figure 3.3: Powers during one HWET cycle

To verify that the change of mass affects the vehicle model correctly a simulation of different masses of the vehicle is done. The mass varies between 1-3 ton, this changes the load current linearly from the point of acceleration. The car with higher mass requires more energy to reach the new speed which also results with higher losses. This is illustrated in Figure 3.5 and 3.4.

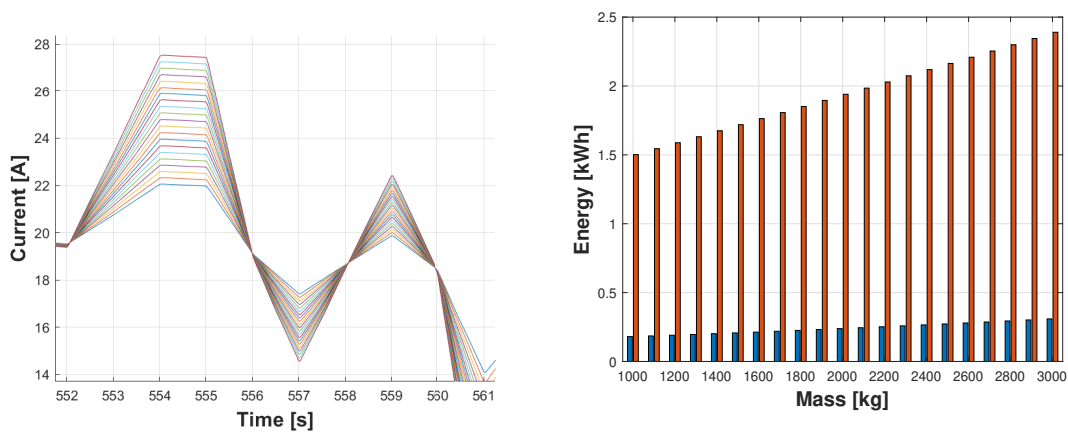


Figure 3.4: Variable mass dynamics difference

Figure 3.5: Variable mass energy consumption total (Orange) and losses in motor (Blue)

3.2 PMSM - Modeling

To limit this report only Permanent magnet synchronous motors (PMSM) is considered. But other alternatives is still viable. Especially in aspects of environmental footprint due to the rare earth magnets commonly used. An average family car has a peak power of 130kW so an similar motor will be used.

3.2.1 Parameters

The motor used is a HVH250-090 because of its long high torque range and peak power of 130kW. An efficiency LUT is derived to be used in Matlab and can be seen in figure 3.7. As seen when comparing between the actual motor efficiency plot from datasheet 3.6 and 3.8 the operational area during the HWFET drive cycle it is operated in an area where the approximation of the efficiency is bad.

Since the range of the car will still meet the requirement of +630km with similar energy capacity as other comparable cars with similar range. This error is neglected since it is beneficial to have the theoretical range as close as possible the actual range. The peak and continuous capability is taken from BorgWarner datasheet around 400V supply voltage [3]

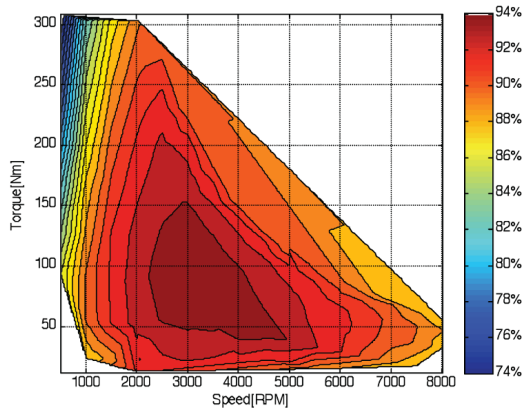


Figure 3.6: Actual motor efficiency HVH250-090 from BorgWarner [3]

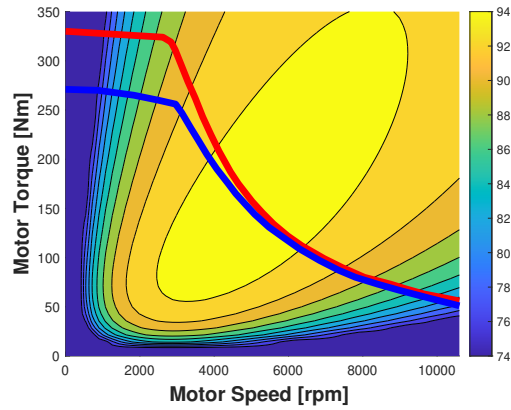


Figure 3.7: Approximation of performance of HVH250 motor. Peak power:Red, Continuous power:Blue line

In addition to this the specifications of the motor according to the datasheet it can handle 600A for 60 sec, has an mass of 57kg and an rotational inertia of 0.086 kgm^2 . Since the lower range of SOC is 350V in Case A the peak power of the motor is 90kW as can be seen in its datasheet [3].

In other words a higher voltage battery is needed or an DC/DC converter to be able to perform with the same power no matter of the SOC. But in this thesis the comparison is more in focus and thereby accepted.

To operate at the motors peak power around 4000 RPM a gearbox ratio of 9 is used. Which corresponds to a road speed of 90km/h.

Not the entire efficiency LUT will be operational. The drive cycle will reach the points shown Figure 3.8 As can be seen when comparing the efficiency plot and the

drive cycle operation area from the HWET standard the motor is over dimensioned for this specific cycle. The 120kW motor is kept since that is a common power performance max for automotives.

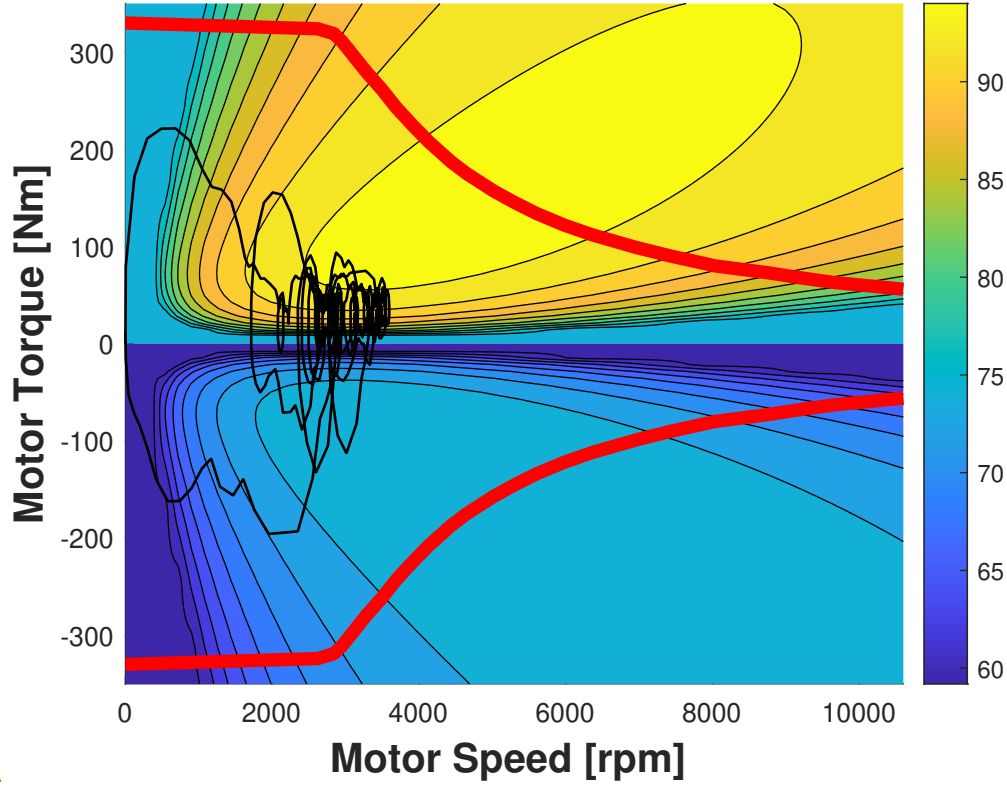


Figure 3.8: Operation area during HWFET driving cycle, where the right bar is the efficiency of the motor [%]

For simplicity sake the regeneration efficiency is assumed to be 80 % since the breaking power in this cycle are around 20kW which can be seen is reasonable with an similar car in Grunditz work [28]. Since the power that can be regenerated is in for average over 40 km/h an average efficiency of 80% is used since the similar size car is used.

Drive cycle HWFET are below the max performance of the motor even at the lowest voltage of the cases, so a comparison of the motors performance will not change allot. Instead the voltage difference of the batteries will be analysed.

The highest regenerative power peak is 23kW which represents approximately an energy of 90Wh. This means that to be able to store this energy it would require at least two stacks of NMC cells ($2 \cdot 96st$) to be able to store the energy. With other words two NMCs in parallel to be able to charge it with a rate of 2C. This makes NMC cells not that good, an option for Case B and C since this would require a high power but relatively low energy to be stored in a low power, high energy battery.

3.3 DC/AC - Inverter

According to [108] SiC traction inverters can reach efficiencies around 99.5% between 250-800V with a peak power of 27kW (one for each motor), with a bus DC-Link of 28uF. It can also be verified that the losses of the inverter is linear depending on output power, also demonstrated in Josefssons work [44].

One of the conclusions from Zhush work [108] is that with an SiC (MOSFET) based inverter has approximately 3.5 times higher Q factor and 3 times lower peak loss in the combined drive cycle (CAFE). This also results with approximately 2 times smaller semiconductor die area. With other words this will result with higher harmonics which also result in higher losses in the battery instead if not designed properly. As previously mentioned, this will be neglected in the model since it is assumed that the internal DC-Link capacitor takes care of most of the harmonics.

3.3.1 Harmonics

The multi-level inverter (MLI) is usually be controlled with Fundamental Selective Harmonic Elimination (FSHE) method to be able to reduce the RMS current to the motor. But an disadvantage with this is that it sets higher stress on the battery, it will produce higher losses but it will not age the battery faster [49].

The angles α_1, α_2 and α_3 describe the instances when the H-bridges should be activated. Depending on their timing the harmonic voltage can be calculated with (3.1). The even harmonics is the ones that will be reaching the battery. The relations are described as

$$U_{ML}(h) = \frac{4}{h\pi} [V_{DC} \cos(h\alpha_1) + V_{DC} \cos(h\alpha_2) + V_{DC} \cos(h\alpha_3)] \quad (3.1)$$

Since a very large battery pack is used in Case A which results with ESR values around $14m\omega$ which are similar to Kerstens descaled test with super- and electrolyte capacitors ($10-100\omega$) [49] and the full extent of an saturated PEMFC capacitive support is unknown the harmonic losses will be neglected in this thesis.

3.4 DC-link

To calculate the specific power and energy of ultra and super capacitors standard "Energy & Power (Based on IEC 62391-2)" is used. The equations used is expressed as

$$E_{max} = \frac{0.5C \cdot V_R^2}{3600} \quad E_G = \frac{E_{max}}{mass} \quad P_U = \frac{0.12V_R^2}{ESR \cdot mass} \quad P_I = \frac{0.25V_R^2}{ESR \cdot mass} \quad (3.2)$$

where the: Maximum Stored Energy:

E_{max} (Wh)

Gravimetric Specific Energy:

E_G (Wh/kg)

Usable Specific Power:

P_U (W/kg)

Impedance Match Specific Power:

P_I (W/kg)

When dimensioning the DC-Link and the rest of the battery the characteristics of the load is vital. An simple calculation of the required capacitance depending on what load is meant to be absorbed seen in (3.3). With a switch frequency at 1kHz and acceptable ripple on 10V as the worst case the minimum capacitance can be calculated. The relations are described as

$$C_{min} = \frac{I_{load}d(1-d)1000}{2 \cdot f_{load} \cdot V_{Ripple}} \quad (3.3)$$

The energy that can be continuously discharged depending on the voltage drop can be calculated with, approximating the load as a ideal sinusoidal current. The relations are described as

$$C_h = -\frac{P_{in} \cdot a \cos\left(\frac{V_{disch} \cdot e^{\pi \cdot i}}{V_{in,max}}\right)}{\left(V_{C_{av}}\right)^2 \cdot \omega \cdot \ln\left(\frac{V_{disch}}{V_{in,max}}\right)} \quad (3.4)$$

Where $V_{C_{av}}$ is the average voltage across the capacitor.

$$V_{C_{av}} = V_{disch} + \frac{V_{inL} \max - V_{disch}}{2} \quad (3.5)$$

Even more aspects must be considered to be able to operate the automotive as practical as possible without adding to much weight.

During simulation it is noticed that a large DC link have similar losses compared to similar mass with LTO cells, similar result with the large battery pack in case A since it's impedance is already very low. In addition to this a high energy storage is needed to be able to provide the power needed for accelerations to not stress the PEMFC to excessively, which is where the main losses are located 3.21.

It is also preferable for the vehicle to be able to store the regenerated power when breaking, which requires a battery pack that can charge at this high rate of power. There is inefficient data know about how high C-rate LTO cells can be charged without consequences as derogation and lifetime. Normally the max charging rate is half of the max discharge rate.

This results with a relatively over dimensioned battery pack, a large DC-link could help with this so the battery can charge during a longer duration but lower intensity. In order to not add to much weight but still be effective there has to be a trade off drivers operation capabilities. In this thesis the capability to still be able utilise max power during a few minutes is prioritised to let case B be more comparable with case A.

Case C on the other hand would be interesting to see with only ultracapacitors as energy bank but since the model is missing an smart controller it is hard to estimate how good the PEMFC stack can cooperate with the capacitor without too high change in voltage during the cycle.

It is neither known how the lifetime of the PEMFC will be affected due to the higher dynamic load compared to if it was parallel with a larger energy bank. The environmental impact calculator GREET has no data about ultracapacitors, so this is why even case C unfortunately will be using LTO cells.

As later will be seen in verification section the load voltage without an DC-link is still reasonable stable with the LTO pack. Which could be even reduced further

with proper planning and control over the PEMFC on when to charge the LTO bank or not.

For example, if the road ahead is a steep hill the PEMFC will be more effective if it slowly charges the LTO stack to the maximum before the hill so it will not need to work as hard that fast. But since this system is not implemented, further work will have to be done to make sure that this is possible.

3.4.1 Parameters

An comparison of the specific power and energy between different energy storage units is seen in table (3.1). The specific power and impedance mach is measured different for the LTO and NMC option. The rest of the capacitors is calculated according to IEC 62391-2:2006, which is also seen in (3.2).

Table 3.1: Specifications of common capacitors and LiB.

* Not calculated according to the IEC standard

| Component | Weight [g] | Energy Density [Wh/kg] | Usable power [kW/kg] | Impedance mach [kW/kg] |
|------------------|---------------|---------------------------|-------------------------|---------------------------|
| 40F [87] | 7.1 | 7.5 | 3.7 | 7.7 |
| 100F [87] | 15.9 | 8.4 | 3.2 | 6.4 |
| 270F [87] | 30.8 | 11.8 | 2.1 | 4.55 |
| Maxwell BCAP[87] | 160 | 4.4 - 6 | 5.9 - 6.9 | 12 - 14 |
| BCAP3400 [75] | 496 | 8.6 | 14.5 | 30 |
| LTO Battery[87] | 128 | 64 | 3.6 * | 3.6* |
| LMO [95] | - | 121 | 2.3 | 2.3 * |
| NMC111 [95] | - | 143 | 2 | 2 * |
| LFP [95] | - | 116 | 1.3 | 1.3 * |
| NMC + LMO/G | 556 | 173 | 0.86 | 0.86* |

As seen in article [84] the usable power and internal resistance can be calculated in several ways. It is seen that the different methods will result with large differences of internal resistance.

Since the cells with unknown cell mass from BatPac uses an unknown calculation method, these values might be needed to be taken as an approximate value. The LTO and NMC+LMO/G cell will use the same method, which is with their known C rate max, NMC+LMO/G has a max C rate of 5C and by dividing them cell mass the result will be the specific power.

By comparing the conventional calculation with the IEC 62391-2:2006 equation (3.2) back to the ESR it is noted that the difference is only 4% compared to the total average ESR as given from the NMC+LMO/G specifications. This is why the ESR is calculated the same as from the LTO given specific power and energy parameters. The drawback with this is that an R-2RC ladder cannot be modelled, more data is needed for this.

When using higher voltage stacks the alternatives becomes less, so if 2 LTO stacks is almost enough it usually better to add another type of cell or capacitor to compensate for it, so another 20kg cell is not needed to be added. But this might

result in extra cost and manufacturing depending on scale. A comparison for each type stacked up to 400V can be seen in table (3.2). Since the max power of the vehicle is 130kW already now LTO and the NMC option seems promising.

Table 3.2: One stack of units specifications to reach 400V

| Component | Weight kg | Energy Density [kWh] | Usable power [kW] | V_{max} | st |
|--------------|--------------|-------------------------|----------------------|-----------|-----|
| Maxwell BCAP | 21.4 | 0.128 | 150 | 3 | 134 |
| BCAP3400 | 66.464 | 0.554 | 934 | 3 | 134 |
| LTO Battery | 20.5 | 1.3 | 73.4 | 2.5 | 160 |
| NMC + LMO/G | 54.48 | 10 | 54.48 | 4.15 | 96 |

3.5 LiB - Modelling

The Open Circuit Voltage (OCV) is represented by a variable ideal voltage source. It is mapped with a look-up table as a function of SOC. The dynamics of the battery is represented with an R+2RC circuit. This is done to approximate the dynamics of the cells, such as mass transport, diffusion time delay and the internal resistance.

The relaxation dynamics of the voltage response will not be taken into account in order to keep the simulation simple. As also seen in Skoogs article [89], the R+2RC is relatively close to the measured voltage, with other words a small error is achieved.

3.5.1 Parameters

Since many parameters is missing from each cell that is desired to be tested more such as the LFP cell limitations had to be made in this thesis. In figure 3.9 the variable R+2RC parameters are compared depending on their SOC, where the last two RC in the LMO case are summed together to be able to compare them. The difference between the time constants depending on chemistry changes a lot [89] which makes it interesting to see which applications they are most suited for. The NMC+LMO/G data is taken from Skoogs and Grunditz work [89] [28]. Where the LMO specifications is taken from the MATLAB library.

3. Methods

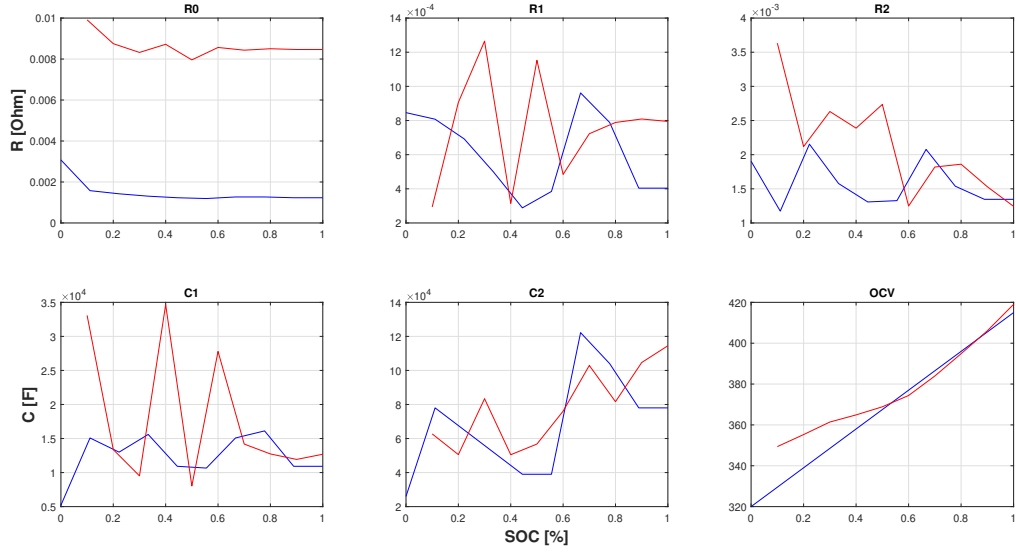


Figure 3.9: NMC+LMO (Blue) vs LMO (Red),

To be able to see what happens to the time constants during the change of SOC a bode diagram is used to illustrate. Figure 3.10 shows the NMC+LMO/G cell and figure 2.3 shows the LMO cell change of dynamics depending on SOC.

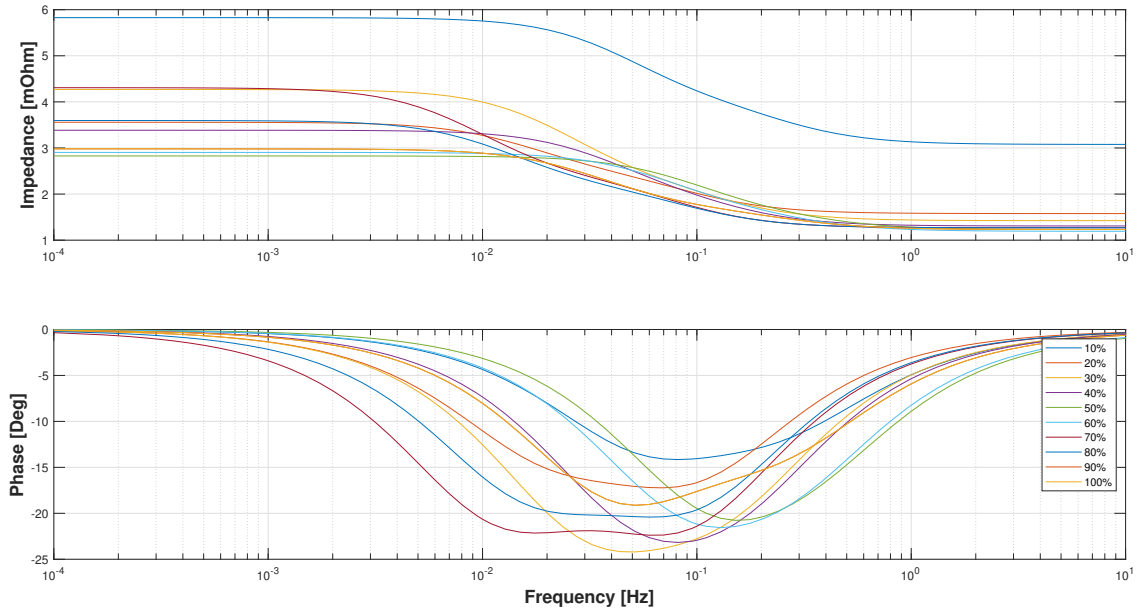


Figure 3.10: NMC R-2RC impedance model, SOC

Since both the DC-link and the LiB is modelled with a lumped impedance, there will be a hysteresis when charging and discharging of the cell voltage depending on the load. Due to not being able to make a control system to set the SOC at a requested state without generating extra losses in case C and B. It is decided to simplify the model and use the average of the SOC dependent parameters, which

also makes the model run much faster. Optimal operation point will be discussed later in this thesis, but it can already be seen that at 40% SOC has low impedance.

3.6 PEM - Modeling

Since internal parameters is hard to come by, MATLABs PEMFC with nominal 85kW was used.

To compliment the missing data from the simulink model parameters from Toyota Mirai is used to fill the gaps. Note that the Simulink model has guaranteed not the same dimensions as the Mirai cells, this might result with a large error in mass estimation. With other words the simulink model might not be able to reach a specific power of 2kW/kg with so much higher cell voltage.

What makes Mirai unique is that they make a thinner PEM layer which gives it a lower cell voltage rating but higher current capability and moisture distribution. This enables the internal humidification but, in this thesis, the external humidification will be assumed for simplicity. For mass calculation the "nominal" cell mass is used, see table (3.3)

Table 3.3: FC parameters of Simulink model and Toyota Mirai. Note that the mass is calculated from with the same $P_{specific}$ as Mirai

| Parameter | Simulink model | Toyota Mirai |
|---|-----------------------------|--------------|
| Stack power P_{nom}/P_{max} | 85/100kW | 88.5/114 kW |
| $Efficiency_{nom}$ | 57 % | |
| Stack Voltage (max) | 469V | 222V |
| Number off cells (series) | 400 | 370 |
| Output Density By Volume: | - | 3.1 kW/L |
| Output Density By Weight: | - | 2.0 kW/kg |
| Weight: cell/($m_{nom}/m_{specific}$) | 90.9*/ 106.2* | 102/119 |
| FC Resistance | 0.17572 ohm | |
| Highest voltage | 1.1729V | 0.6 V |
| Nom utilazation: | H2 95,24 % , O2 50,03 % | |
| Nominal Consumption | H2= 794,4 lpm, Air 1891 lpm | |
| Exchange current | 24,1mA (I0) | |
| Exchange coefficient | 1.1912 | |
| System temprature | 368 K (T) (94,85C) | 80C |
| Nom Air & Fuel pressure | 3 bar | 2.5 bar |

LUT are made of the modelled PEMFC to see its performance dependence on operating temperature. It is seen that it is supposed to be more effective at even higher temperature then it is made to operate around. Even if this might be true it is not possible since it's not made to be able to operate at any higher temperature. To simplify the model the operating temperature is always 85C°.

According to the model used the nominal operation temperature is needed to reach maximum power output, which is how it should be and is also shown in Figure 3.11. Note that the transitions between the colours is actually smooth.

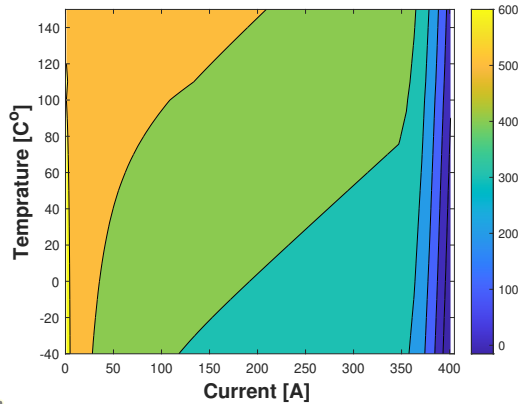


Figure 3.11: LUT of the modelled PEMFC voltage [V]

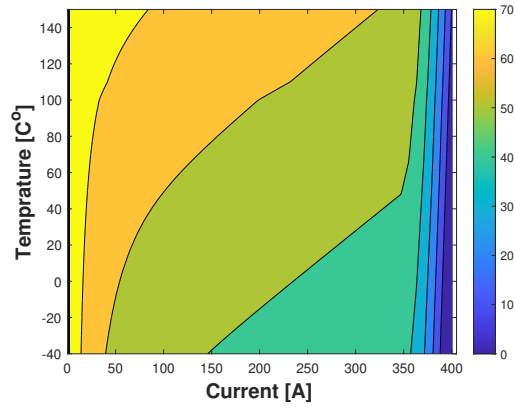


Figure 3.12: LUT of the modelled PEMFC Efficiency [%]

With an LUT of the hydrogen needed to supply a certain current depending on the temperature it could be used to calculate the exact flow that is needed to fulfil the electric demands fast. Of course this will change during its lifetime so at least an extra dimension is needed.

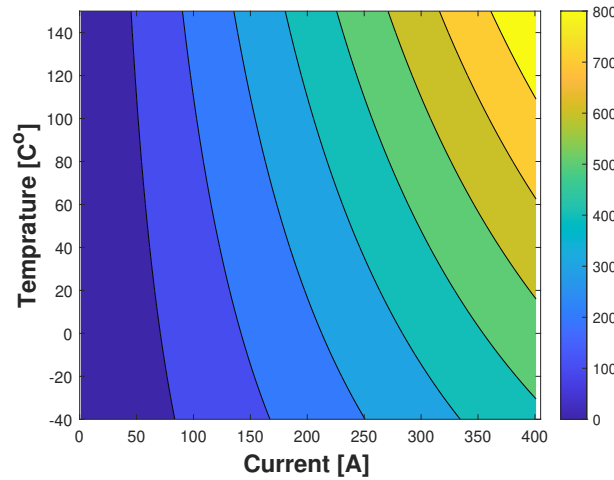


Figure 3.13: LUT of the modelled PEMFC hydrogen flow [l/min]

3.6.1 DC/DC - converter

For PEMFC packs with lower voltage than a LiB it is necessary to use a DCDC to be able to be compatible. When the voltage at the end of the PEMFC operating range of interest is higher than the LiB, a DC/DC is not needed. It is not entirely sure that it will not result in more losses when the voltage of the PEMFC is scaled to high but after discussion with Hillander it is an appropriate assumption[37].

With other words, that the internal voltage of the PEMFC is not stiff as a battery but can be chosen with the hydrogen flow to reach the desired internal voltage. The maximum efficiency was measured to be over 96.5 % [97] which is comparatively higher than conventional converters with the same voltage gain. As

also seen in Wai's article, the losses are not linear but the difference of the efficiency is small so the average efficiency is used in model for simplicity.

3.6.2 Controller

To ensure a longer life time expectancy a slow control is necessary according to Emanuelssons thesis [20], depending on operation cycles the lifetime of the call can change with a factor 10. An optimal solution would be to integrate a controller with the drivers planned route so the PEMFC can prepare the battery for the expected events for optimal performance and derogation.

If there was no LiB to support the PEMFC it would have been hard to control in it's activation area. The controllable areas can be calculated with equations (3.7) and (3.6) which are explained in Woo's article [104]. The relations are described as

$$P_{\max} = \frac{V_b^2 (R_L A_m)}{(\rho_m + R_L A_m)^2} \quad (3.6)$$

$$P_{\min} = \left(2F \frac{Q_{H_2, \min} P_{H_2}}{A_m R T} \right)^2 (R_L A_m) \quad (3.7)$$

R_i - Internal resistance of membrane-electrode assembly (ohm)

R_L - Load resistance (ohm)

R_s - Shunt resistance (ohm)

V_b - Battery voltage of fuel cell (V)

p_m - Membrane resistivity

A_m - Active area of membrane-electrode assembly (cm²)

F - Faraday's constant (96469 C/mol)

P_{H_2} - Partial pressure of hydrogen (bar)

P_w - Water vapor pressure bar

P - Power delivered to the load impedance (W)

Q_{H_2} - Hydrogen flow rate (mL/min)

R - Gas constant

3.6.3 Hydrogen - Fuel tank

Nominal pressures of hydrogen in FCV are around 700 bar [6] [42]. This is an sweet-spot of pressure where reasonable materials can be used without making it to costly, dangerous or heavy.

To calculate the mass of hydrogen stored in the tank (2.15) is used. To estimate the SOC of the tank the mass of the flow used is subtracted from the total mass of hydrogen in the tank, this works up until the pressure of the tank is around 3 bar which is around 0.5% of the total capacity.

3.6.3.1 Design

There are many safety factors and alternative materials that can be used, but to simplify it the same as [42] will be used since not within the scope of this thesis. More about safety and standard can be found in [78].

It is described in the Argonne Department of Energy article the relation of gravimetric capacity (wt%) depending on what material being used, number of tanks and the capacity. In an weight perspective it is beneficial with one tank but two is needed due to safety aspects.

To compare with TOYOTA Mirai which weigh 87,7 kg and contains 5kg of hydrogen. Since hydrogen contains 39.7 kWh/kg the energy density of the container 77,4kWh or 0.9kWh/kg and they are using two fuel tanks. [43].

This will result in a wt% of 5,7 which surpasses expectations from USAs energy government 2015. However, with the same principle as in the article, by using one tank the weight to capacity ratio is increased even further. Then again, this is not as safe as with two tanks nor legal in Sweden. One of the materials used to reach 12.50 wt% is MgC60 nano-lamellae for hydrogen storage applications, and can be read more about in Wangs article [101].

An expel to show how important the temperature of the tank is to be able to store more can be seen in Figure 3.14. This is with a tank with a capacity of 100l and 700 bar. It is seen in figure that the storage capabilities is slightly exponential which makes it extra important to store it cold, which can be a challenge with a FCV.

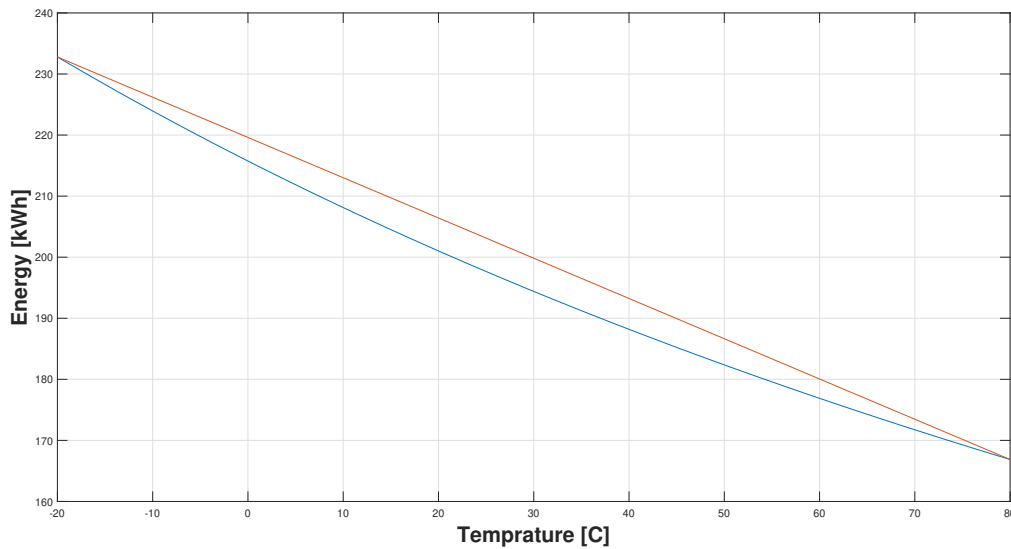


Figure 3.14: Energy storage depending on temperature, Blue line is the energy stored and Red line is visual linear reference

3.6.4 Air - Compressor

According to [104] the air flow is the hardest to control mainly due to its delay. As discussed previously by always having a higher flow of air then needed will saturate the need of O_2 .

If the air is filtered from carbon dioxide it could extend the lifetime even further [47]. This gives the reason to implement a Carbon Capture and Storage (CCS) system which would be interesting to investigate what potential effect it could have.

Both in aspects of captured carbon dioxide and the PEMFCs increased lifetime. This must be a passive solution since the active methods would use a lot of power.

3.6.5 Water

As the water flows in the channels it alters the effective area of the MEA, thus changing the internal resistance of the fuel cell [104]. This makes it important to have a clean exit for the water so the anode and cathode is not getting filled. The relation can be found as (3.8).

$$A_m = \frac{\rho_m}{(V_b/2F) RT/Q_{H_2} P_{H_2}^{\text{in}} - R_L} \quad (3.8)$$

3.6.6 Verification of dynamics

By sweeping the PEMFC load current linearly we can plot it's VI characteristics. The result can be seen in chapter 3.11 where the temperature is also swept. The efficiency and hydrogen flow required is also up to expectations.

An alternative is to always saturate the hydrogen flow to be able to handle the load directly. This leads to a low total efficiency since a lot of fuel is wasted according to the model. In practice the excess hydrogen is compressed back to the inlet and separated from any water that might have leaked through the membranes.

Unfortunately this loop is not integrated properly into the model. Except the power as an approximated constant power load of 500W combined with all other hydrogen accessories witch is described in Figure 3.28. With this constant power load it is meant to symbolise the constant saturation of the system. With an instant access of air and hydrogen, the dynamics of the system can be seen together with the LiB in figure 3.15.

The control of both the fuel gases after the step is not controlled ideal for neither from a losses and lifetime perspective. Figure 3.16 shows the total step response of the paired stacks, it is seen that the PEMFC could help the LiB more to keep the same voltage but the controller is missing.

This could be a further work on how to control it properly to be able to prepare the LiB for the step and ramp up of the current. The LiB voltage is the internal voltage on the terminal voltage.

The controller implemented slows down the model with a factor of 1000 and adds more losses even if a re-loop is implemented. Since a comparison still can be made between the cases it's decided to use the automatic control which has the least losses. A further investigation on the controller and re-loop has to be done.

3. Methods

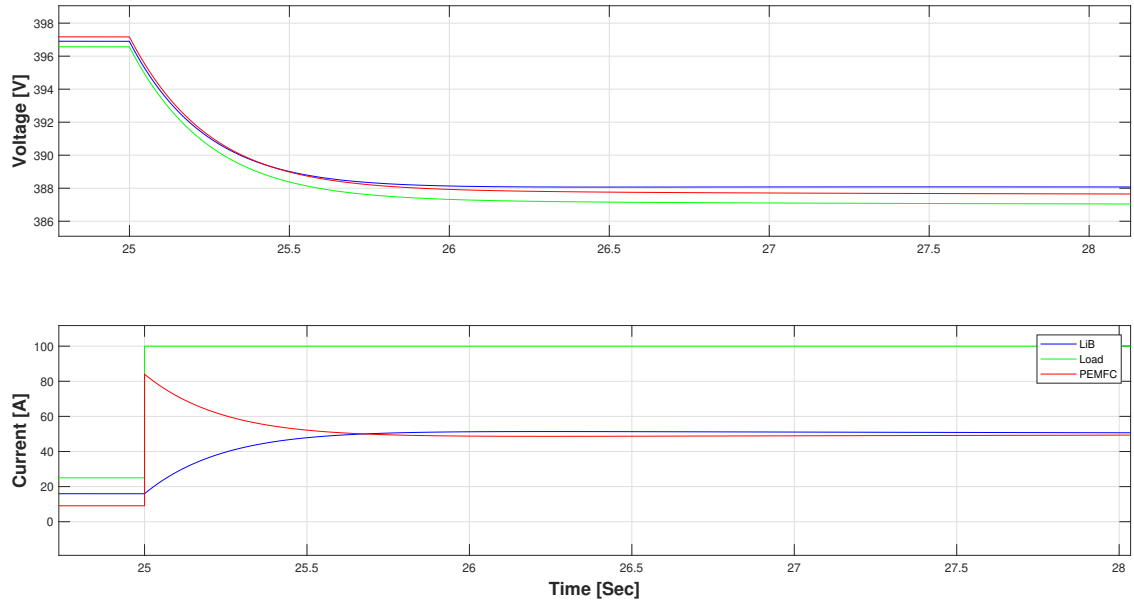


Figure 3.15: Dynamics of PEMFC stack within parallel

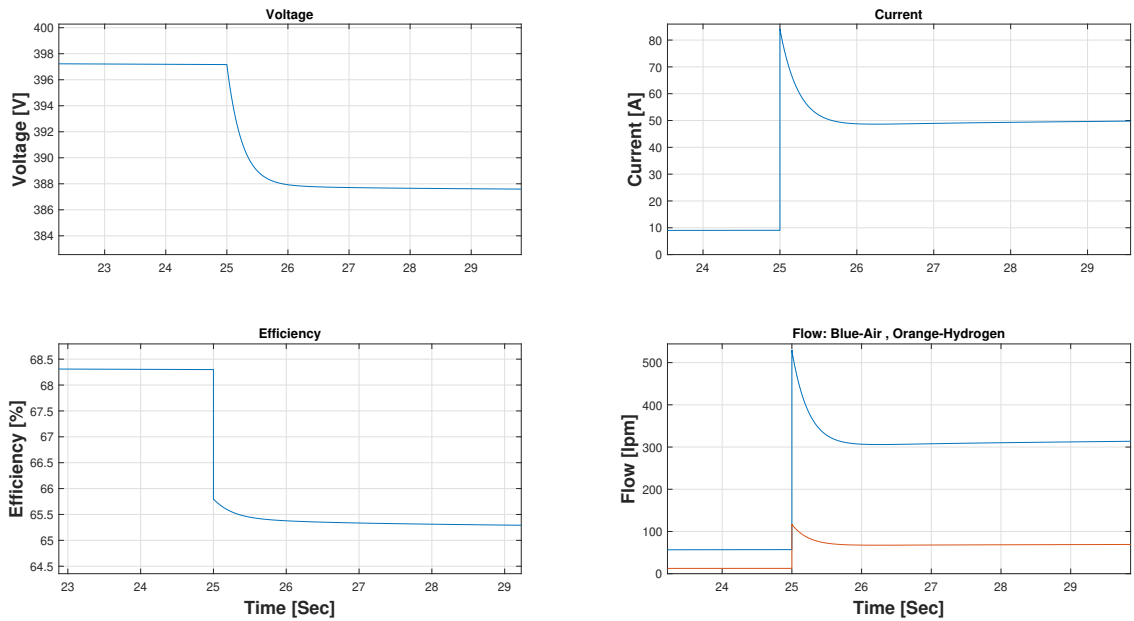


Figure 3.16: Dynamics of both PEMFC and stack in parallel with load voltage and current

According to [52] [9] [37] the dynamics of PEMFC retention effect is similar to LiB after current interruption. This is because the effective area of the catalyst decreases. This effect is neglected in this thesis due to simplicity.

3.7 Dynamics of systems

3.7.1 PEMFC and LiB

To be able to provide full power to the LiB the PEMFC needs to be able to hold high enough voltage. This is demonstrated in figure 3.17. Since it is optimal to hold the LiB around 10-20% SOC to extend its lifetime there is no need for a higher voltage then seen in figure since it can provide more then nominal power in that SOC area.

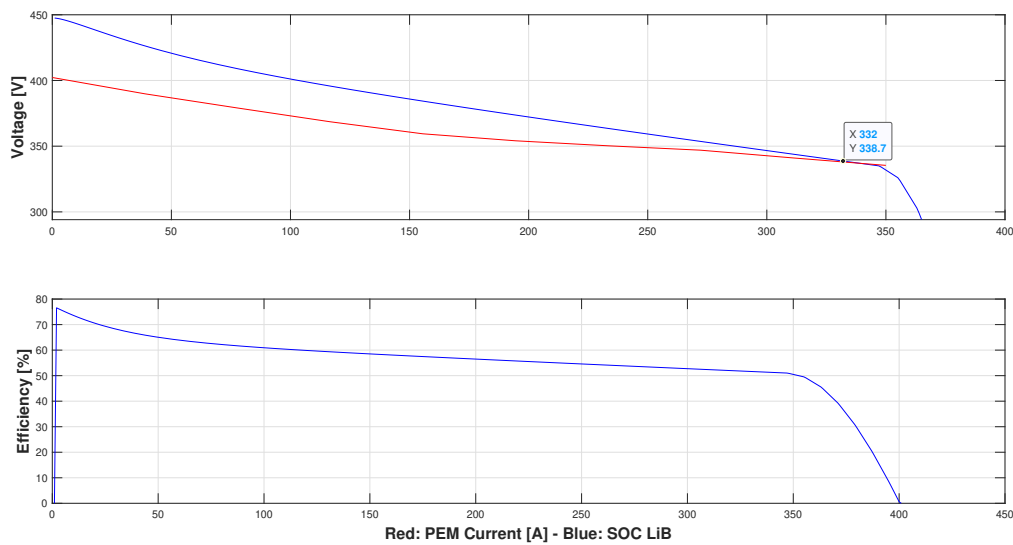


Figure 3.17: PEMFC VI characteristics at 90 $^{\circ}\text{C}$,

This also means that if the SOC of the LiB is high the PEMFC will not be able to provide for the full power, which means that another energy source needs to be able to provide for the fully rated power at this range, depending on design.

An unclear aspect of this is what efficiency the PEMFC will have when operating at a lower voltage then it would have at that certain load alone. As will be seen in the results the efficiency decreases with the voltage when the terminal voltage is lower than according to its V-I graph. In other words, the question is if there will be additional restive losses. After discussion with Hillander [37] an assumption with no additional losses is reasonable due to the ability to control fuel.

An alternative to this is to use a DCDC between the PEMFC and the LiB to make it possible to use a smaller PEMFC stack to supply a higher voltage LiB, which enables more design opportunities. This is also the way a few car manufacturer takes, for example Toyota. With the same stack power they find their new cells with lower voltage 20% more effective with an DC/DC compared to an solution as Figure 3.17 describes. This and more can be read in Hasegawas article [32].

Hasikos article shows how a step response is supposed to look in practice without a LiB as support nor saturated gas supply [33]. When implementing the controller that is supposed to control the compressor TF together with the FC it resembles

3. Methods

Hasikos tests except slower.

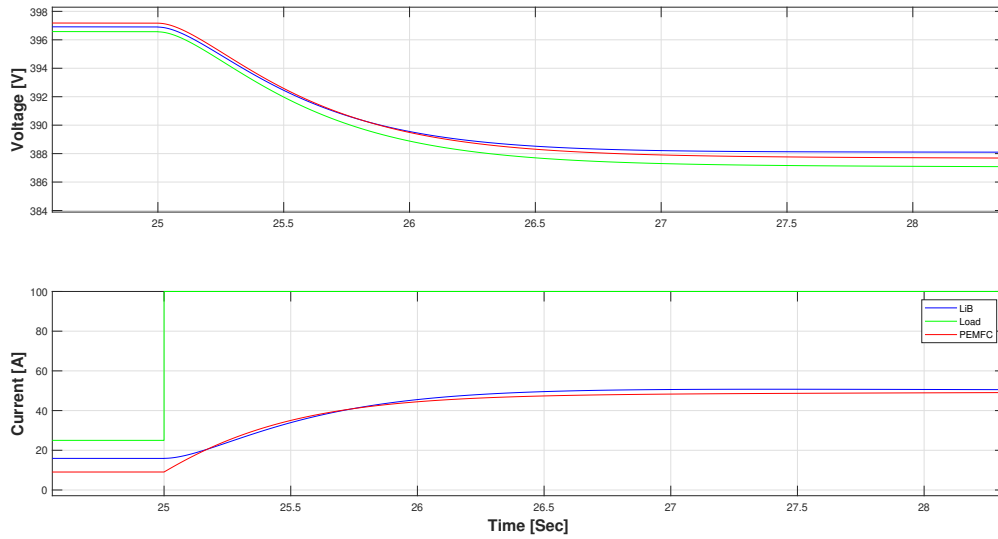


Figure 3.18: LiB and PEMFC cooperation during step with PID controlled compressor, PEMFC stack with LiB, 85kW

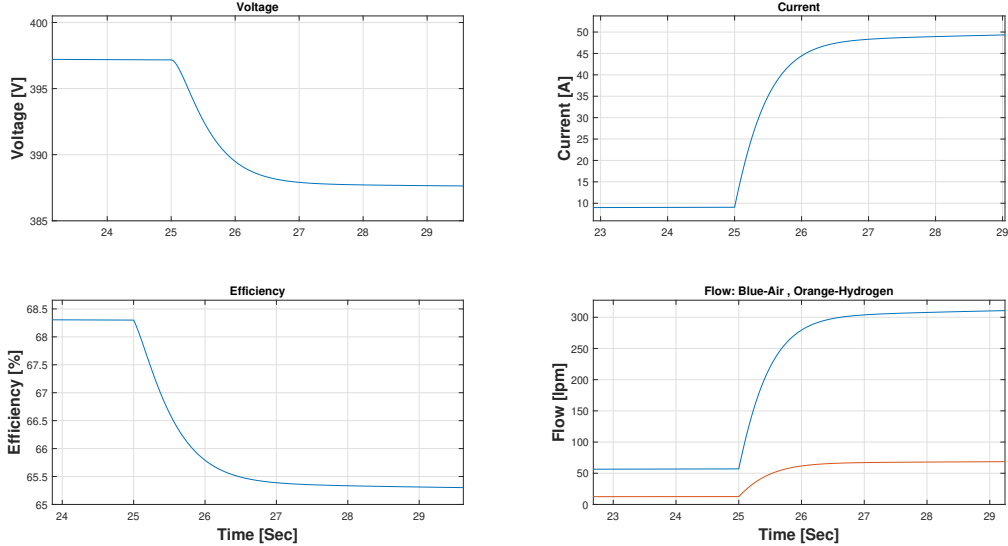


Figure 3.19: PEMFC parameters during LiB and PEMFC cooperation under step load with PID controlled compressor, PEMFC stack with LiB, 85kW

Since the start-up time of a LT-PEMFC from an ambient temperature of 20°C would be approximately 3 min depending on catalyst material. 5min from 0°C This means that the LiB used together with the PEMFC needs to be able to supply the power needed for the driver during this time if the FC is cold. In a worst case scenario it would need to power 130kW for 3 minutes that would amount to a 6.5kWh

battery which is 5 parallel LTO cells (106kg) at 3C or 138kg of NMC+LMO/G with 5C.

If LFP cells was used instead it could supply it for 6 min with a 100kg pack. Of course an NMC111 or LMO buffer would be more efficient electrically but the benefit of LFP in terms of environmental impact is lower which will later be discussed. More specifications about the LFP cell would be needed but it's potential especially with the solid-state version would be a a better match for case B and C. Due to its high operation temperature and decent energy to power ratio.

As seen in Figure 3.20 the PEMFC keeps the battery around 80% SOC but it needs to be regulated properly to allow the battery to make the load voltage steady. In this figure an over dimensioned battery is used to show how stable load voltage and PEMFC current can be achieved with a large energy bank.

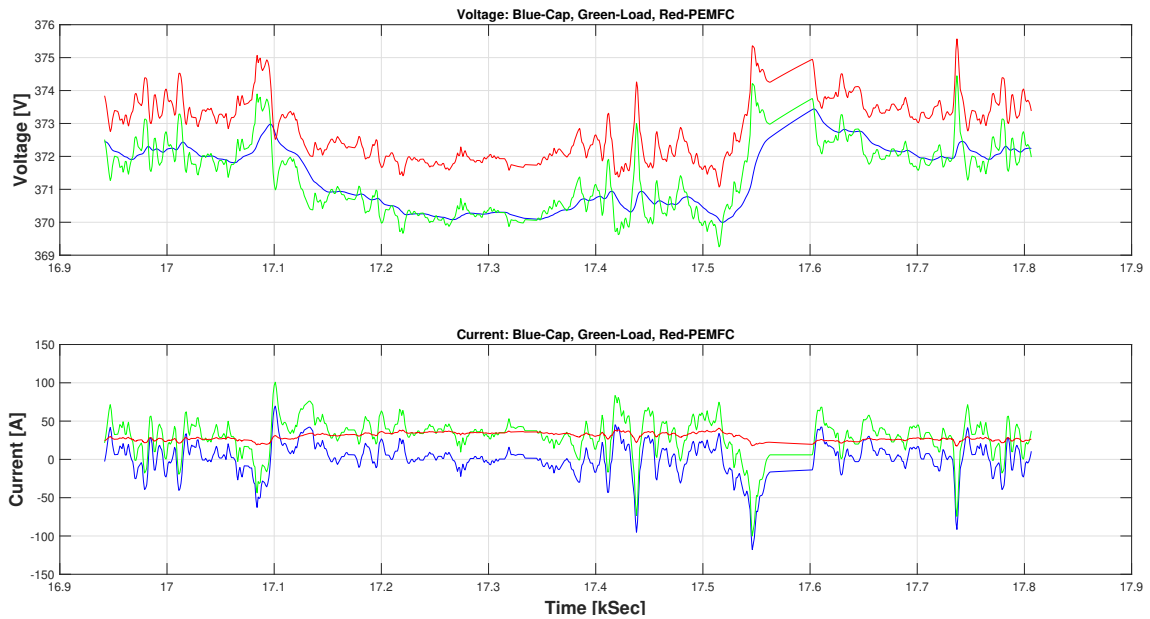


Figure 3.20: Self regulated saturated PEMFC stack verification, Nominal power 85kW

Seen in figure 3.21 that the higher voltage it is operating around the higher efficiency reached. The nominal efficiency at 85kW is 57% so by working in its activation region its efficiency is much higher than an under dimensioned cell. Note that it's unknown if the efficiency is dependent on the voltage or not in practice when coupled up with a LiB. For simplicity this is accepted for the time being.

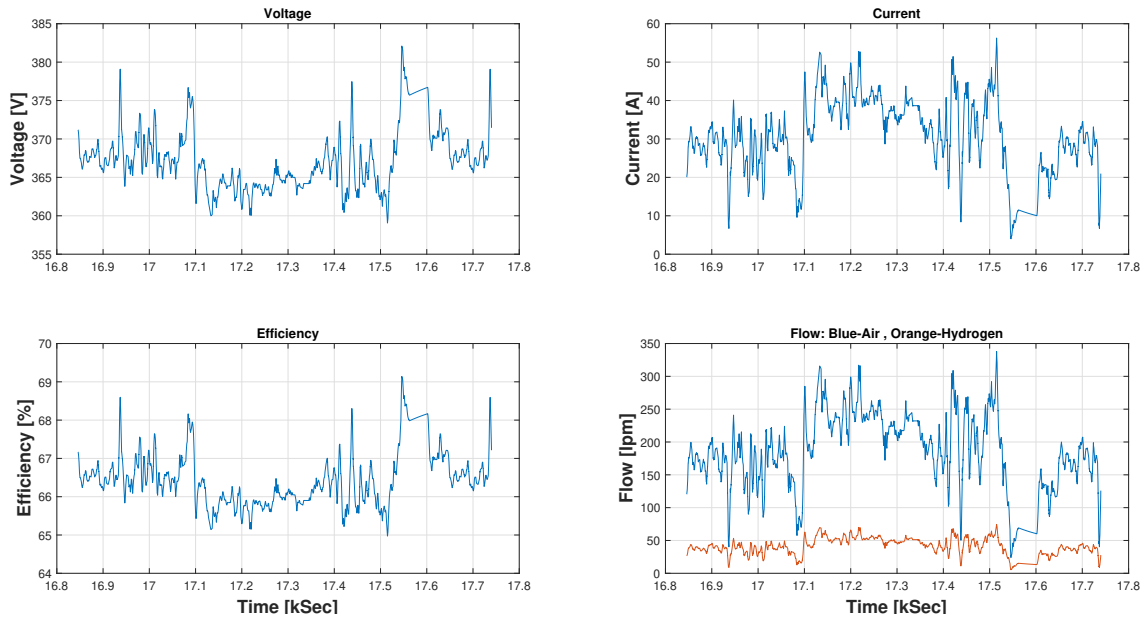


Figure 3.21: Verification of PEMFC stack dynamics during cycling for case C, Nominal power 85kW stack

The cycle in figure 3.20 shows that the PEM keeps delivering power even if the load is lower and recharges the LiB pack. If the control is properly calibrated it is possible to increase the current to charge the LTO instead of decreasing while the load decrease, then the effect at the moment 16.8kSec would be more common. Especially at 16.3kSec but since the current remains the same it does not recharge the LTO and has to react to next power spike faster. The load voltage difference is good at this SOC, it would be interesting to see how it looked like at lower SOC with an controlled PEMFC that would give a more stable support during the hole cycle.

3.7.2 LiB & PEMFC potential of life

As discussed in the theory section about Wikners results [103] it is potential to extend the battery lifetime by operating it differently. An benefit with PEMFC is that now it's possible to control exactly how to charge the LiB pack.

In case B in this study would require an additional control system to be able to operate the LiB at lower SOC range to still have power left for example an overtake on the highway and it is required to accelerate past an obstacle. This means that the control system would have to prepare for a similar event and break from the optimal operation.

With Wikners information it can also be concluded that in Case A its preferable to dimension the battery around 1C to increase its lifetime, to keep the range of the vehicle high.

In case B and C it's preferable to operate around 4C since the capacity is not as important since it's not the main energy storage and it's more important to keep the internal resistance low. Thereby the hysteresis, ripple and losses can be minimized. What makes this even better is that this is exactly what is preferred to also cut

costs and material usage, for both case B and C.

3.8 Cost

The main data that have been gathered is for LiB packs and are taken from the BatPac software and PEMFC costs from James work [42] [43]. BatPac is a commonly used software that includes many aspects in great detail to be able to approximate the total cost of the battery pack. For each case it resizes the cells to fill the request of the case.

Even if BatPac and James data has a relatively low error margin, a 25% error is assumed since the costs are not all from same date and the difference depending on geographical location and when the data is taken. The date of the data matters a lot because this is a fast-growing industry where everything changes fast, everything from specifications of the cells to manufacturing costs.

3.8.1 DC-Link

There are many types of capacitors and their cost varies a lot depending on layout. According to [49] super capacitors costs around 32.8 \$ per kg or 10k % per kWh. In the same article it's shown how similar the reduction of losses depends on the cost with the different options.

The main change seen is the mass difference comparing the 3 options Electrolytic, Supercapacitor, and battery. Where a battery adds around 20% more mass for the same losses. The capacitors can reach even higher reduction of losses compared to a larger battery. Since the results are so similar between the super cap and electrolyte options the cost of the super cap is used for both cases.

A case with no lithium and using a larger DC-link instead of the LTO cells would have been interesting to investigate. Since the controller does not work for the PEMFC, the cycling will be to unstable with a lower capacity of the secondary energy storage.

3.8.2 LiB

Bat Pac is used to estimate the cost of the LiB pack. 7 different types of cars cases are used with the same cell chemistry are generated. From these cases an approximation of what cases in between would cost with approximated function, seen in figure 3.22.

Note that the cost is with an NMC 50-50% LMO cell instead of a 70% NMC and 30% LMO type, of which the latter one is used in the electrical model. This is assumed to be similar due to insufficient data. An 100kWh battery will approximately cost 100k\$ and weigh 535kg.

3. Methods

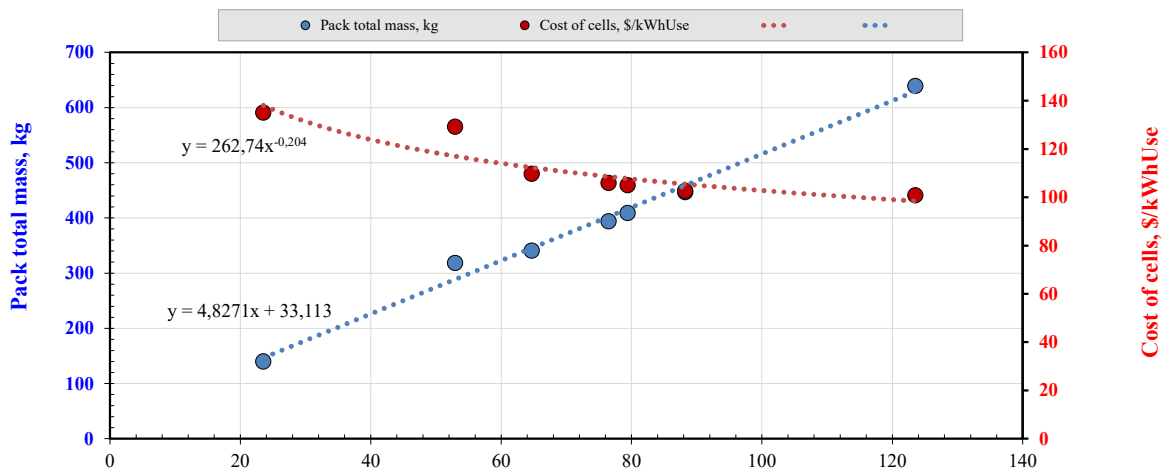


Figure 3.22: Cost of NMC/LMO+G cell depending on battery pack dimensions, BatPac

Battery 7 is the last battery pack data point to the right in Figure 3.22 which has the most similar performance as the battery used in case A. In figure 3.23 the detailed total cost breakdown is presented to illustrate how the budget layout is distributed. As can be seen the product is not very labour heavy, the main costs is it's material and purchased products.

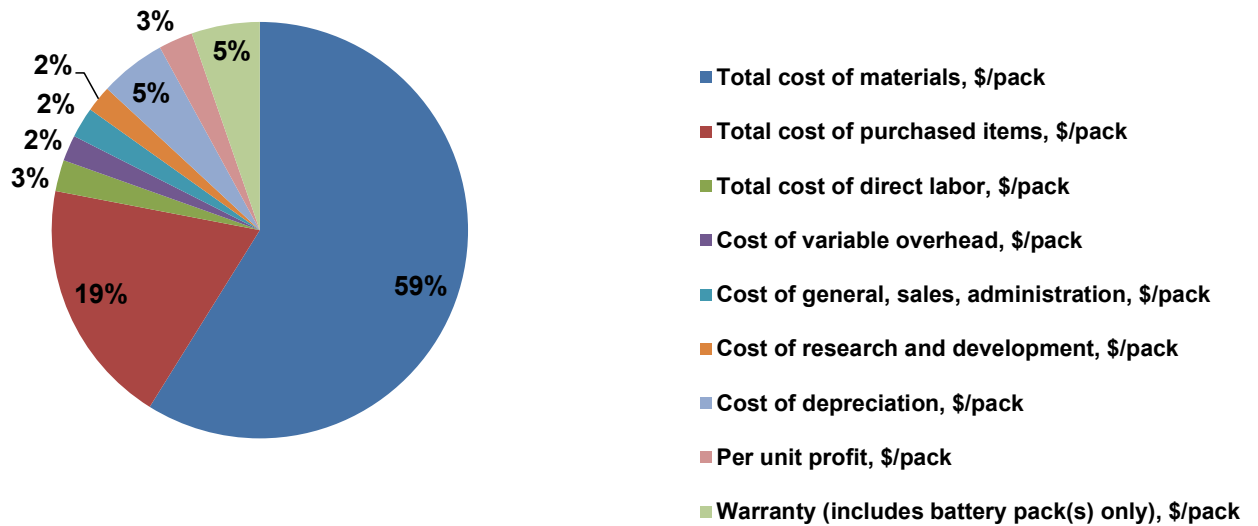


Figure 3.23: Total cost of NMC/LMO+G cell breakdown of different processes and material

A breakdown of the material costs can be seen in Figure 3.24, the main cost of the material is the lithium which is categorised under positive active material.

This is due to the increasing demand and lack of resources. This is one of the reasons why recycling of lithium has to improve to be able to reach both the lower middle class and in this way avoiding high environmental impact.

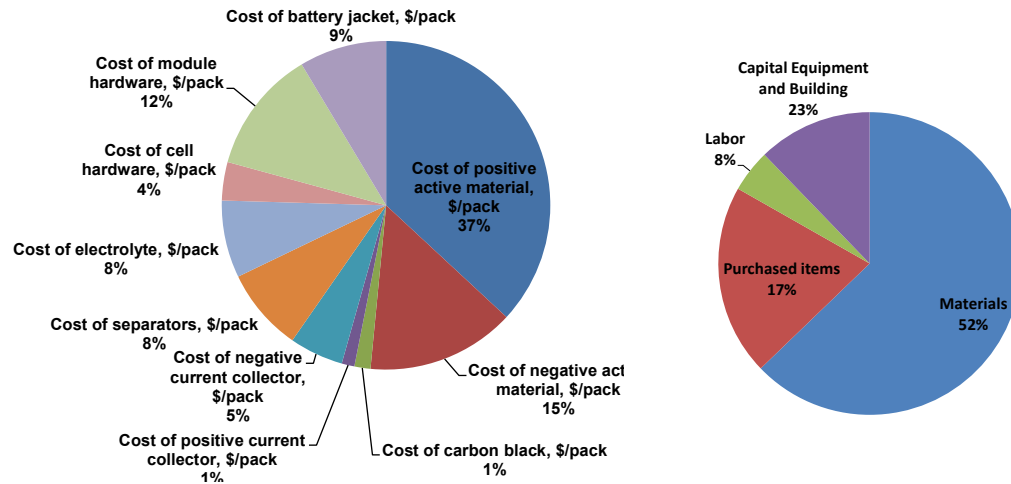


Figure 3.24: Pack cost of NMC/LMO+G cell breakdown of different parts. Grouped total breakdown of cost to the right

According to BatPac the cheapest cells are NCA for larger energy storage systems in vehicles. This is because of its high specific capacity. A more environmentally friendly cell, LFP which has a much lower energy capacity costs only 10% more than the NMC/LMO+G cell, see figure 3.25.

For both battery packs ethylene glycol water (EG-W) is used as coolant in the packs cooling system. The manufactured units is 100k per year.

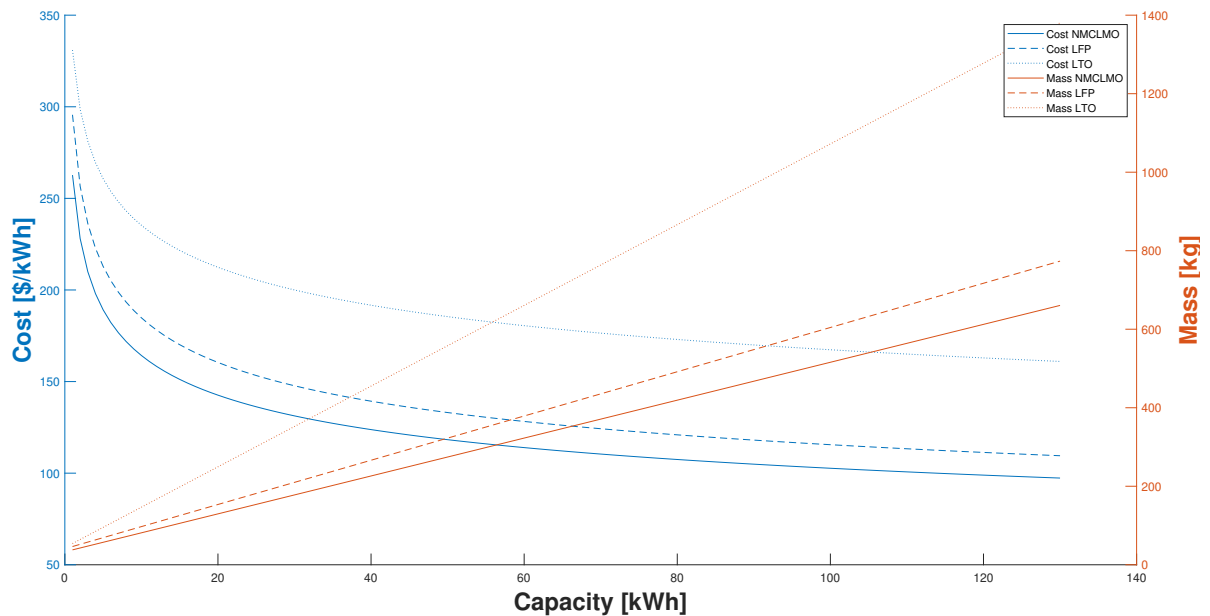


Figure 3.25: Cost comparison of LiB pack depending on capacity, data is from BatPac

The cost of the battery pack depending on power will show that LTO cells are the most effective choice, see figure 3.26. For the same max power performance LFP has approximately 3 times higher mass compared to LMO-LTO battery pack.

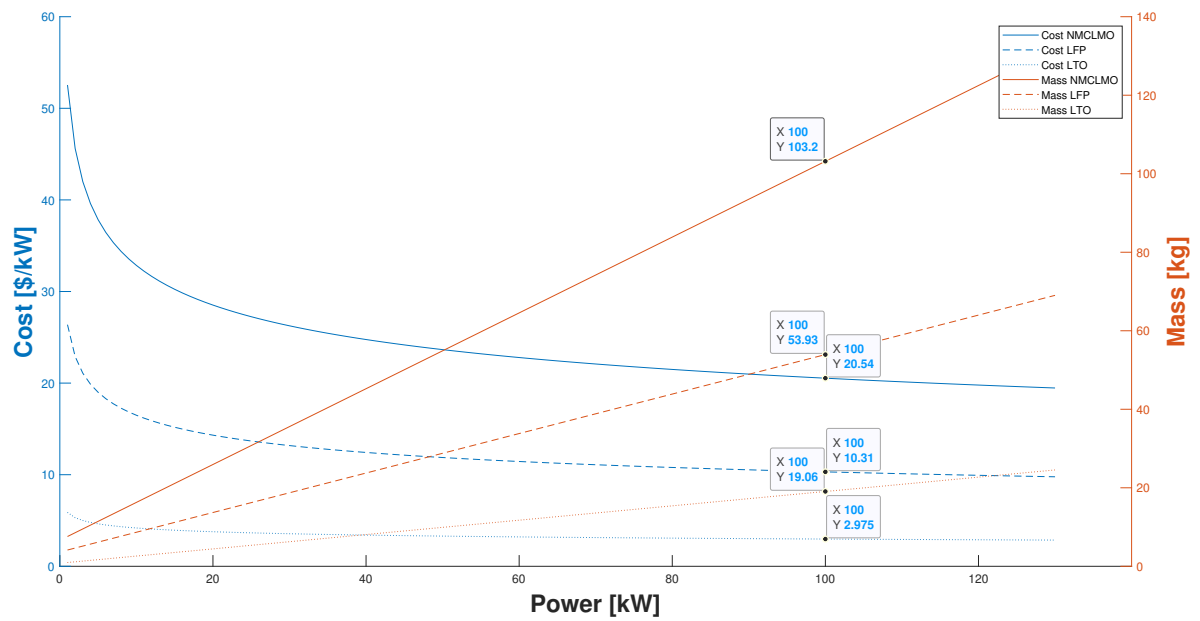


Figure 3.26: Cost comparison of LiB pack depending on power, data is from BatPac

3.8.3 PEMFC

The cost of fuel cells has changed drastically lately, with new solutions that uses non rare materials will be able to trim down the costs hopefully even further. According to Energiforsk article [69](p 28) a high power PEMFC in combination with a lower power battery is the most cost effective choice. With other words a 100kW PEMFC with 30kW battery.

This results in that either the driver would have to drive slow in the beginning while the PEMFC is heating up or wait before being able to drive. In the same article they approximate a cost of 4.4k\$ for an stack system with a capacity of 100kW which can be seen in figure 3.27. A more accurate number will be calculated with the help of James work [42] and later compared.

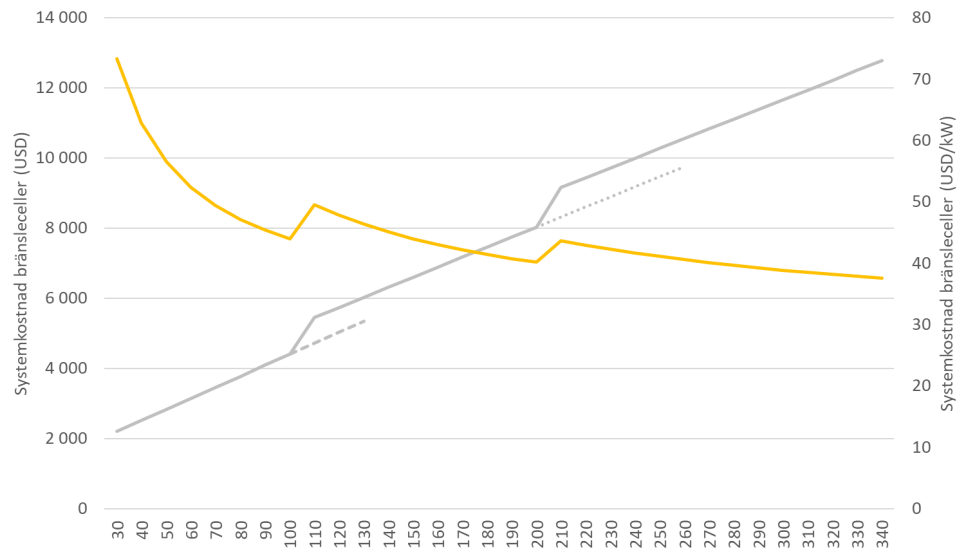


Figure 3.27: Cost function of PEMFC depending on nominal kW capabilities, from [69] ©

The cost breakdown of PEMFC stack can be seen in table (3.4). A 100kW nominal power will result in an cost of 2k\$ with the same production rate as for the LiB pack of 100k units annually in year 2020. One of the most expensive part with a PEMFC is the catalyst which is usually made out of platinum.

HT-PEMFC have started to use an iron based catalysts [72] which is more sustainable in all 3 aspects. But similar solutions have not been done for automotive grade cells so far.

Table 3.4: Detailed prediction of stack cost for the 2020 auto technology system with 100k systems manufactured annually [42]

| Part | Unit | Cost |
|---------------------------------|--------------------------|-------|
| Net power | kW _{net} | 80 |
| Gross power | kW _{gross} | 87,9 |
| Bipolar plates (stamped) | \$ / stack | 387 |
| Membranes | \$ / stack | 188 |
| d-PtNi cataly | \$ / stack | 617 |
| CCM Acid wash | \$ / stack | 14 |
| GDLs | \$ / stack | 149 |
| M& E hot pressing | \$ / stack | 8 |
| M& E cutting & slitting | \$ / stack | 5 |
| MEA Sub-Gaskets | \$ / stack | 91 |
| Coolant Gaskets (Laser Welding) | \$ / stack | 41 |
| End Gaskets (Screen Printing) | \$ / stack | 1 |
| End Plates | \$ / stack | 37 |
| Current Collectors | \$ / stack | 5 |
| Compression Bands | \$ / stack | 6 |
| Stack Housing | \$ / stack | 6 |
| Stack Assembly | \$ / stack | 39 |
| Stack Conditioning | \$ / stack | 28 |
| Total Stack Cost | \$ / stack | 1,643 |
| Total Stacks Cost (Net) | \$ / kW _{net} | 20.53 |
| Total Stacks Cost (Gross) | \$ / kW _{gross} | 18.69 |

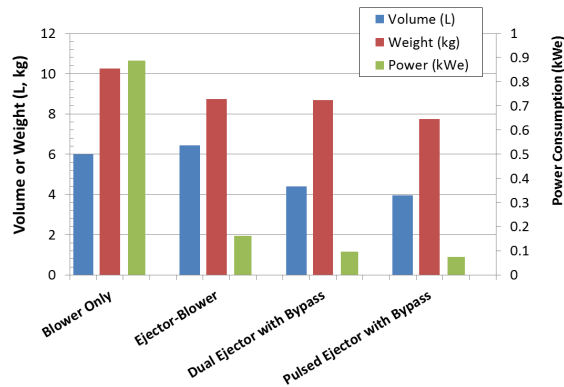
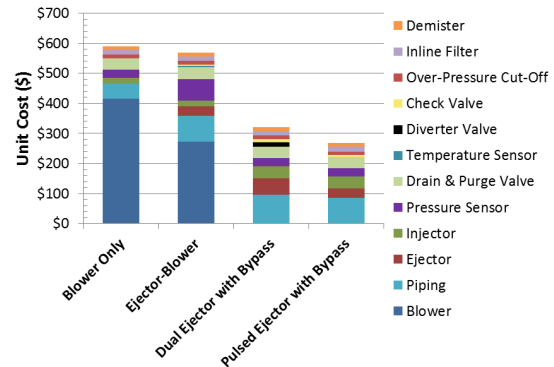
The total cost of the BOP system will amount to 2.56k for 100kW according to table(3.5). Which sums the cost up to approximately the same as Energifors results. The FCV cars manufactured today is not yet close to these production rates. The predicted costs for Toyota Mirai stacks is 120 dollar per kW_{net} with a production of 3000 annually, where the BOP system costs approximately 61.65 dollar per kW_{net} .

This amounts to 18k \$ per hydrogen system which really explains why it is important to scale up production to be able to reach the broad public. By using a passive PEMFC, a much simpler air loop could be used which is one of the main costs of the Balance of Plant (BOP), so far this is not possible.

Table 3.5: Detailed balance of plant cost for the 2020 auto technology system 100k systems productions annually [42], with a +/- 10 % cost certainty

| Part | Unit | Cost |
|----------------------------------|--------------|-------|
| Air Loop | \$ / system | 932 |
| Humidifier & Water Recovery Loop | \$ / system | 167 |
| High-Temperature Coolant Loop | \$ / system | 351 |
| Low-Temperature Coolant Loop | \$ / system | 68 |
| Fuel Loop | \$ / system | 279 |
| System Controller | \$ / system | 97 |
| Sensors | \$ / system | 28 |
| Miscellaneous | \$ / system | 125 |
| Total BOP Cost | \$ / system | 2,048 |
| Total BOP Cost (Net) | \$ / kWnet | 25.6 |
| Total BOP Cost (Gross) | \$ / kWgross | 23.3 |

James also approximates the mass and the additional power consumption from the equipment of the fuel system which is 1,2kW, see figure 3.28, this will be used in the model of this thesis. The total additional mass without the tank is 35kg, tank 95kg with a capability of 5kg hydrogen [43].

**Figure 3.28:** Volume, weight, and parasitic load of each of the four H2 re circulation systems modelled by SA [43]**Figure 3.29:** Cost breakdown for 500k units sold annually [42]

3.8.4 Cost - fuel

The fuel of cost depending on location can change a lot depending on infrastructure, demand and access. From Energiforsks results, a higher cost with FC dominated FCV when driving longer ranges because of the higher cost of hydrogen compared to the electric costs.

This is a hard approximation because one of the main features of hydrogen is that it can be used as an energy buffer from excess green energy which might not be valued the same as the common grid electricity.

3.9 Material usage - Manufacturing footprint

3.9.1 DC-Link

Generally capacitors makes the least footprint due to commonly materials is used especially for electrolyte capacitors. Even lithium capacitors have started to appear (LIC). The degradation function of each differ between the cases but here only doubled layered ultracapacitors will be discussed. Maxwells highest specific energy capacity ultracapacitors lifetime can be seen in figure 3.30. LiB's EOL is around 80% of capacity rating has been reached. Their lifetime is surprisingly low but this will change depending on circumstances. For example how close their operating cycle is to their max ratings.

The same goes for the increase of the ESR. Here it's seen that the rated ESR are not the actual until 2/3 of its lifetime, Figure 3.31. Since even more energy is needed then this, and LTO cells have such a high specific power, these capacitors will not be used. But in a case where LFP cells are used instead, these ultracapacitors would be interesting to investigate again.

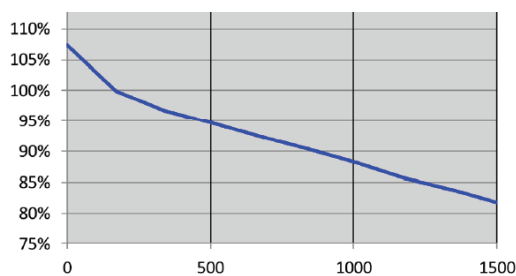


Figure 3.30: Accelerated ageing capacity performance, $V=3$ at $65C^{\circ}$, Average capacity (%)

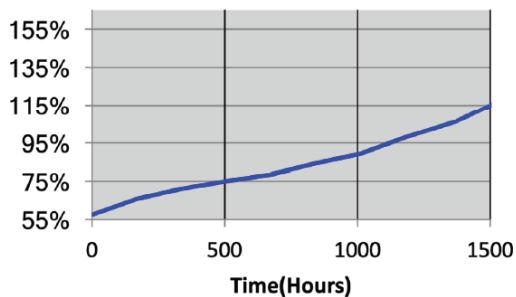


Figure 3.31: Accelerated ageing ESR performance, $V=3$ at $65C^{\circ}$, Average capacity (%)

3.9.2 LiB

By using cells with more common materials that can be recycled and with sustainable manufacturing methods that does not make an excessive environmental impact is an important step towards a sustainable future.

Even the NMC+LMO/G cell which is used to derive the price of the pack the NMC532 in a 50-50% ratio with LMO. The cell from the electric investigation will be used here, which was a 70-30% mix, see figure 3.32.

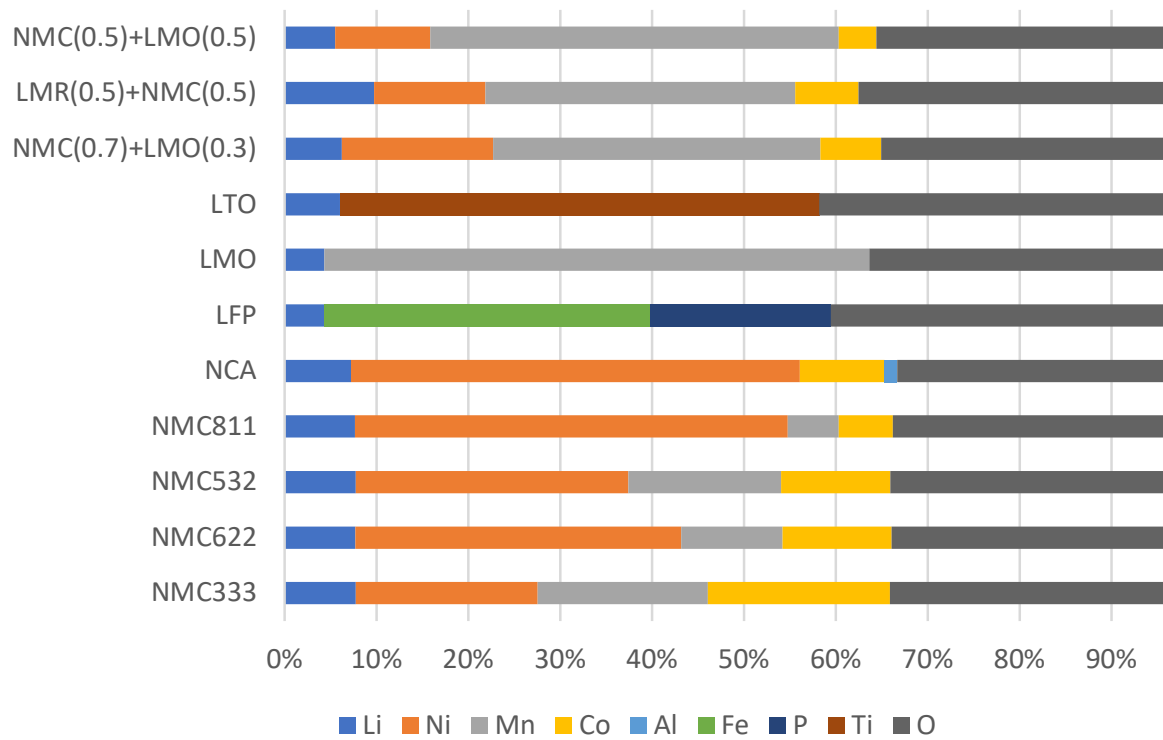


Figure 3.32: Ratio of material used in chemistry depending on total mass [%]

The more energy dense cells shown in 3.32 is using more lithium compared to the rest. More investigation is needed to see how much can be recycled from each case but here only an example of NMC+LMO/G from BatPac will be shown. Approximately 6kg cells is needed to reach 1kWh capacity, according to GREET around 1.6% of the battery pack is $LiPF_6$. This results with almost the same amount as the total amount recycled seen in table (3.6).

Table 3.6: Recoverable Metals from 50-50% NMC+LMO/G per kWh. Data from BatPac

| Material | Amount recycled [kg/kWh] |
|---------------------------------------|--------------------------|
| Lithium in Electrodes and Electrolyte | 0,08 |
| Cobalt in positive electrode | 0,12 |
| Nickel in positive electrode | 0,29 |
| Manganese in positive electrode | 0,75 |
| Aluminium content | 0,91 |
| Copper content | 0,47 |
| Steel, compression plates and straps | 0,020 |

GREET is used to analyse energy and emission pollution and usage depending on what materials, manufacturing methods used. To normalise the results the average of the ratio between the specific energy capacity and energy used during the manufacturing per ton material, see Figure 3.33.

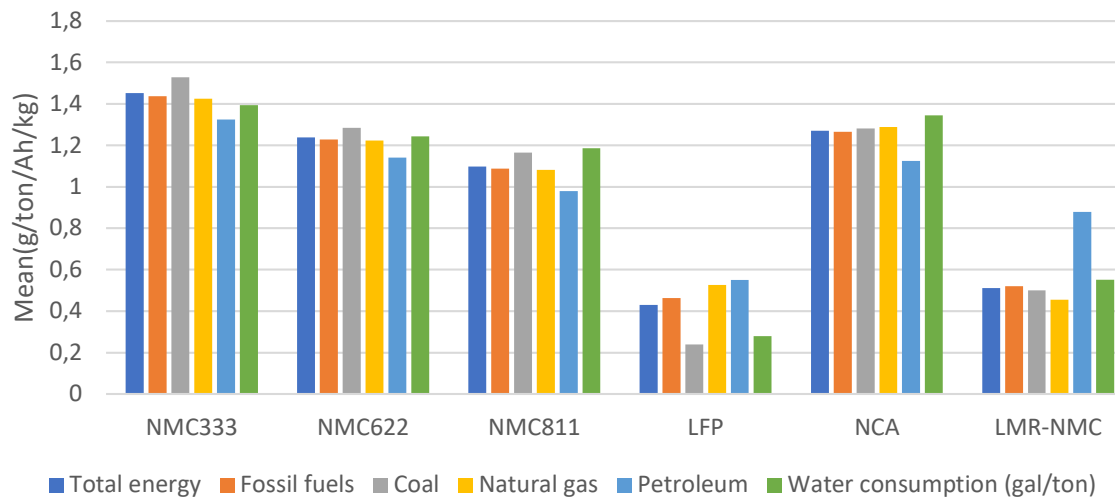


Figure 3.33: Normalised energy usage for cathodes, with other words the average of the ratio between the specific energy capacity and energy used per ton of material, data from GREET

Same normalisation as before but instead the individual emissions related to each cathode type can be seen in figure 3.34. Without the need of comparing each cell it's seen that LFP are by far the most sustainable type in aspects of energy capacity and environmental impact.

GREET software does not have an approximation on emission and energy consumption during processing of titanium LTO cells are not included in this thesis. Unfortunately there is neither enough data found about NMC+LMO/G and LMO cells which is why they are not in this comparison. Figure 3.32 shows that it uses less lithium and rare metals compared to the more energy dense materials. More LFP LCA analysis can be found in [41].

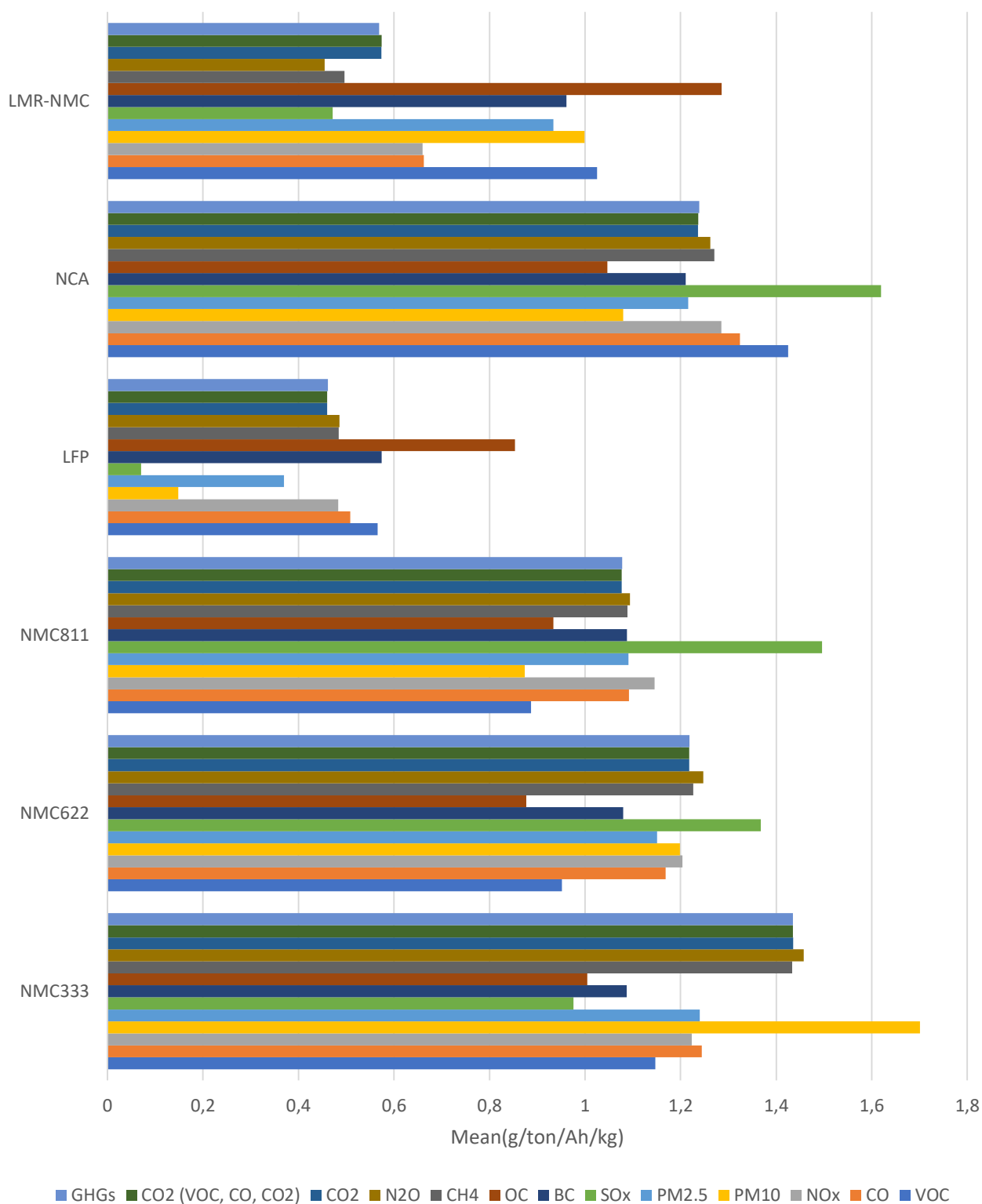


Figure 3.34: Normalised emissions released, with other words the average of the ratio between the specific energy capacity and energy (mmBtu) used per ton of material.

GHGs is the total gases and CO₂(VOC, CO, CO₂) the total is the total data from GREET

3.9.3 Material used for PEMFC system

Stropnik have composed a list of materials used for each kW of [91] a 100kW PEMFC stack that represents 170kWh of hydrogen which translates to a slightly lower capacity then compared to case B and C in this thesis.

Table 3.7: Materials used for each kW of PEMFC, including BOP system. Data from [91]

| | Material | Unit | Value |
|--------|---------------------|------|---------|
| Stack | Graphite | kg | 4.5 |
| | PVdC | kg | 1.1 |
| | Aluminum | kg | 0.3 |
| | Chromium steel | kg | 0.1 |
| | Glass fibers | kg | 0.1 |
| | PFSA (Nafion®) | kg | 0.07 |
| | Carbon black | kg | 0.0008 |
| | Platinum | kg | 0.00075 |
| BoP | Steel product | kg | 3.7 |
| | HDPE | kg | 1.5 |
| | Chromium steel | kg | 1.1 |
| | Cast iron component | kg | 0.8 |
| | Aluminum | kg | 0.75 |
| | PP granulate | kg | 0.25 |
| System | Electricity | kWh | 16.9 |

Analysis show that only 0.75 g of platinum in the manufacturing phase contributes, on average, 60% of the total environmental impacts of the manufacturing phase [91].

An HT-PEMFC on the other hand can without noble material reach a power density of 1/4 of the LT-PEMFC used in this research. Even if the added mass makes it a viable solution it operates of around 200C° which makes the thermal management even harder than the LT-PEMFC which already is tricky since the only thing that needs to be hot is the stack and the rest is sensitive to that amount of heat.

3.9.4 Environmental impact - Cases

This is the data that will later be used to compare in the result section. Note that an EV has a 30% less lifetime compared to FCV according to GREET so the total emission and energy used will

Table 3.8: Case comparison of emission and energy used

| Btu or grams per mile | Case A | Case B | Case C |
|-----------------------|---------|----------|----------|
| Lifetime VMT | 121206 | 173151 | 173151 |
| Total energy | 1107 | 844 | 876 |
| Fossil fuels | 962 | 766 | 793 |
| Coal | 307 | 226 | 229 |
| Natural gas | 547 | 459 | 479 |
| Petroleum | 106 | 81 | 86 |
| Water consumption | 0,147 | 0,0585 | 0,0642 |
| CO2 | 69 | 54 | 56 |
| CO2 (VOC, CO, CO2) | 71 | 55 | 56 |
| CH4 | 0,176 | 0,141 | 0,1455 |
| N2O | 0,00154 | 0,00127 | 0,00132 |
| GHGs | 77 | 59 | 61 |
| VOC: Total | 0,276 | 0,195 | 0,194 |
| CO: Total | 0,18 | 0,14 | 0,138 |
| NOx: Total | 0,0884 | 0,0613 | 0,0633 |
| PM10: Total | 0,0366 | 0,0189 | 0,0193 |
| PM2.5: Total | 0,0156 | 0,00873 | 0,00897 |
| SOx: Total | 0,551 | 0,224 | 0,228 |
| BC: Total | 0,001 | 0,000469 | 0,000487 |
| OC: Total | 0,00161 | 0,000869 | 0,000902 |

4

Results

In this section the description of each case design will be presented and their results will then be discussed. The environmental aspect will be normalised in order to be able to compare them in all three aspects of a sustainable design.

4.1 System verification

In this section the three model cases will be examined and compared. They will all travel the The Highway Fuel Economy Driving Schedule (HWFET) represents highway driving conditions under 100 km/h for 16.5km repeatably. The load will repeat until the equivalent distance of 630km is reached which approximately takes 8h and 30min.

4.1.1 EV - Case A

Case A energy reservoir is only the 94kWh battery pack excluding the small DC-link filter at the AC/DC inverter. This is because such a large battery pack results in a low internal impedance which translates to a battery efficiency of 99% and a total propulsion efficiency of 86%. After 630km the SOC is 9% with a new battery which is compared in figure 4.8.

Since the battery voltage will decrease during the complete discharge of the battery and the load power will remain the same higher current is needed to full fill the driver's requests. This will also result in an increase of losses at the lower SOC levels since higher currents is needed.

If no extra DC/DC is used between the battery and the DC/AC inverter the motor will not have high enough voltage to be able to provide the nominal 130kW at the higher SOC range.

4. Results

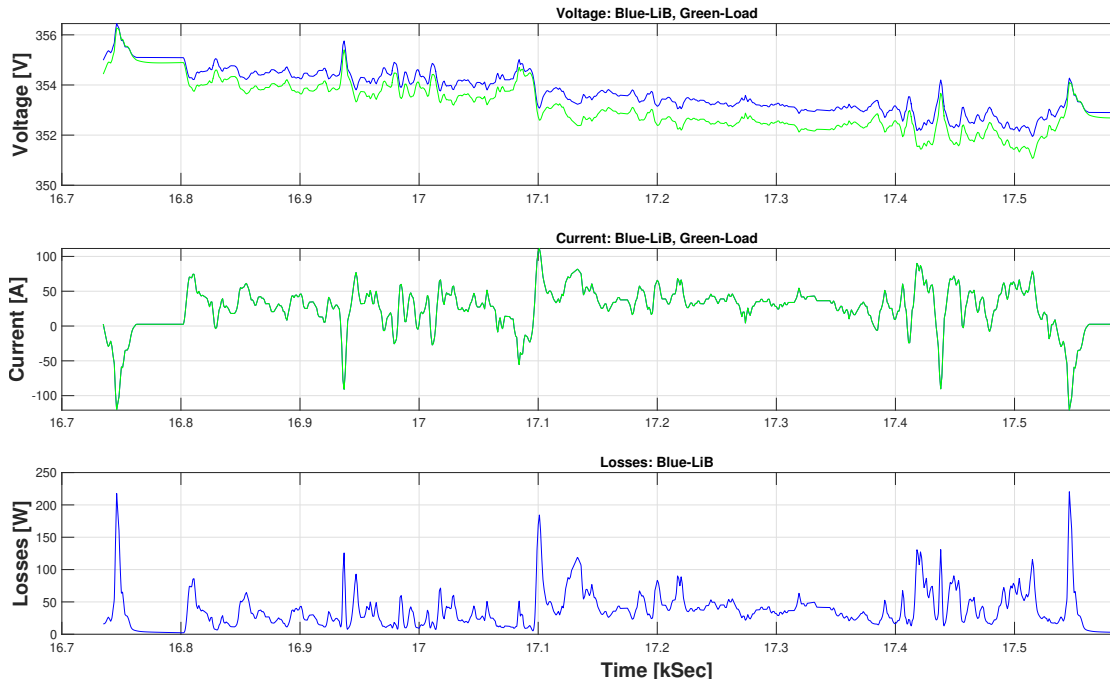


Figure 4.1: Operation of case A during one cycle

4.1.2 FCV with DC/DC - Case B

Case B relies on mainly on the additional LiB pack for higher power dynamics. Which only enables it to drive with full power for a few minutes. Then it has to slow down to recharge the LTO stack while driving. But compared to case A both case B and C can provide full power no matter on SOC. The total propulsion efficiency of this case is 54%, this is similar to commercial solutions according to [54].

Figure 4.2 shows it's performance during one cycle, the LTO cell can absorb all the energy when breaking, resulting in the highest voltage ripple of 15V. With a cooperative control system between the PEMFC and LiB it would be possible to reduce the voltage ripple even more.

Due to saturated version of the PEMFC model the faster dynamics will still be taken care of with the PEMFC. But practically the LTO cell will take more responsibility of the dynamics.

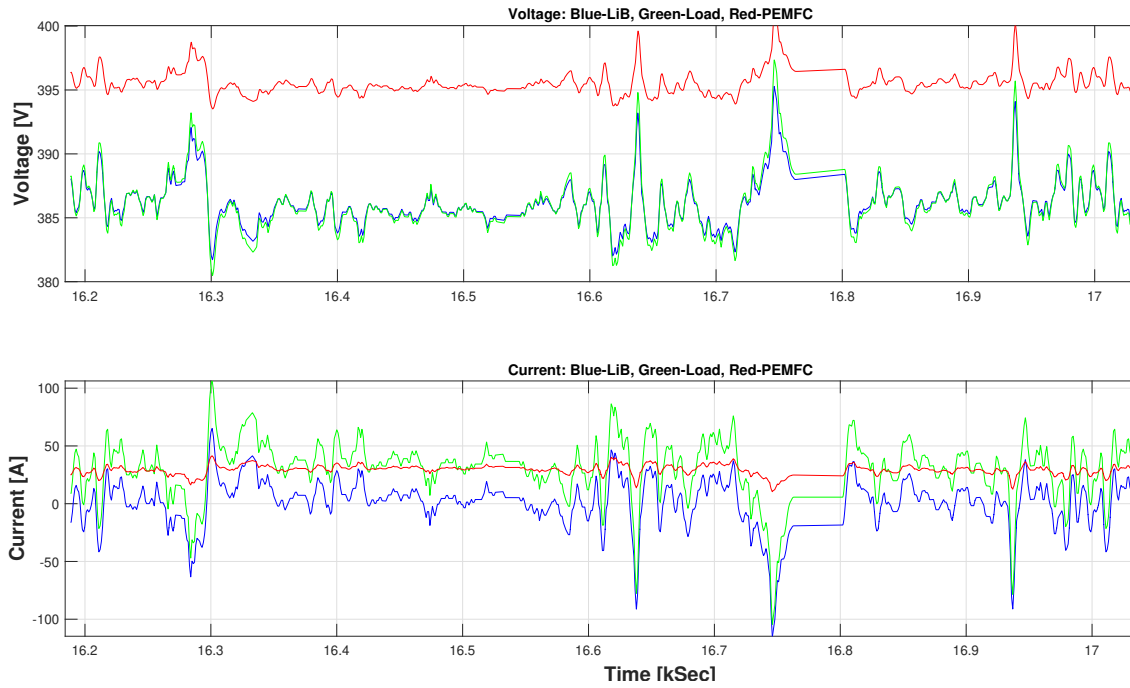


Figure 4.2: Operation of case B PEMFC during one cycle

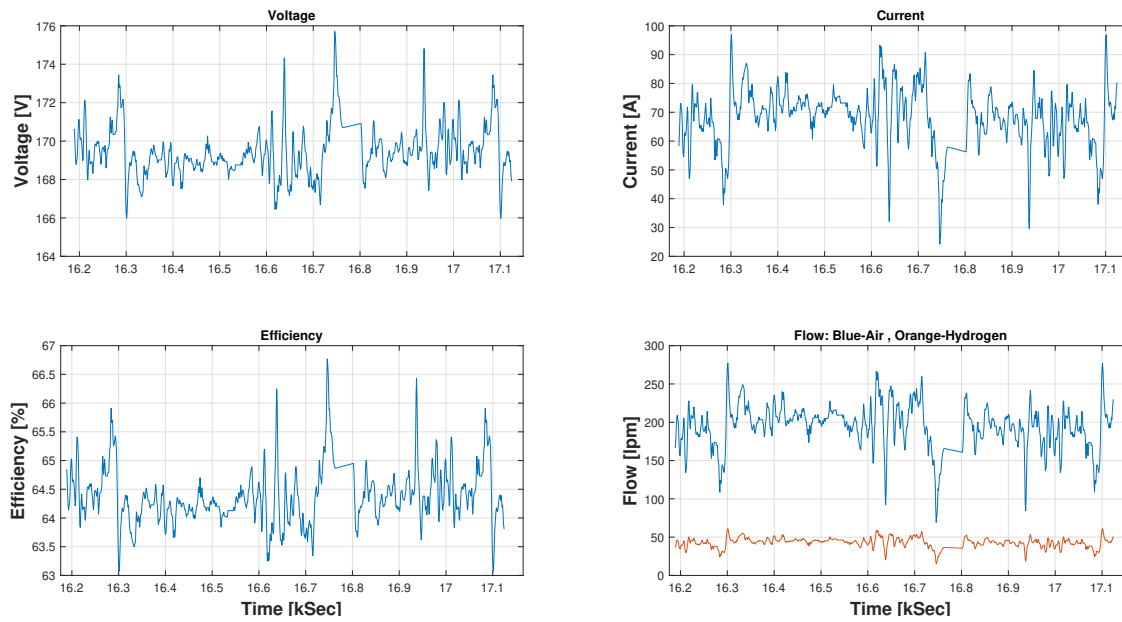


Figure 4.3: Operation of case B during one cycle, activation and ohmic region

4.1.3 FCV - Case C

In this case the tactic is to dimension the PEMFC to be able to provide for the max power and use a LTO link to stabilise the voltage ripple and be able to absorb the regenerated power.

At lower power cycles this results in the possibility to operate in the very high

4. Results

efficiency range which translates to a total proportion efficiency of 58% which drastically will drop at higher power cycles.

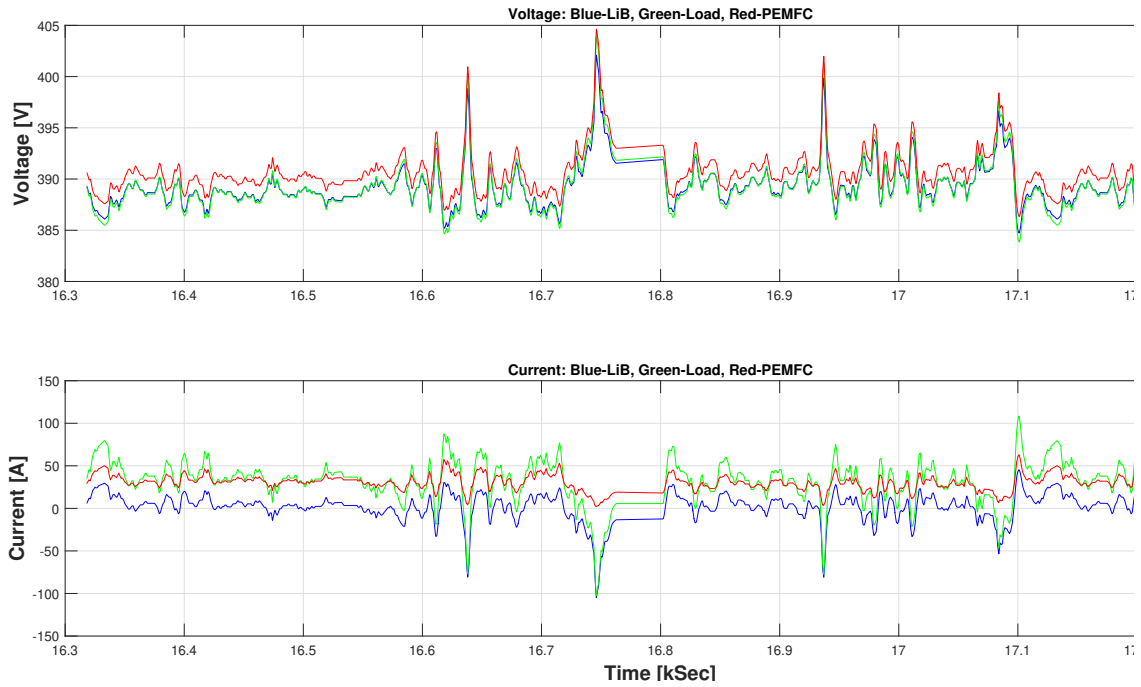


Figure 4.4: Operation of case C during one cycle

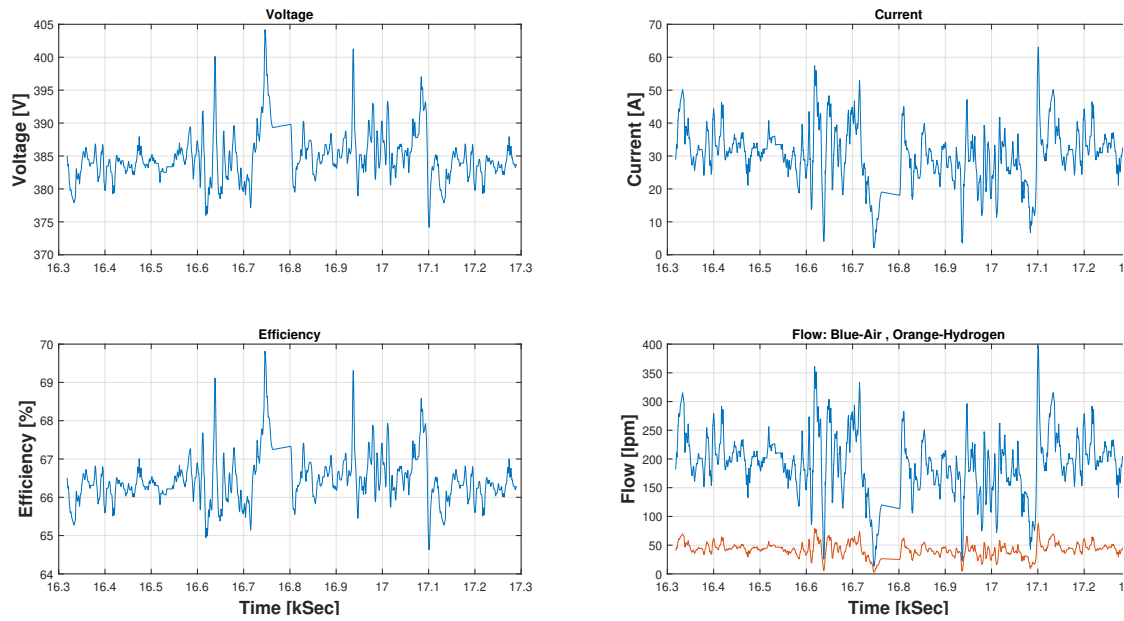


Figure 4.5: Operation of case C during one cycle

4.1.4 Limitation to model

The DC/DC and DC/AC inverter are modelled as linear components, and its dynamics is only approximate transfer functions.

The motor is operated at constant voltage but the battery draws the same power no matter of DC voltage, this is acceptable at lower power cycles since the motor is still not operating over its max power at the lowest battery voltage.

To utilise the full potential a PEMFC and LiB system a smart control system is necessary to increase the synergy between them, resulting in higher efficiency and less voltage difference. This would also be needed in high power cycles and a recycle loop for the hydrogen flow, so the unused hydrogen does not go to waste.

The utilities in the BOP system use a constant power load which is not the real case, just as everything else it does not operate with the same efficiency all the time but at least a linear approximation would be needed.

4.2 Comparison of cases

The final comparison task between the cases requires a method to try to measure how sustainable they are. In other words, three criteria for a sustainable automotive in this thesis scope, sociological (performance), economical (Cost) and environmental impact.

This is not fair in all cases since not all data is available so many assumptions have been made, this increases the accuracy of the approximations a lot.

With the substantial smaller LiB pack of LTO cells, similar efficiency have been reached compared to case A in terms losses in the battery pack. Figure 4.6 shows how even a smaller LTO stack can decrease its losses when a larger PEMFC stack is used, without increasing the total losses more then 40kW stack in case B which can be seen in Figure 4.9. If the losses from the PEMFC stack are neglected, case B and C still require a lot more energy compared to Case A, see Figure 4.7.

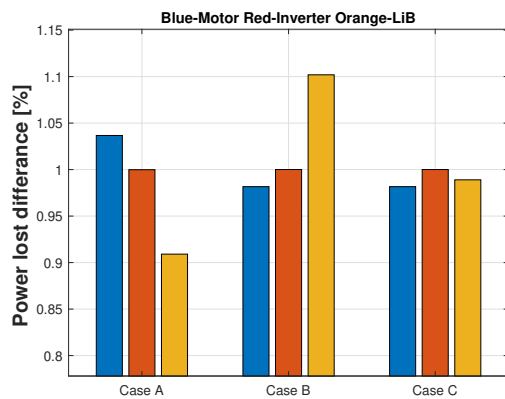


Figure 4.6: Normalised common power losses comparison cases

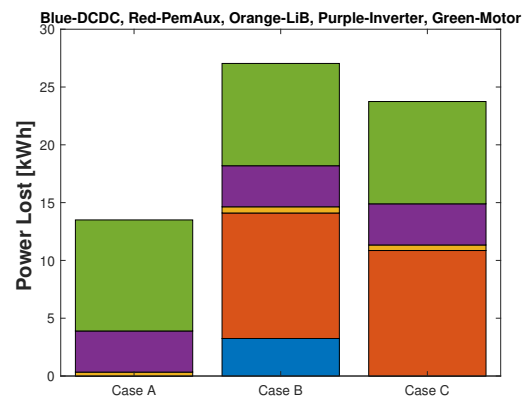


Figure 4.7: Electrical losses case comparison, not including PEMFC losses

According to GREET, an EV has a 30% lower lifetime driving distance compared to a FCV, 195062km compared to 278660km. One of the major differences between the lifetime of the PEMFC and the EV is that EOL of LiB is at 80% energy capacity where PEMFC has a 50% power capacity. In addition to this, GREET approximates

4. Results

the same lifetime of Case B as C which cannot be the case. So a large error tolerance is needed here.

The EOL range is calculated when all cases have driven the same distance and compared to their new range, see Figure 4.8.

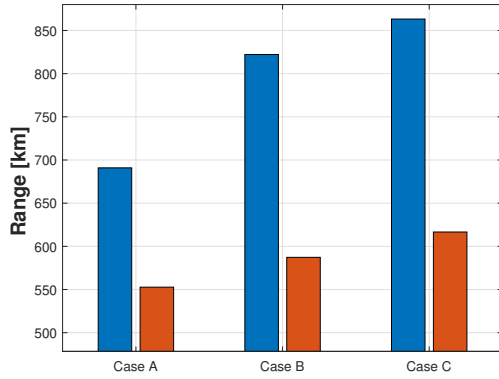


Figure 4.8: Range old and new after EVs lifetime of 195Mm

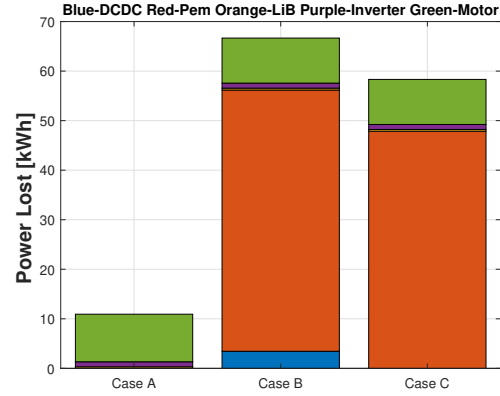


Figure 4.9: Total electrical losses case comparison

Where "PemAux" is the losses from extra auxiliaries that is required for the hydrogen and air fuel system. that includes Blower, ejector blower, dual ejector with bypass, pulsed ejector with bypass which can be seen in the Figure 3.28.

Since both cases are driving the same cycle the same extra auxiliary power is assumed. This is not the real case because case C would for example require higher power compressors which will result in higher losses and heavier.

When summarising the total mass of all energy storage units, the results is that case B and C are less than half of the battery pack mass of case A, see Figure 4.11. Where the added DC/DC is included in the accessories total mass.

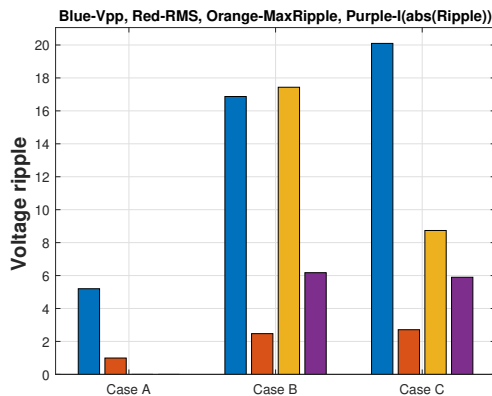


Figure 4.10: Different type of ripple only for comparison purposes: Highest peak to peak, RMS, Max derivative, Volume of ripple

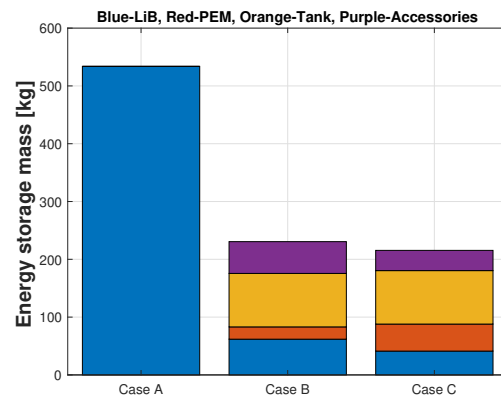


Figure 4.11: Total mass of energy storage case comparison

A real comparison between these three cases and other cars is not ideal since they use different drive cycles. But according to their total capacity and power it is seen that commercial cars put more pressure on the PEMFC except the Mercedes case which uses something similar to LMO cells which can be seen with the ratio between the power and energy capacity, see table 4.1 references to compare to other car manufacturers

Table 4.1: Comparison between commercial FCV and the three cases inspected in this thesis, the rest of the table is taken from [69]

| Car | FC (kW) | Battery (kW) | Battery (kWh) | Motor (kW) | Range km | Comment |
|--------------------------|---------|--------------|---------------|------------|----------|-------------------------------|
| Toyota Mirai | 114 | 32 | 1,59 | 113 | 658 | NiMH Cells |
| Hyundai iX 35 FC | 100 | 24 | 1,68 | 100 | 424 | |
| Hyundai NEXO | 95 | 40 | 2,8 | 120 | 592 | |
| Honda Clarity Fuel Cell | 103 | 346 V | - | 129 | 586 | |
| Mercedes-Benz GLC F-CELL | 112 | 129 | 9 / 13,8 | 147 | 500 | Power optimised cells assumed |
| Tesla S | - | - | 89 | 165 | 610 | NCA-G/Si |
| Case A | - | 556 | 94 | 130 | 680-550 | NMC+LMO/G cells |
| Case B | 40 | 222 | 3,95 | 130 | 840-601 | LTO cells DCDC used |
| Case C | 100 | 148 | 2,63 | 130 | 876-626 | LTO cells |

4.2.1 Cost comparison

The cost of Case A is done with BatPac and case B&C is from different sources where none of them involve costs such as warranty or earnings. The cost and mass of the DCDC has a large error margin, it is close to impossible to know, since not that many step-up converters are available with a similar step-up ratio. The results of the summarised costs of the energy storage system can be seen in Figure 4.12

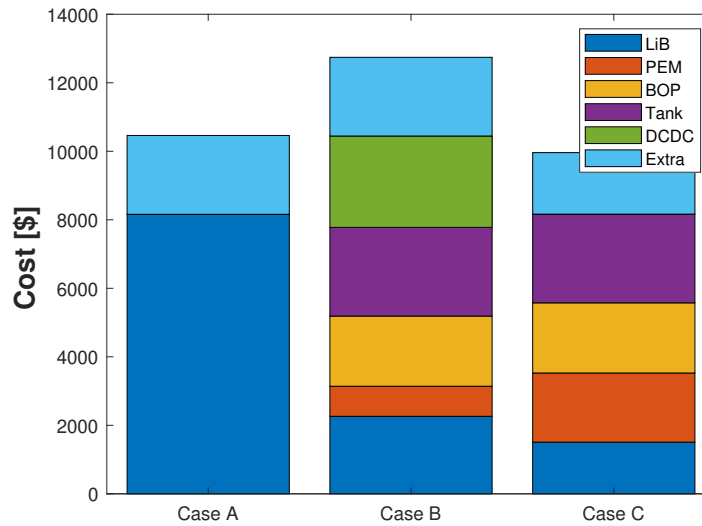


Figure 4.12: Cost of each case, Blue-LiB, Red-PEM, Orange-BOP, Purple-Tank, Green-DCDC

4.2.2 Environmental impact comparison

Case A in the GREET software uses a 100kWh of LMR/NMC+G which is the most environmental friendly of the NMC family that GREET has to offer, see Figure 3.33 and 3.34, case B and C uses 200kW of LFP cells which is approximately double the mass of the LTO stack used in the model which is meant to still make the cases comparable.

LFP is chosen since that is the type that would have been perfect in Case B and C both because of it's a good energy to power ratio and good thermal capabilities. Unfortunately not enough LFP data was found to be able to use it in the model.

LTO cells are still a good match for FCV but if LFP cells still can perform similar even if it results in triple the weight it would still be an interesting case comparison.

When comparing case B and C it is seen in the figures that they have very similar total emission and the energy usage with same parameters, expect for the reduction of PEMFC power.

With SSLBs LFP cells will be more viable not only in terms of energy capacity but it will also be able to operate in even higher temperatures which makes it more suited for FCV applications [105] [83].

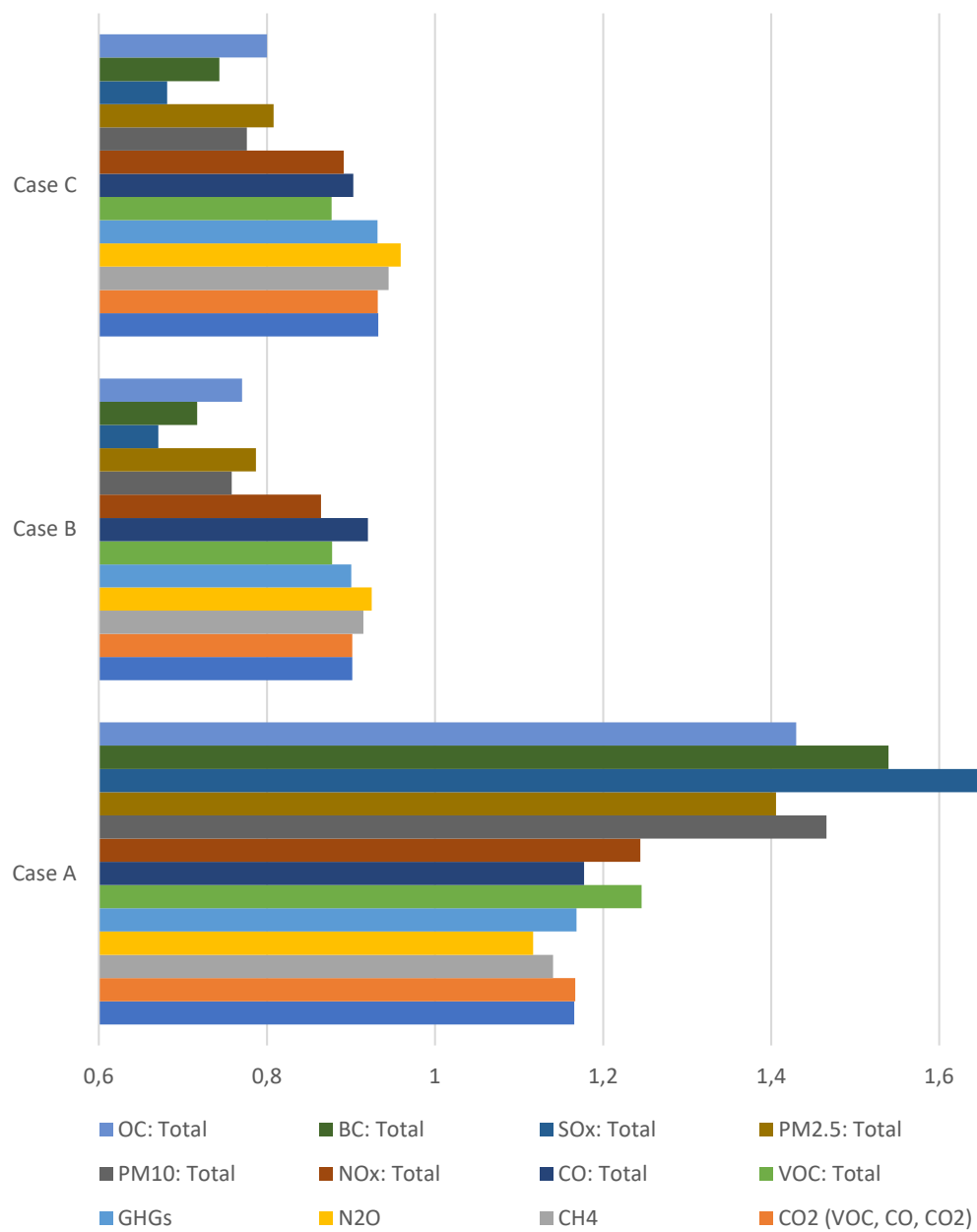


Figure 4.13: Emission comparison between cases, data from GREET

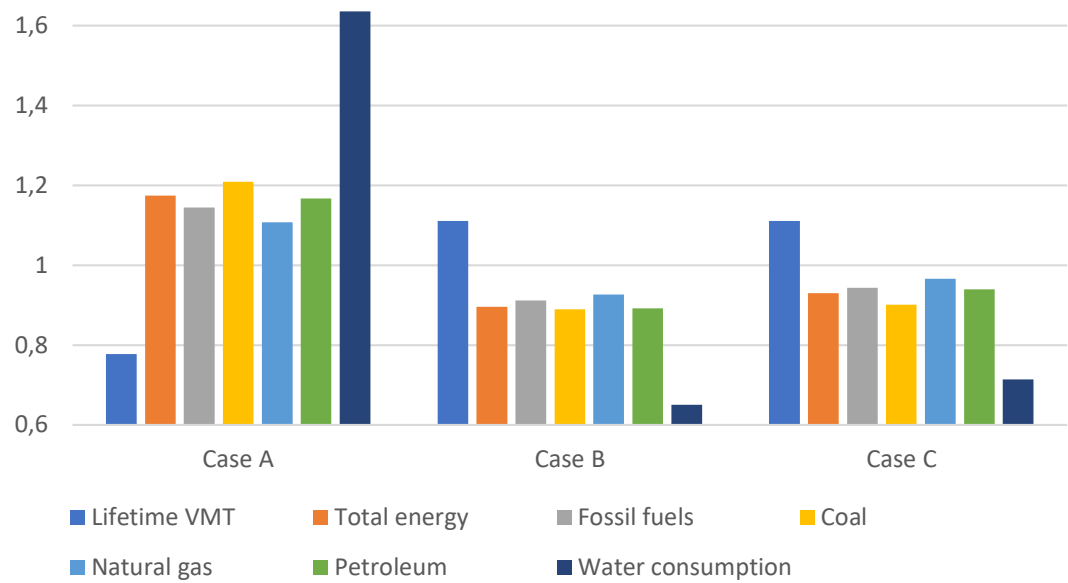


Figure 4.14: Energy usage caparison between cases, data from GREET

5

Conclusion

Due to the lack of data and fast moving development, the comparison between the cases needs to be observed with an $\pm 25\%$ error margin. The probable reason why Case B and C seem to have an incredible range compared to similar commercial cars is due to how cold they can keep the hydrogen tank and the relatively fast degradation.

To make out for the large difference in range degradation, the average value is taken between the new and old unit. Even if LTO cells and NMC/LMO+G could be used in the environmental impact comparison, the most generous case of cell type was given as case A, see Figure 3.34, it still resulted with a large difference compared to case B and C, see Figure 5.1.

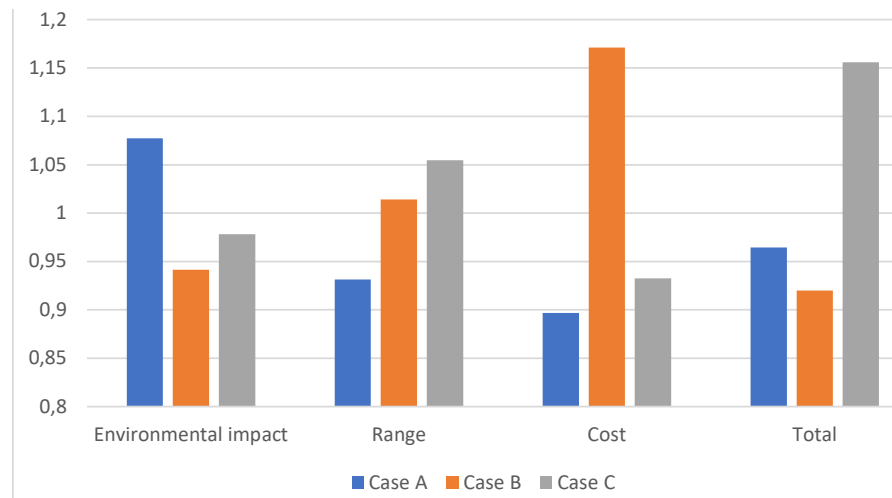


Figure 5.1: Sustainability comparison between the three cases [%]

Both EV and FCV have yet a lot room for improvement, EV does not require the same large infrastructure that FCV needs which has to be taken into account as well.

For the moment it's important to find alternative solutions to be able to not only have the opportunity to use a wider range of resources but use them where they can do the most impact.

6

Future work

There have been many assumptions in this thesis which needs to be investigated further to be able to verify the benefits of FCV compared to EV. The main topics that needs investigation are listed beneath.

- Analyse LTO cells footprint versus alternative options as a power bank. For example LFP cells, especially with the new SSBL technology [105] [83].
- Implement NMC+LMO/G and LTO cell environmental impact into GREET software.
- Implement and analyse LFP cell into Matlab model.
- Investigate LT-PEMFC degradation, including "flushing"/ cleaning the catalyst possibility's.
- Implement an empirical ageing model of each device into the Matlab model to more accurately approximate their lifetime.
- Find more data about cost and environmental impact of the DC/DC that can be used for case B for an more accurate comparison.
- Make an control system which improves the cooperation between the PEMFC and LiB pack, to be able to prepare the LiB / DC-Link for obstacles ahead.
- Use parameters from the same actual PEMFC cell instead of assuming two cells has the similar performance.
- Test an LT-PEMFC in practice to verify assumptions of operation and performance, including dynamics.
- Implement the environmental impact calculations into Matlab to be able compare the cases instantly.
- Investigate the possibility of filtering the air from carbon dioxide, to extend the life time even further [47]. Alternatively a passive Carbon Capture and Storage (CCS)

Bibliography

- [1] (2020 Mirai). URL: https://www.toyota.com/mirai/assets/modules/carpagehowitworks/Docs/MY20_Mirai_eBro_FuelCellTech.pdf.
- [2] (9) (PDF) Permanent magnet motor efficiency map calculation and small electric vehicle consumption optimization. URL: https://www.researchgate.net/publication/325554576_Permanent_magnet_motor_efficiency_map_calculation_and_small_electric_vehicle_consumption_optimization.
- [3] (Datasheet). URL: https://cdn.borgwarner.com/docs/default-source/default-document-library/remy-pds---hvh250-090-sheet-euro-pr-3-16.pdf?sfvrsn=a142cd3c_11.
- [4] A. Adib and R. Dhaouadi. *Performance Analysis of Regenerative Braking in Permanent Magnet Synchronous Motor Drives*. Tech. rep. URL: www.astesj.com.
- [5] P. Akiki et al. “Performance comparison of a doubly-salient motor with multi-V-shape ferrite magnets Performance comparison of a doubly-salient motor with multi-V-shape ferrite magnets Performance comparison of a doubly-salient motor with multi-V-shape ferrite magnets”. In: (2016), pp. 199–206. DOI: 10.1109/SPEEDAM.2016.7525826. URL: <https://hal.archives-ouvertes.fr/hal-01433976>.
- [6] L. Alfredsson. *Oral discussion about FC and hydrogen storages*. Apr. 2020.
- [7] “Alternative marine fuels _ Prospects based on multi-criteria decision analysis involving Swedish stakeholders _ Elsevier Enhanced Reader”. In: ().
- [8] J. Anderson et al. *Fire Spread due to Thermal Runaway in a Lithium-ion Battery Cell*. Tech. rep.
- [9] Y. Chang et al. *Humidification strategy for polymer electrolyte membrane fuel cells – A review*. Nov. 2018. DOI: 10.1016/j.apenergy.2018.08.125.
- [10] K. T. Chau, M. Cheng, and C. C. Chan. *Electric Machines and Power Systems*. Tech. rep. 1999, pp. 1055–1067.
- [11] A. Chaudhry. *Investigation of Lithium-ion battery parameters using pulses and EIS*. Tech. rep.
- [12] H. Dai, B. Jiang, and X. Wei. “Impedance characterization and modeling of lithium-ion batteries considering the internal temperature gradient”. In: *Energies* 11.1 (2018). ISSN: 19961073. DOI: 10.3390/en11010220.
- [13] *DATASHEET BC SERIES ULTRACAPACITORS FEATURES AND BENEFITS**. Tech. rep.
- [14] “Design strategy for reducing manufacturing and assembly complexity of air-breathing Proton Exchange Membrane Fuel Cells (PEMFC) _ Elsevier Enhanced Reader”. In: ().

- [15] H. A. Dhahad et al. *Experimental Study Of The Operating Temperature Effect On The Performance of PEM Fuel Cell*. Tech. rep. 2016. URL: <https://www.researchgate.net/publication/311886634>.
- [16] M. Dudek et al. "Power sources involving ~ 300W PEMFC fuel cell stacks cooled by different media". In: (). DOI: 10.1051/4.
- [17] *Dynamometer Drive Schedules / Vehicle and Fuel Emissions Testing / US EPA*. URL: <https://www.epa.gov/vehicle-and-fuel-emissions-testing/dynamometer-drive-schedules>.
- [18] *Electrical Energy Storage*. Tech. rep.
- [19] M. W. Ellis, M. R. Von Spakovsky, and D. J. Nelson. "Fuel Cell Systems: Efficient, Flexible Energy Conversion for the 21st Century". In: *Proceedings of the IEEE* 89.12 (2001), pp. 1808–1817. ISSN: 00189219. DOI: 10.1109/5.975914.
- [20] S. Emanuelsson and J. Persson. *Design of a fuel cell system Design of a specification of requirements for a fuel cell system for the electric power generation in a 77-foot sailing ship*. Tech. rep.
- [21] H. K. Esfeh and M. K. A. Hamid. "Temperature effect on proton exchange membrane fuel cell performance Part II: Parametric study". In: *Energy Procedia*. Vol. 61. Elsevier Ltd, 2014, pp. 2617–2620. DOI: 10.1016/j.egypro.2014.12.261.
- [22] "fcto_fuel_cells_comparison_chart". In: ().
- [23] J. P. M. Figueiredo, F. L. Tofoli, and R. L. Alves. "Comparison of non-isolated DC-DC converters from the efficiency point of view". In: *COBEP 2011 - 11th Brazilian Power Electronics Conference*. 2011, pp. 14–19. ISBN: 9781457716447. DOI: 10.1109/COBEP.2011.6085174.
- [24] *Final Report*. Tech. rep. 2018.
- [25] M. Gavrilas et al. *EPE 2016 : proceedings of the 2016 International Conference and Exposition on Electrical and Power Engineering (EPE)*. ISBN: 9781509061297.
- [26] I. D. Gimba et al. "Theoretical Energy and Exergy Analyses of Proton Exchange Membrane Fuel Cell by Computer Simulation". In: *Journal of Applied Chemistry* 2016 (2016), pp. 1–15. ISSN: 2356-7171. DOI: 10.1155/2016/2684919.
- [27] M. Grahm, M. Taljegard, and S. Brynolf. *Electricity as an Energy Carrier in Transport-Cost and Efficiency Comparison of Different Pathways*. Tech. rep. 2018.
- [28] E. A. Grunditz and Chalmers tekniska högskola. Division of Electric Power Engineering. *Design and assesment of battery electric vehicle powertrain, with respect to performance, energy consumption and electric motor thermal capability*, p. 217. ISBN: 9789175974125.
- [29] E. A. Grunditz and Chalmers tekniska högskola. Division of Electric Power Engineering. *Design and assesment of battery electric vehicle powertrain, with respect to performance, energy consumption and electric motor thermal capability*, p. 217. ISBN: 9789175974125.
- [30] *Handbok – Tillstånd till hantering av brandfarliga gaser och vätskor*. ISBN: 9789173837521.

-
- [31] *Handbok – Tillstånd till hantering av brandfarliga gaser och vätskor*. ISBN: 9789173837521.
 - [32] T. Hasegawa et al. “Development of the Fuel Cell System in the Mirai FCV”. In: *SAE Technical Papers*. Vol. 2016-April. April. SAE International, Apr. 2016. DOI: 10.4271/2016-01-1185.
 - [33] J. Hasikos et al. “Operational optimization and real-time control of fuel-cell systems”. In: *Journal of Power Sources* 193.1 (Aug. 2009), pp. 258–268. ISSN: 03787753. DOI: 10.1016/j.jpowsour.2009.01.048.
 - [34] H. He et al. “Model Predictive Control with Lifetime Constraints Based Energy Management Strategy for Proton Exchange Membrane Fuel Cell Hybrid Power Systems”. In: *IEEE Transactions on Industrial Electronics* (Mar. 2020), pp. 1–1. ISSN: 0278-0046. DOI: 10.1109/tie.2020.2977574.
 - [35] H. He et al. “Model Predictive Control with Lifetime Constraints Based Energy Management Strategy for Proton Exchange Membrane Fuel Cell Hybrid Power Systems”. In: *IEEE Transactions on Industrial Electronics* (Mar. 2020), pp. 1–1. ISSN: 0278-0046. DOI: 10.1109/tie.2020.2977574.
 - [36] *Headway Battery LiFePO₄ - 38120*. URL: http://www.evliithium.com/Headway_Battery/50.html.
 - [37] J. Hillander. *Oral discussion about HT- and LT-PEMFC systems*. May 2020.
 - [38] A. Holm. *SiC Converter for Electrical Vehicle-DC-Link Ripple*. Tech. rep.
 - [39] M. M. Hussain, I. Dincer, and X. Li. “A preliminary life cycle assessment of PEM fuel cell powered automobiles”. In: *Applied Thermal Engineering* 27.13 (Sept. 2007), pp. 2294–2299. ISSN: 13594311. DOI: 10.1016/j.applthermaleng.2007.01.015.
 - [40] Institutul de Cercetări pentru Industria Electrotehnică et al. *2019 Electric Vehicles International Conference (EV) : Icpce Solar Park, Bucharest, Romania, October 3-4, 2019*. ISBN: 9781728107912.
 - [41] C. S. Ioakimidis et al. “Life Cycle Assessment of a Lithium Iron Phosphate (LFP) Electric Vehicle Battery in Second Life Application Scenarios”. In: *Sustainability* 11.9 (May 2019), p. 2527. ISSN: 2071-1050. DOI: 10.3390/su11092527. URL: <https://www.mdpi.com/2071-1050/11/9/2527>.
 - [42] B. D. James. “Hydrogen Storage System Cost Analysis”. In: September 2018 (2011). DOI: 10.13140/RG.2.2.34567.85927.
 - [43] B. D. James et al. “Mass Production Cost Estimation of Direct H₂ PEM Fuel Cell Systems for Transportation Applications: 2017 Update Fuel Cell System and Hydrogen Storage Cost Analysis View project Cost Analysis of Transportation Fuel Cell Power Systems View project”. In: (2017). DOI: 10.13140/RG.2.2.36532.55683. URL: www.sainc.com.
 - [44] O. Josefsson. *THESIS FOR THE DEGREE OF LICENTIATE OF ENGINEERING Energy Efficiency Comparison Between Two-level and Multilevel Inverters for Electric Vehicle Applications*. Tech. rep.
 - [45] A. Jossen. “Fundamentals of battery dynamics”. In: *Journal of Power Sources* 154.2 (Mar. 2006), pp. 530–538. ISSN: 03787753. DOI: 10.1016/j.jpowsour.2005.10.041.

- [46] J. Kacprzyk, R. Bello Perez, and N. T. Nguyen. *Advances in Intelligent Systems and Computing Volume 1039 Series Editor*. Tech. rep. URL: <http://www.springer.com/series/11156>.
- [47] A. Kannan et al. “Three-layered electrolyte membranes with acid reservoir for prolonged lifetime of high-temperature polymer electrolyte membrane fuel cells”. In: *International Journal of Hydrogen Energy* 45.1 (Jan. 2020), pp. 1008–1017. ISSN: 03603199. DOI: 10.1016/j.ijhydene.2019.10.186.
- [48] M. Karlström et al. *Can fuel cells become a mass-produced option globally for heavy-duty trucks 2030+?* 2019. ISBN: 978-91-7673-604-3. URL: www.energiforsk.se.
- [49] A. Kersten et al. “Battery Loss and Stress Mitigation in a Cascaded H-Bridge Multilevel Inverter for Vehicle Traction Applications by Filter Capacitors”. In: *IEEE Transactions on Transportation Electrification* 5.3 (2019), pp. 659–671. ISSN: 23327782. DOI: 10.1109/TTE.2019.2921852.
- [50] M. Kubicka et al. “The temperature effect on the electrochemical performance of sulfur-doped limn₂ o₄ in li-ion cells”. In: *Nanomaterials* 9.12 (Dec. 2019). ISSN: 20794991. DOI: 10.3390/nano9121722.
- [51] E. Kulldorff. *Illustrative work of FC systems*. May 2020.
- [52] J. Larminie and A. Dicks. *Fuel Cell Systems Explained*. West Sussex, England: John Wiley & Sons, Ltd., Feb. 2003, pp. 1–406. ISBN: 9781118878330. DOI: 10.1002/9781118878330. URL: <http://doi.wiley.com/10.1002/9781118878330>.
- [53] S. Lazarou, E. Pyrgioti, and A. Alexandridis. *PEM fuel cell equivalent circuit models: A review Nanofluids for High Voltage applications View project Dealing with the emerging European electric energy challenges using advanced simulation capabilities View project*. Tech. rep. 2008. URL: <https://www.researchgate.net/publication/260597805>.
- [54] H. Lohse-Busch et al. “Automotive fuel cell stack and system efficiency and fuel consumption based on vehicle testing on a chassis dynamometer at minus 18 °C to positive 35 °C temperatures”. In: *International Journal of Hydrogen Energy* 45.1 (Jan. 2020), pp. 861–872. ISSN: 03603199. DOI: 10.1016/j.ijhydene.2019.10.150.
- [55] A. O. Lukman et al. *Modeling and Simulation of Hydrogen Storage Device for Fuel Cell Plant*. Tech. rep. 2012, pp. 604–612.
- [56] A.-F. Mahrous et al. “Experimental Investigation of the Operating Parameters Affecting Hydrogen Production Process through Alkaline Water Electrolysis”. In: *International Journal of Thermal and Environmental Engineering* 2.2 (Dec. 2010), pp. 113–116. ISSN: 19237308. DOI: 10.5383/ijtee.02.02.009.
- [57] P. Manoj Kumar and V. Parthasarathy. “A passive method of water management for an air-breathing proton exchange membrane fuel cell”. In: *Energy* 51 (2013), pp. 457–461. ISSN: 03605442. DOI: 10.1016/j.energy.2012.12.015.
- [58] M. Mayur et al. “Lifetime Prediction of a Polymer Electrolyte Membrane Fuel Cell under Automotive Load Cycling Using a Physically-Based Catalyst Degradation Model”. In: *Energies* 11.8 (Aug. 2018), p. 2054. ISSN: 1996-

1073. DOI: 10.3390/en11082054. URL: <http://www.mdpi.com/1996-1073/11/8/2054>.
- [59] MC Power Series BOOSTCAP® Ultracapacitors MC Power Series BOOSTCAP® Ultracapacitors Round, Terminal Type. Tech. rep. URL: www.maxwell.com.
- [60] M. Meeus and M. Meeus -Emiri. *Overview of Battery Cell Technologies Overview of battery technologies Bridging the Innovation Gap*. Tech. rep.
- [61] A. S. Menesy, H. M. Sultan, and S. Kamel. *Extracting Model Parameters of Proton Exchange Membrane Fuel Cell Using Equilibrium Optimizer Algorithm*. ISBN: 9781728156552.
- [62] Y. Miao et al. *Current li-ion battery technologies in electric vehicles and opportunities for advancements*. Mar. 2019. DOI: 10.3390/en12061074.
- [63] *Model S Efficiency and Range | Tesla Sverige*. URL: https://www.tesla.com/sv_SE/blog/model-s-efficiency-and-range?redirect=no.
- [64] S. T. Myung et al. *Nickel-Rich Layered Cathode Materials for Automotive Lithium-Ion Batteries: Achievements and Perspectives*. Jan. 2017. DOI: 10.1021/acsenergylett.6b00594.
- [65] A. C. N Reilley and R. W. Murray. *FormulaSheet*. Tech. rep.
- [66] B. Naourez et al. *Permanent magnet motor efficiency map calculation and small electric vehicle consumption optimization Design and Faults Diagnosis in Permanent Magnet Synchronous Motors View project Recent Advances in Electrical Systems View project*. Tech. rep. 2018. URL: <https://www.researchgate.net/publication/325554576>.
- [67] F. Ning et al. "Flexible and Lightweight Fuel Cell with High Specific Power Density". In: *ACS Nano* 11.6 (June 2017), pp. 5982–5991. ISSN: 1936086X. DOI: 10.1021/acsnano.7b01880.
- [68] J. Partridge and D. I. Abouelamaimen. "The role of supercapacitors in regenerative braking systems". In: *Energies* 12.14 (2019). ISSN: 19961073. DOI: 10.3390/en12142683.
- [69] H. Pohl. *Kostnadsfunktion för traktionära bränslecellssystem*. 2018. ISBN: 9789176735558. URL: www.energiforsk.se.
- [70] H. Pohl. *Kostnadsfunktion för traktionära bränslecellssystem*. 2018. ISBN: 9789176735558. URL: www.energiforsk.se.
- [71] H. Pohl. *Research Institutes of Sweden COST FUNCTION FOR AUTOMOTIVE FUEL CELL SYSTEMS RISE VIKTORIA*. Tech. rep. 2019.
- [72] *Polymer Fuel Cells - DTU Energy*. URL: <https://www.energy.dtu.dk/english/Research/Fuel-Cells/PEM-Fuel-Cells>.
- [73] J. W. Pratt et al. *SANDIA REPORT Proton Exchange Membrane Fuel Cells for Electrical Power Generation On-Board Commercial Airplanes*. Tech. rep. 2011. URL: <http://www.ntis.gov/help/ordermethods.asp?loc=7-4-0#online>.
- [74] J. W. Pratt et al. *SANDIA REPORT Proton Exchange Membrane Fuel Cells for Electrical Power Generation On-Board Commercial Airplanes*. Tech. rep. 2011. URL: <http://www.ntis.gov/help/ordermethods.asp?loc=7-4-0#online>.

- [75] *PRODUCT GUIDE Maxwell Technologies® BOOSTCAP® Ultracapacitors*. Tech. rep. 2009.
- [76] J. T. Pukrushpan, A. G. Stefanopoulou, and H. Peng. “Control of Fuel Cell Breathing”. In: *IEEE Control Systems* 24.2 (2004), pp. 30–46. ISSN: 1066033X. DOI: 10.1109/MCS.2004.1275430.
- [77] M. Robinius et al. *Comparative Analysis of Infrastructures: Hydrogen Fueling and Electric Charging of Vehicles Comparative Analysis of Infrastructures*. ISBN: 978-3-95806-295-5.
- [78] RVS Technical Campus, IEEE Electron Devices Society, and Institute of Electrical and Electronics Engineers. *Proceedings of the Second International Conference on Electronics, Communication and Aerospace Technology (ICECA 2018) : 29-31, May 2018*. ISBN: 9781538609651.
- [79] I. P. Sahu et al. “Performance study of PEM fuel cell under different loading conditions”. In: *Energy Procedia*. Vol. 54. Elsevier Ltd, 2014, pp. 468–478. DOI: 10.1016/j.egypro.2014.07.289.
- [80] F. Saidani et al. “Lithium-ion battery models: A comparative study and a model-based powerline communication”. In: *Advances in Radio Science* 15 (Sept. 2017), pp. 83–91. ISSN: 16849973. DOI: 10.5194/ars-15-83-2017.
- [81] U. Sarma and S. Ganguly. “Design optimisation for component sizing using multi-objective particle swarm optimisation and control of PEM fuel cell-battery hybrid energy system for locomotive application”. In: *IET Electrical Systems in Transportation* 10.1 (Mar. 2020), pp. 52–61. ISSN: 20429746. DOI: 10.1049/iet-est.2018.5053.
- [82] R. Schmuck et al. *Performance and cost of materials for lithium-based rechargeable automotive batteries*. Apr. 2018. DOI: 10.1038/s41560-018-0107-2.
- [83] J. Schnell et al. “Prospects of production technologies and manufacturing costs of oxide-based all-solid-state lithium batteries †”. In: *1818 / Energy Environ. Sci* 12 (2019), p. 1818. DOI: 10.1039/c8ee02692k.
- [84] H.-G. Schweiger et al. “Comparison of Several Methods for Determining the Internal Resistance of Lithium Ion Cells”. In: *Sensors* 10.6 (June 2010), pp. 5604–5625. ISSN: 1424-8220. DOI: 10.3390/s100605604. URL: <http://www.mdpi.com/1424-8220/10/6/5604>.
- [85] L. H. Seim. *Modeling, Control and Experimental Testing of a Supercapacitor/Battery Hybrid System-Passive and Semi-Active Topologies*. Tech. rep.
- [86] Y. H. Seo et al. “Development of active breathing micro PEM fuel cell”. In: *International Journal of Precision Engineering and Manufacturing - Green Technology* 1.2 (2014), pp. 101–106. ISSN: 21980810. DOI: 10.1007/s40684-014-0014-3.
- [87] S. Skoog. *Component and system design of a mild hybrid 48 V powertrain for a light vehicle*. 2020. ISBN: 9789179053239. URL: www.chalmers.se.
- [88] S. Skoog. “Electro-thermal modeling of high-performance lithium-ion energy storage systems including reversible entropy heat”. In: *Conference Proceedings - IEEE Applied Power Electronics Conference and Exposition - APEC*. Institute of Electrical and Electronics Engineers Inc., May 2017, pp. 2369–2373. ISBN: 9781509053667. DOI: 10.1109/APEC.2017.7931031.

-
- [89] S. Skoog. “Parameterization of equivalent circuit models for high power lithium-ion batteries in HEV applications”. In: *2016 18th European Conference on Power Electronics and Applications, EPE 2016 ECCE Europe*. Institute of Electrical and Electronics Engineers Inc., Oct. 2016. ISBN: 9789075815245. DOI: 10.1109/EPE.2016.7695340.
 - [90] S. Skoog and S. David. *Parametrization of Linear Equivalent Circuit Models over Wide Temperature and SOC spans for Automotive Lithium-Ion Cells using Electrochemical Impedance Spectroscopy*. Tech. rep.
 - [91] R. Stropnik et al. “Critical materials in PEMFC systems and a LCA analysis for the potential reduction of environmental impacts with EoL strategies”. In: *Energy Science and Engineering* 7.6 (Dec. 2019), pp. 2519–2539. ISSN: 20500505. DOI: 10.1002/ese3.441.
 - [92] R. Stropnik et al. “Critical materials in PEMFC systems and a LCA analysis for the potential reduction of environmental impacts with EoL strategies”. In: *Energy Science & Engineering* 7.6 (Dec. 2019), pp. 2519–2539. ISSN: 2050-0505. DOI: 10.1002/ese3.441. URL: <https://onlinelibrary.wiley.com/doi/abs/10.1002/ese3.441>.
 - [93] *Technical Assessment of Compressed Hydrogen Storage Tank Systems for Automotive Applications Nuclear Engineering Division*. Tech. rep. 2010. URL: www.anl.gov.
 - [94] *The data is taken from BatPac software*. Tech. rep. 2019.
 - [95] *The data is taken from GREET software*. Tech. rep. 2019.
 - [96] S. Ullah et al. “A permanent magnet assisted switched reluctance machine for more electric aircraft”. In: *Proceedings - 2016 22nd International Conference on Electrical Machines, ICEM 2016*. Institute of Electrical and Electronics Engineers Inc., Nov. 2016, pp. 79–85. ISBN: 9781509025381. DOI: 10.1109/ICELMACH.2016.7732509.
 - [97] R. J. Wai and R. Y. Duan. “High step-up converter with coupled-inductor”. In: *IEEE Transactions on Power Electronics* 20.5 (Sept. 2005), pp. 1025–1035. ISSN: 08858993. DOI: 10.1109/TPEL.2005.854023.
 - [98] C. Wang, M. H. Nehrir, and S. R. Shaw. “Dynamic models and model validation for PEM fuel cells using electrical circuits”. In: *IEEE Transactions on Energy Conversion* 20.2 (June 2005), pp. 442–451. ISSN: 08858969. DOI: 10.1109/TEC.2004.842357.
 - [99] H. Wang et al. “Flexible and Adaptable Fuel Cell Pack with High Energy Density Realized by a Bifunctional Catalyst”. In: *ACS Applied Materials and Interfaces* 12.4 (Jan. 2020), pp. 4473–4481. ISSN: 19448252. DOI: 10.1021/acsaami.9b18511.
 - [100] S. Wang and Y. Xu. *Battery Electric Vehicle with a Fuel Cell Stack A System Study of Propulsion Concepts and Scenarios Master’s thesis in Electrical Engineering*. Tech. rep.
 - [101] Y. Wang et al. “Mg@C60 nano-lamellae and its 12.50 wt% hydrogen storage capacity”. In: *International Journal of Hydrogen Energy* 44.29 (June 2019), pp. 15239–15245. ISSN: 03603199. DOI: 10.1016/j.ijhydene.2019.04.104.

- [102] S. Wessel. *Open-Source FCPEM-Performance and Durability Model (FC-APOLLO): Consideration of Membrane Properties on Cathode Degradation*. Tech. rep. 2014.
- [103] E. Wikner and Chalmers tekniska högskola. Division of Electric Power Engineering. *Ageing in commercial li-ion batteries : lifetime testing and modelling for electrified vehicle applications*, p. 114. ISBN: 9789179051662.
- [104] C. H. Woo and J. B. Benziger. “PEM fuel cell current regulation by fuel feed control”. In: *Chemical Engineering Science* 62.4 (Feb. 2007), pp. 957–968. ISSN: 00092509. DOI: 10.1016/j.ces.2006.10.027.
- [105] S. Xiong et al. “Design of a Multifunctional Interlayer for NASCION-Based Solid-State Li Metal Batteries”. In: *Advanced Functional Materials* (Apr. 2020), p. 2001444. ISSN: 1616301X. DOI: 10.1002/adfm.202001444. URL: <http://doi.wiley.com/10.1002/adfm.202001444>.
- [106] M. Zeraoulia, M. E. H. Benbouzid, and D. Diallo. *Electric motor drive selection issues for HEV propulsion systems: A comparative study*. Nov. 2006. DOI: 10.1109/TVT.2006.878719.
- [107] X. Zhang et al. “Performance analysis of a proton exchange membrane fuel cell based syngas”. In: *Entropy* 21.1 (Jan. 2019). ISSN: 10994300. DOI: 10.3390/e21010085.
- [108] J. Zhu et al. “High efficiency SiC traction inverter for electric vehicle applications”. In: *Conference Proceedings - IEEE Applied Power Electronics Conference and Exposition - APEC*. Vol. 2018-March. Institute of Electrical and Electronics Engineers Inc., Apr. 2018, pp. 1428–1433. ISBN: 9781538611807. DOI: 10.1109/APEC.2018.8341204.